Assessment of Design Provisions for Open I-Section under Combined Flexure and Torsion

by

Jing Zhang

A thesis submitted to the Graduate Faculty of
Auburn University
in partial fulfillment of the
requirements for the Degree of
Master of Science

Auburn, Alabama
August 4, 2012

Keywords: flexure, torsion, ultimate strength, serviceability

Approved by

Hassan H. Abbas, Chair, Assistant Professor of Civil Engineering
James S. Davidson, Associate Professor of Civil Engineering
Mary L. Hughes, Lecturer of Civil Engineering

Abstract

In civil structures, the members often encounter a combined loading of flexure and torsion, which has a strong influence on the members' behavior and capacity, especially for those beam sections with relatively weak torsional resistance, such as the commonly used I-shaped sections. To ensure both the safety and the economy of design result, the validity of different design methods for combined flexure and torsion should be investigated before any practical applications are attempted.

In this thesis, finite Element (FE) models are developed and verified using theoretical analysis and experimental results in the literature. The influence of a number of key parameters on the behavior, ultimate strength, and serviceability of representative I-shaped beam members are investigated via the finite element method FEM approach. The current main design methods for combined flexure and torsion are also evaluated based on the FE simulation results. Suggestions are made regarding the applicability of the design methods studied in this thesis for the ultimate strength prediction of I-shaped beam members.

Acknowledgement

First, I would like to thank Dr. Abbas and Dr. Davidson for their continuous guidance and support of my study and research at Auburn. The knowledge and insights they shared with me are truly invaluable, without which this thesis would not have been possible. I would also like to thank Dr. Hughes for her encouragement and effort which have definitely helped with the completion of this thesis. Many thanks to the faculty of the Civil Engineering Department at Auburn University for their inspiring and interesting classes that I have been fortunate enough to take. I also owe a lot of thanks to my friends and classmates with whom I have spent a lot of pleasant times.

Last, but not the least, I would like to thank my dear family members; their support and encouragement carry me to where I am.

Table of Contents

List of Tables

List of Figures

Chapter 1. Introduction

1.1. Overview

Commonly used open sections in steel building construction (e.g., wide flange I-shapes) are poor in resisting torsion. Therefore, it has been advisable in practice to design and detail members with open sections in such a way to eliminate or minimize torsional effects. However, in practice, the loads may not act through the shear center of the section, in which case the member is subject to a mixture of torsion and flexure.

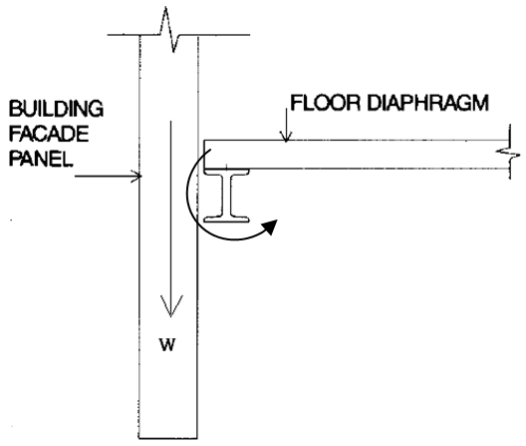

Figure 1 Torsion in spandrel beam

For example, for the structure shown in Figure 1, the weight of the vertical rigid façade elements is transferred eccentrically with respect to the shear center of the spandrel beam, thus causing torsion. Moreover, the vertical load acting between the two end supports produces bending moment about the strong axis of the spandrel beam. Hence, the spandrel beam is subject to combined flexure and torsion. Similarly, for the structure shown in Figure 2, the weight of the wall and the slab also cause both flexure and torsion in the beam. Proper design criteria are needed to address design situations such as those depicted in Figures 1 and 2.

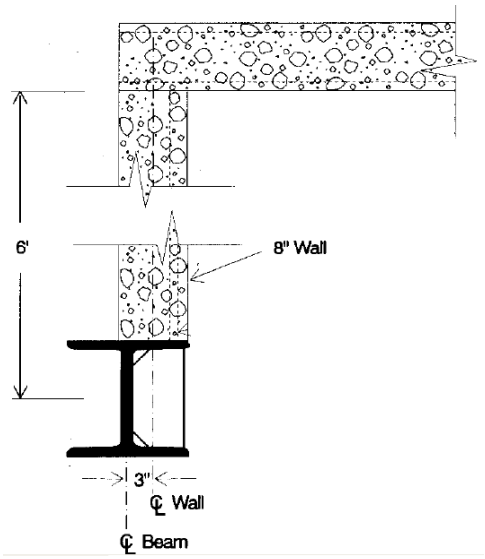

Figure 2 Torsional load in a support beam.

1.2. Motivation

Current AISC design provisions for I-sections under combined flexure and torsion are based upon an elastic analysis approach that involves the superposition of stresses caused by flexure and torsion. Stresses are usually calculated using established theories of structural mechanics, and the beam is designed such that the resulting maximum stress anywhere in the beam does not exceed a limiting stress that depends upon the limit state considered. This approach is used whether the Allowable Strength Design (ASD) method or Load and Resistance Factor Design (LRFD) method is used (AISC 2010). Elastic analysis of I-sections subject to torsion requires the solution of a third or fourth order ordinary differential equation (ODE) whose independent variable is the angle of twist. Although closed-form mathematical solutions are available for beams with standard support and loading conditions, they are considered impractical for use in design. Seaburg and Cater (2003) present these solutions graphically in the form of normalized charts for beams with standard support and loading conditions. Nonetheless, this procedure is often viewed by engineers to be cumbersome and onerous.

Researchers at the University of Alberta in Canada (Estabrooks and Grodin, 2008) and the University of Sydney in Australia (Pi and Trahair, 1994b) have recently proposed to use an ultimate strength limit state design approach in lieu of the elastic analysis approach described above. This approach can significantly simplify the design process by eliminating the need to solve the ODE or investigate critical combinations of flexural and torsional stresses.

In this thesis, the viability of this recently-proposed strength limit state design approach will be assessed in comparison with the AISC elastic design approach.

1.3. Research Objectives

The objectives of this research were as follows:

- Generate finite element (FE) analysis results that can be used to assess the AISC design provisions for I-shaped steel beams under combined flexure and torsion.
- Investigate the effect of a number of key parameters on the behavior of I-shaped steel beams under combined flexure and torsion.
- Assess recently proposed ultimate strength design approaches for combined flexure and torsion.

1.4. Scope and Approach

The scope of this research study is analytical in nature. The general-purpose commercially available finite element (FE) analysis package ABAQUS was employed. Because FE analysis was used as the only means of analysis in this research, it was necessary to ensure that the FE models could accurately predict the behavior in both the elastic and inelastic range of behavior. To this end, FE models were developed, then their results validated via two means: (1) the models' elastic response was validated by comparison with well-established elastic analysis theories, and (2) the models' inelastic response was validated by comparison with experimental results reported in (Estabrooks and Grondin 2008). After the models were validated, they were used in a subsequent parametric study to investigate the influence of several key parameters on the behavior.

Instead of performing a comprehensive study of all parameters affecting the behavior of I-shaped steel beams subject to combined flexure and torsion, this research focuses on a small number of key parameters and some variables. These parameters and variables include the beam slenderness ratio, the moment-to-torque ratio, the ratio of pure warping to torsional resistance, and the ratio of flexural to torsional stiffness. The parametric study included a total of 30 simulations of simply supported beams with varying lengths and moment-to-torque ratios under an eccentrically-applied load at the mid-span section.

1.5. Tasks

To achieve the objectives of this research, the following tasks were completed:

- Review previous research
- Develop and verify FE models in ABAQUS
- Validate the FE analysis results
- Develop and conduct a parametric study
- Analyze the influence of the parameters on the behavior
- Compare FE analysis results with AISC design criteria and recently proposed ultimate strength design approaches
- Make recommendations and suggestions for future research

1.6. Thesis Organization

This thesis is organized into five chapters. Chapter 1 provides a brief overview of the problem considered in this thesis, and introduces the objectives as well as the approach of this research. In Chapter 2, relevant theories and current methodologies for predicting the elastic and inelastic behavior of I-shaped beams under combined bending and torsion are reviewed. The FE modeling approach and validations studies are presented in Chapter 3. The parametric study and its results are reported in Chapter 4. Finally, in Chapter 5, the main results and conclusions of this thesis as well as recommendations for future research are presented.

1.7. Notation

The notation used in this thesis follows AISC Steel Construction Manual 13th Edition (2010) and is listed in Appendix A. United States customary units of measurement are used throughout this thesis unless otherwise specified.

Chapter 2 Literature Review

2.1. Overview

Current AISC design provisions for I-shaped steel beams restrict the stresses due to combined flexural and torsional loading effects to within the elastic range of behavior (AISC 2010). However, recent research studies have shown that the load-carrying capacity can be significantly higher if post-yielding behavior is considered. In this chapter, first, existing theories and methodologies for the elastic analysis of I-shaped beams subject to flexure, torsion, and combined flexure and torsion are reviewed. Then, theoretical and research results pertaining to the ultimate capacity of I-shaped beams subject to combined flexural and torsional loading are presented, with a primary focus on interaction equations proposed in the literature for the ultimate strength limit state. Finally, research results that employed finite element (FE) analysis studies for members under combined flexure and torsion will be reviewed.

2.2. Elastic Analysis

2.2.1 Elastic Analysis for Torsion

The torsional resistance of a given member is attributed to two distinct resistance mechanisms as established by Saint Venant in the 1850s. These resistances are pure (St. Venant, uniform) torsion and warping torsion, which are established separately as a function of rotational deformation.

Pure torsion is characterized by the development of cross-sectional shear stresses as each cross-section resists the adjacent cross-section's twist; the pure torsion resistance is thus a function of longitudinal rotation and shear rigidity. Certain cross sections (e.g., circular cross sections) resist the applied torsional loads by pure torsion solely. This may be attributed to the fact that such cross sections do not warp even if the applied torsional loads are nonuniform or if the member is rotationally restrained. For open I-shaped thin-walled cross sections, however, the applied torsional loads will be resisted by pure torsion only if the applied torsional loads are uniform and the member is not rotationally restrained. This may be attributed to the fact that I-shaped cross sections do experience cross-sectional warping due to torsional loads (Seaburg and Carter, 2003). The shear stress distribution of a typical I-shaped section in pure torsion is shown in Figure 3. An illustration of aarping deformations in I-shaped sections is shown in Figure 4.

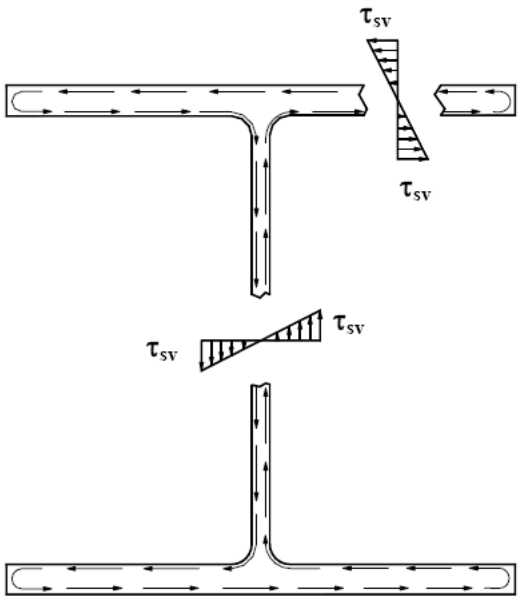

Figure 3 Shear stress distribution due to pure torsion, (Estabrooks and Grondin, 2008).

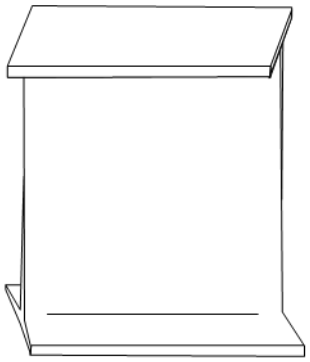

Figure 4 Idealized warping deformation of I-shapes (Seaburg and Carter, 2003).

Galambos (1968) expresses the maximum shear stress due to pure torsion for open cross-sections composed of thin-walled rectangular elements as:

$$\tau_{sv} = Gt_m\theta' \qquad (2.1)$$

where G is the shear modulus of rigidity, t_m is the maximum cross-sectional thickness , and θ' is the change of the rotation angle per unit length. The total pure torsion resisted by a particular cross-section is represented by:

$$T_{sv} = GJ\theta' \tag{2.2}$$

where J is the polar moment of inertia which is a geometric property of the cross-section. For I-sections, J can be closely approximated using the following equation:

$$J = \sum bt^3/3 \tag{2.3}$$

where b and t are the length and thickness of each cross-sectional element, respectively. Various modifications have been proposed to adjust the J term for end effects and fillet geometry, as referenced by Driver and Kennedy (1987).

Cross-sections that do not exhibit uniform shear strains at all points on the same radius, with respect to the shear center, will warp when subjected to torsion (Hibbeler 2008). Warping effects cause cross-sectional elements to deform out of plane. When this tendency to deform is restrained or when the applied torsional loads are nonuniform, shear and normal warping stresses will develop.

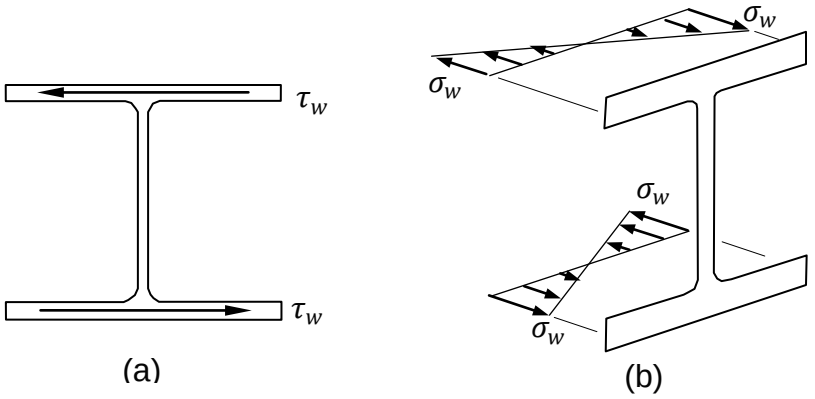

Figure 5 (a) Shear stress in flanges due to warping torsion. (b) Normal stress distribution due to warping torsion.

The warping deformations of I-shaped cross sections can be visualized as the lateral deformation of the flanges in opposite directions as shown in Figure 4. The warping resistance of I-shaped cross sections can be represented by equal and opposite transverse shear stresses in the flange that occur in conjunction with transverse flange bending (bi-moment), as shown in Figure 5(a). Figure 5(b) shows the distribution of normal stress due to warping torsion. The shear and normal stresses in the flanges of I-shaped cross sections can be expressed respectively as:

$$\tau_w = -ES_w\theta''' \tag{2.4}$$

and

$$\sigma_w = -EW_n\theta'' \tag{2.5}$$

where E is the modulus of elasticity, the normalized warping function W_n and the warping static moment S_w are determined by the section geometry, and θ'' and θ''' are the second and third derivatives of the angle of twist with respect to the distance along the length of the beam.

The resultant of the shear stresses represents the transverse shear force, while, the resultant of the normal stresses represents the bi-moment. The transverse shear force and the bi-moment are self equilibrating forces that act on the cross-section. The total warping torsion resisted by a particular cross-section is represented by:

$$T_w = -EC_w\theta''' \tag{2.6}$$

where C_w is the warping constant of the cross-section. The resistance due to the combination of pure and warping torsion for concentrated torque is given by the following differential equation:

$$T = T_{sv} + T_w = GJ\theta' - EC_w\theta''' \tag{2.7}$$

The solution of this differential equation depends upon loading and boundary conditions, and requires the determination of constants of integration. Statically determinant members require three boundary conditions to be satisfied, while an additional boundary condition is required for each additional degree of indeterminacy (Pi and Trahair 1995a). It is important to note that web deformations are neglected in the development of warping resistance, which provides approximate but adequate solutions (Kubo et al. 1956) except for unstiffened plate girders (Salmon and Johnson 1980), as reported by Driver and Kennedy (1987). Also, interactions between normal and shear stress are neglected in the equations used; Pastor and Dewolf (1979) developed differential equations that consider such interactions, as reported by Bremault et al. (2008), however, their equations are complicated, and are not suitable for design purpose.

2.2.2 Elastic Analysis for Flexure

The elastic analysis for flexure of I-sections is well established and prior knowledge of theory supporting this section is assumed, as it is not covered here. The stress distributions due to flexure and shear are generally determined based upon generalized distributions based on basic structural mechanics theories. The internal moment is carried by normal stresses that vary linearly from zero at the elastic neutral axis to a maximum at the extreme fibers of a cross-section. The

shear stress distribution generally follows a pattern where the transverse shear is carried primarily by the web, while offsetting shear stresses occur in the flanges. These stress distributions are developed and superimposed with those obtained through the elastic torsion methods to obtain the maximum normal and shear stresses which are generally restricted to elastic behavior as described below.

2.2.3 Elastic Analysis for Combined Flexure and Torsion

For the elastic analysis of I-shaped steel beams under combined flexure and torsion, generally two sets of stresses are superimposed: (1) normal stresses due to flexure and warping torsion, and (2) shear stresses due to flexure, pure torsion, and warping torsion. The equations used are presented in detail in Chapter 3 with the aid of an example. Determining the cross section that controls design of an open section can be the most challenging part of the analysis, as each stress effect changes along the length of the member according to its loading and support conditions. In addition, each force effect distributes stress differently within a given cross-section. The stress values are typically obtained by solving for the exact solution using graphical design aids such those provided by Seaburg and Carter (1997), and any interactions between normal and shear stresses are assumed to be negligible. This is justified due to the rarity that the maximum shear and normal stresses occur at the same cross-section and location within that cross-section to warrant interaction consideration.

There are alternative design procedures based upon elastic theory as summarized by Driver and Kennedy (1987). Such methods include the flexural analogy, in which the torsion is assumed to be resisted solely by a flange shear force couple, which overestimates the normal stresses. The β-modifier method modifies the flexural analogy to reduce the over-conservatism through the use of a reduction factor based upon the loading, connection, and geometry of the beam; graphical design aids using this method are presented by Lin (1977). The bi-moment method, introduced by Walker (1975), establishes torsion resistance due to bi-moments, which represent the flexural capacity of the flanges; the effects of both flexure and torsion are superimposed without consideration for interaction. Finally, Salmon and Johnson (1980) proposed a simplified analysis that approximated the flange moments as in the flexural analogy, but modifies the warping restraint appropriately for relatively long beams, in which the effect of warping restraint dissipation is considered. Bremault et al. (2008) provide more detail into alternative or modified elastic approaches in the literature review provided in their works.

2.3 Ultimate Strength Analysis

2.3.1 Ultimate Strength of I-shaped Sections Subjected to Torsion

There has been significant research that describes the response to torsion in the inelastic range of behavior; however, a widely accepted and empirically verified method for determining the torsional capacity of I-shapes has proven to be difficult. This is primarily due to the difficulty in describing the warping torsion behavior and large rotation behavior. Although expressions have been proposed for determining the warping displacements of cross-sections, no analytical solutions for the inelastic behavior of warping torsion have been presented to date, as reported by Pi and Trahair (1994b). Some current research is described below in an effort to present the various methods that are used to obtain the ultimate strength of I-sections subjected to torsion. The torsional ultimate strength is later used in the interaction equations for combined flexure and torsion.

General torsion theory includes the sand heap analogy, as developed by Nadai in 1931, which describes the constant shear stress under full yielding, for solid sections, as being equivalent to the slope of a sand heap piled on the cross-section. The rooftop analogy was used by Nadai in 1954 to describe the elastic-plastic torsion of various cross sections including open sections. Elastic-plastic solutions specific to I-sections were also presented by Christopherson (1940); this work is further discussed by Pi and Trahair (1993b, 1994a, 1994b) in their various literature reviews.

The majority of past work describing torsion of thin-walled open sections has been under the assumption of small deformations; the following works consider small deformation assumptions to approximate the warping torsion of I-shaped cantilever beams. Boulton (1962) developed a lower bound theorem of this scenario. Dino and Merchant (1965) proposed the Merchant upper bound as the ultimate capacity for I-shaped cantilever beams. Augusti (1966) verified the Merchant upper bound limit and proposed a method that falls between the upper and lower bounds.

Recently, there has been significant research using the FE method to predict the inelastic torsion capacities of beams; Pi and Trahair (1994b) summarized some of these recent studies, which are not reiterated here. The mitre model, which describes the shear strain distribution over the cross-section, has been used by Billinghurst et al. (1991) to develop an elastic-plastic solution for various cross sections. Chen and Trahair (1993) applied this method in their analytical work

specific to I-sections. Only the recent FE analysis results of Pi and Trahair (1994c) are furthered reviewed below. As mentioned, more information on relevant analytical methods prior to the works discussed here is provided by Pi and Trahair (1994b).

There have been some experimental research results produced for I-shapes subjected to torsion in the inelastic range. However, this information is limited and somewhat dated. Boulton (1962) tested two specimens while allowing warping and observed capacities beyond those predicted by the small rotation theory used for comparison. The specimens attained large rotations, which increases resistance due to what is termed the helix effect (or Wagner effect), as described below. Dino and Gill (1964) also conducted tests to find capacities larger than anticipated, as reported by Pi and Trahair (1995b). Farwell and Galambos (1969) tested five specimens and reported capacities beyond theoretical plastic capacities based on small rotation theory used for comparison. It is important to note that the theoretical capacities were based upon small rotation assumptions, while I-shaped specimens fail at significantly large rotations. Simplifying assumptions in regard to deformation behavior may have significant consequence as shown through the work of Pi and Trahair (1995b).

Pi and Trahair (1995b) compared results of alternate assumptions with regard to torsional behavior. In one analysis, they compared small twist analysis to that of large twist analysis. For the large twist analysis, the effects of Wagner stresses (helix effect) were considered. It is important to note that these assumptions were of little consequence in the elastic range, and did not significantly alter the elastic material behavior approximations, but had significant effects in the inelastic range.

For open thin-walled members, the assumption of small rotation is arguably erroneous, due to the associated low torsional rigidities, which make them susceptible to larger rotations. In general, models that assume small rotations and neglect strain hardening have torsional capacities that reach a limiting torsion value corresponding to torsional plastic collapse mechanism formation; however, the incorporation of large rotation analysis shows significant increases in ultimate capacity at large rotations (Pi and Trahair 1994b), as shown in Figure 6. This resistance is further increased when strain hardening effects are considered, as illustrated in Figure 7. Furthermore, increased resistance due to the formation of what is termed Wagner stresses can significantly increase capacity and alter the failure mode, as discussed by Trahair (1995b).

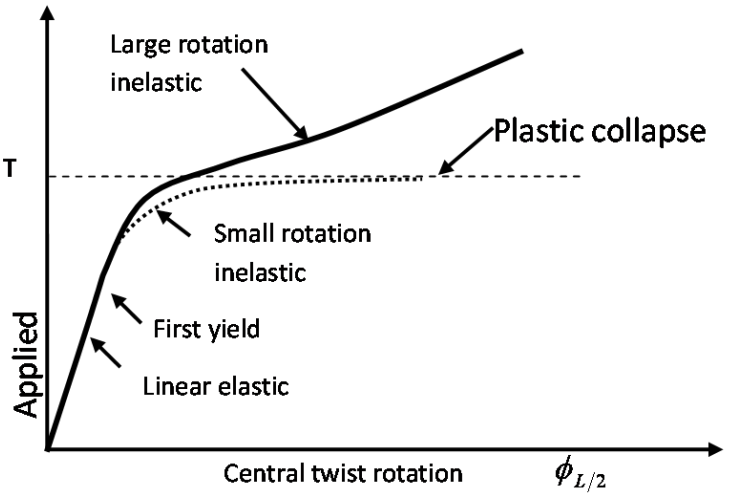

Figure 6 Typical torsion/deformation relationship comparison (Pi and Trahair, 1994b).

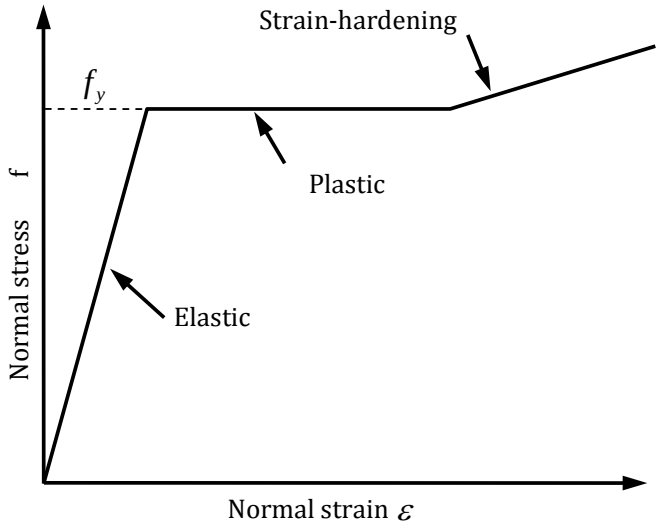

Figure 7 Typical strain/strain relationship used in inelastic modeling (Pi and Trahair, 1994b)

Wagner stresses (helix effect) result from additional longitudinal elongation of a member's flange tip when subjected to torsion as illustrated in Figure 8. These deformations are only significant when relatively large rotations are encountered. The incorporation of Wagner stress alters the behavior of the pure torsion resistance, as described by Pi and Trahair (1994c), resulting in the failure of the cross section before full plastification is reached. It has been shown by the experimental results of Farwell and Galambos (1969) that such a failure is due to the rupture of the flange tips under tensile stress.

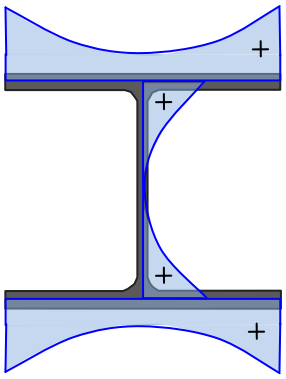

Figure 8 Typical Distribution of Wagner Stresses (Pi and Trahair, 1994b)

Selected research and torsional capacity derivations are discussed below to highlight the development of current understanding.

Dinno and Merchant (1965)

Dinno and Merchant (1965) proposed what is called the Merchant upper bound for the ultimate capacities of cantilever beams, which sums the pure and warping torsion capacities of the support cross-section without considering any interaction, which coined the upper limit connotation; this is shown not to be a true upper bound by Pi and Trahair (1994c) (due to the small rotation assumptions used) who incorporate this method into their torsion capacity approach, as described below. This method proposes that the cross sectional plastic capacity for a cantilever beam, T_p, be determined by:

$$T_p = T_{up} + \frac{M_{fp} h}{L} \tag{2.8}$$

where T_{up} is the pure torsion plastic capacity, which is approximated using the sand heap analogy, as described in the works of Pi and Trahair below. The second term represents the warping torsion plastic capacity of the cross-section, which depends upon the length L of the cantilever and the bi-moment, $M_{fp} h$, where h is the distance between upper and lower flange centroids. M_{fp} represents the flange plastic moment which is given by:

$$M_{fp} = \frac{\sigma_y b_f^2 t_f}{4} \tag{2.9}$$

Driver and Kennedy (1987)

Driver and Kennedy (1987) developed a method for determining the plastic torsion capacity that also sums the individual capacities of pure and warping torsion. These capacities are based upon tests conducted on cantilever beams subjected to combined torsion and bending. These tests showed that the normal tensile stresses in the flange f can reach the ultimate tensile stress. It was also assumed that high compressive strains can be attained without local buckling.

The authors proposed that the pure torsion resistance can be determined using the sand heap analogy as:

$$T_{shu} = \frac{1}{6}\left[4t_f^3 + 6\left(b_f - t_f\right)t_f^2 + 3\left(d - 2t_f\right)t_w^2 + t_w^3\right]\frac{\sigma_u}{\sqrt{3}} \qquad (2.10)$$

which is similar to equation (2.16) below except that here the ultimate tensile stress, σ_u, rather than the yield tensile stress, σ_y, is used as the failure criterion. The warping torsion resistance is given by:

$$T_{wu} = \left[\frac{Kb_f^2 t_f\left(d - t_w\right)}{L}\right]\sigma_u \qquad (2.11)$$

where, again, the ultimate tensile stress is used as the failure criterion. The warping component of torsional resistance under various loading and end conditions can be considered through the use a warping factor K. The value of K depends on the boundary and the loading conditions. For a beam pinned at both ends, when the torque is concentrated at the mid-span, $K = 1$. When the torque is uniformly distributed along the beam, $K = 1/2$. More details about the warping factor for different boundary and loading conditions can be found in (Driver and Kennedy, 1987).

Pi and Trahair (1994a)

Pi and Trahair (1994a) modified the capacities described by Dinno and Merchant (1965) to incorporate other types of structural members, and proposed the use of the upper bound for design. The analytical work of Pi and Trahair (1994a) made an effort to establish the conservatism of this method, which has advantages of computational ease and the fact that it relies on familiar concepts of plastic analysis to obtain the torsional capacity of I-shapes. This method is applicable to any idealized end and loading condition typically found in design. In particular, according to Pi and Trahair, the normalized plastic collapse load factor λ_{tp} equals the sum of two plastic load factors, as follows:

$$\lambda_{tp} = \lambda_{up} + \lambda_{wp} \tag{2.12}$$

where λ_{up} and λ_{wp} are the uniform torsion collapse load factor, and the warping torsion collapse load factor, respectively. These factors are proportional to the applied torsion load $T_{applied}$ as:

$$\lambda_{up} = \frac{T_{applied}}{2T_{up}} \tag{2.13}$$

$$\lambda_{wp} = \frac{T_{applied}}{T_{wp}} \tag{2.14}$$

where T_{wp} is the warping plastic torque. The torsional strength is considered adequate when

$$\lambda_{tp} \leq \phi_t \tag{2.15}$$

where ϕ_t is a performance (resistance) factor for torsion, which is usually taken as 0.9. Each torsional factor is a function of the collapse mechanism required and the respective plastic cross section resistance. The plastic torsion capacity of an I-shaped cross-section is given by:

$$T_{up} = \tau_y \left[b_f t_f^2 \left(1 - \frac{t_f}{3b_f} \right) + \frac{h t_w^2}{2} + \frac{t_w^3}{6} \right] \tag{2.16}$$

where τ_y is the shear yield stress taken as $\sigma_y / \sqrt{3}$ according to the von Mises yield criterion, and b_f and t_f are the width and the thickness of the flanges, respectively, t_w is the web thickness, and h is the clear distance between flanges. Rotational hinges form when a collapse mechanism is reached.

For a torsionally pinned beam with a concentrated torque at midspan, the critical torque associated with torsion plastic collapse caused by warping is given by:

$$T_{wpc} = \frac{4M_{fp}h}{L} \tag{2.17}$$

where M_{fp} is given by equation (2.9). The collapse mechanism is determined using typical flexural plastic collapse methods where the flanges bend laterally. When the location of hinge formation is not obvious, the upper and lower bound analysis approaches of flexural plastic analysis must be incorporated, such as the case for distributed torsional loading.

This method was verified through FE analysis results. The analysis compared small rotation, large rotation without Wagner stresses, and large rotation with Wagner stresses. The case without Wagner stresses assumed that an axial restraint prevented elongation of the member. The analyses results were compared with experimental results obtained from Farwell and Galambos (1969), which showed close agreement with the large rotation model that incorporated Wagner resistance. In addition, the effects of large rotation analysis were compared to small rotation analysis for the bimoments, pure torsion, and strain hardening effects.

2.3.2 Ultimate Strength of I shapes Subjected to Flexure

The methods for determining the ultimate capacity of compact I-shapes with regard to flexural action is well established and not covered in detail here. There are two primary methods that are used in typical flexural design: the first yield design and the plastic design. The first yield approach limits the load-carrying capacity to the level where the maximum Von Mises stress in the beam is the yield stress, which leads to a very conservative and uneconomical design.

The plastic design may be performed for one hinge, or for as many hinges as possible until the structure becomes unstable (Osterrieder and Kretzschmar, 2006). It is most common to use a first hinge approach, where full plastification of a single cross-section represents the ultimate capacity of a member. This method is used to find the resistance of members in LRFD design techniqueswherethe design loads use elastic load analysis techniques. The majority of all work performed to date uses this approach to detemine the ultimate flexural capacity that is incorporated into interaction equations of combined loading design techniques. The ultimate flexural capacity (M_p) is defined as

$$M_p = \sigma_y . Z \tag{2.18}$$

where the plastic section modulus Z for an I-shape section is approximated by the following formula (Megson, T.H.G ,2005)

$$Z = \left[bt_f \left(h - t_f \right) + t_w \left(h - 2t_f \right)^2 / 4 \right] \tag{2.19}$$

When the member is not compact, its flexural resistance is controlled by lateral torsion buckling (LTB). This resistance value is taken as the ultimate flexural resistance. The susceptibility to LTB is related to unbraced length, loading configuration, and cross-sectional properties.

2.3.3 Interaction between Flexure and Torsion

Dinno and Merchant (1965)

Dinno and Merchant (1965) conducted tests on six I-shaped compact beams. The beams were subjected to combined torsion and moment, yet details of the loading methods were given. In this reference, a curve was proposed for considering the combined interaction between flexure, warping torsion, and pure torsion:

$$\left(\frac{M}{M_p}\right)^2+\left(\frac{T}{T_p}\right)^2=1 \qquad (2.20)$$

which extends the work by Hodge (1959) on closed cross-sections. This curve has been shown to be an upper limit on the member's capacity by Augusti (1966). However, it has been revised to consider compact sections not susceptible to LTB effects (Pi and Trahair 1993a, 1994c). When the section is non-compact, LTB effects are present, and the curve has been shown to be unconservative when the modified slenderness increases above 1.0. The modified slenderness is defined in (2.21) by Pi and Trahair (1994c):

$$\lambda=\sqrt{\left(M_{px}/M_{yz}\right)} \qquad (2.21)$$

where M_{px} is the major axis full plastic flexure moment of the cross section, and M_{yz} is the classical elastic flexural torsional buckling moment of a simply supported beam in uniform bending given by Timoshenko and Gere(1961):

$$M_{yz}=\sqrt{\frac{n^2\pi^2EI_y}{L^2}\left(GJ+\frac{n^2\pi^2EI_w}{L^2}\right)} \qquad (2.22)$$

where I_y is the second moment of inertia about the minor axis, I_w is the warping section constant, L is the length of the beam, and n is the number of equally spaced braces. For unbraced beams, $n=1$. For centrally braced beams, $n=2$.

Kollbrunner et al (1978).

Kollbruner et al. (1978) tested a cantilever I-shaped steel beam with a compact section. The section was fixed at one end to prevent warping and was subjected to combined loading through an eccentrically applied load. The ultimate strength of the specimen was defined by limiting the maximum normal strain to five times the yielding strain. The failure criterion is not described. Through this work, a parabolic interaction equation was proposed for the interaction of the plastic

capacity of the flanges of a cross-section with respect to flexure and torsional bi-moments, represented by

$$\left(\frac{M - M_{wp}}{M_{fp}^2} \right)^2 + \frac{B}{B_p} = 1, \qquad (2.23)$$

where B is the flange bimoment, B_p is the plastic flange bi-moment, M_{wp} is the plastic bending moment of the web, and M_{fp} is the plastic bending moment of the flanges. This method assumes normal stress actions are of primary concern, and does not consider shear interaction. Equation (2.23) is applicable to cantilever and fixed-fixed end conditions.

Trahair and Pi (1994c)

Trahair and Pi (1994c) incorporated their analytical work of combined flexure and torsion into a set of comprehensive design methodologies that account for the stability issues of LTB and local buckling for flexural action. The approach was to propose alternate interaction equations and analysis techniques to account for local stability classifications, where the local buckling criterion remained the same as that for pure flexure.

The proposed interaction for Class 1 (compact) beams allows all resistances to be calculated using plastic analysis techniques separately, where the flexural capacity incorporates LTB strength reduction effects typical of flexural analysis. The combination should satisfy the following equation:

$$\lambda_{ip}^2 + \lambda_{tp}^2 \leq \phi^2 \qquad (2.24)$$

where ϕ is the performance factor, and is usually taken as 0.9. The λ_{ip} term in (2.24) represents the plastic collapse load factor for in-plane bending:

$$\lambda_{ip} = \frac{M_{applied}}{M_{ipc}} = \frac{M_{applied}}{Z_x \sigma_y} \qquad (2.25)$$

where $M_{applied}$ is the applied bending moment. M_{ipc} is the critical bending moment, σ_y is the yield normal stress of the material, and Z_x is the plastic section modulus.

The λ_{tp} term in (2.24) is the plastic collapse load factor for torsion, based upon individual resistances of pure and warping torsion resistances as in (2.12).

The interaction equation proposed for Class 2 and 3 sections (noncompact and slender, respectively) is as follows:

$$\left(\frac{M}{\phi M_y}\right)+\left(\frac{T}{\phi T_y}\right)\leq 1 \qquad (2.26)$$

The M and T terms are applied loads from plastic load analysis. The M_y term is the design moment capacity considering LTB effects, and the T_y term is the torsional capacity. For Class 2 sections, T_y is computed based on a first yield elastic analysis. For Class 3 sections, T_y is computed based on a local buckling analysis for Class 3 sections. The particular local buckling procedures for torsion are not given, and little work has been done in this area; however, it is rare that a Class 3 (slender) section will be selected for flexural action, making the lack of attention appropriate.

The moment vs. torsion values at failure are compared to the proposed interaction equation of Dinno and Merchant (1965), discussed previously. Pi and Trahair (1994c) found that the Dinno and Merchant interaction does not account for LTB effects adequately, and provided an alternative expression applicable to combined bending and free torsion, which considers LTB effects for cases with slenderness ratios up to 1.41; the interaction depends upon bracing conditions and is given by

$$\left(\frac{PL}{4M_{bx}}\right)^{\gamma_x}+\left(\frac{Pe}{2T_p}\right)^{\gamma_z}=1 \qquad (2.27)$$

where P is the concentrated force load, e is the eccentricity of with respect to the shear center of the section. The γ_x and γ_z terms depend upon the bracing configuration where $\gamma_x = 2.0$ and $\gamma_z = 1.0$ for continuously braced beams, and $\gamma_x = 1.0$ and $\gamma_z = 1.0$ for centrally braced and unbraced beams. The M_{bx} term represents the flexural-torsional buckling strength of the member given by $M_{bx} = \alpha_m \alpha_s M_p \leq M_p$, where the α_m and α_s terms represent a moment modification factor and slenderness reduction factor, respectively. T_p is the maximum internal torque at plastic collapse.

Driver and Kennedy (1987)

Driver and Kennedy (1987) performed tests on four cantilever sections loaded in combined flexure and torsion. For each case, while the flexural action was kept approximately constant with a

vertical load in the same direction, the eccentricity of the applied load was increased from case 1 to 4, thereby increasing torsion. The lengths and sections were selected with the intent of minimizing the lateral torsional buckling effects, while making the effects of both warping and pure torsional resistances significant.

Based on the failure points and corresponding strains, an interaction diagram was proposed, as shown in Figure 9. The points on the interaction diagram are described as follows:

Point E: Represents the plastic capacity of the cross-section under pure flexure;

Point F: Torsional capacity, which equals the sum of sand heap torsion plus warping torsion (ultimate);

Point G: Torsional capacity vs. plastic capacity of the web;

Point H: Sand heap torsion vs. plastic capacity of the cross-section.

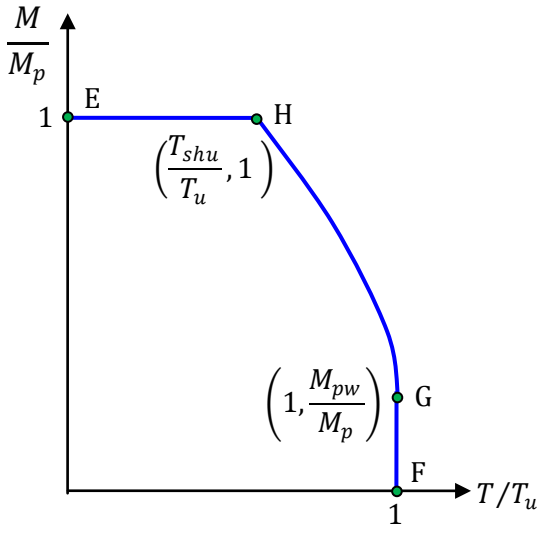

Figure 9 Interaction diagram proposed by Driver and Kennedy (1987).

Due to local stability effects, the plastic capacity of the cross-section for flexure is obtained using the yielding criteria. The torsional capacity is obtained using the ultimate torsional strength as failure criteria. The end conditions of the member are addressed in the computation of the warping resistance. When the flanges are carrying both bending normal stresses and warping normal stress, the interaction is described by a parabolic curve extending from its vertex at G to H.

Driver and Kennedy (1987) also proposed an interaction diagram for class 3 beams, which can reach the yield moment M_y before local buckling occurs. This interaction diagram is shown in Figure 10. The torsional capacity is also obtained using yielding as the failure criteria. The interaction between flexure and torsion is accounted for by simply joining points G and H using a straight line.

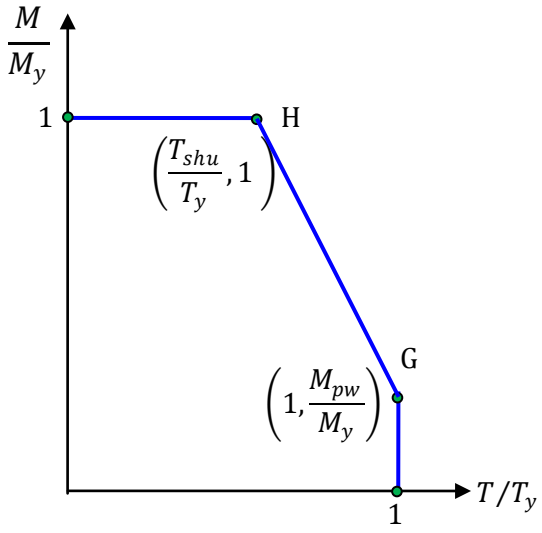

Figure 10 Interaction diagram by Razzaq and Galambos (1979)

The interaction diagrams by Driver and Kennedy (1987) can be used in a design methodology that incorporates lateral torsional buckling. However, this method has recently been considered unconservative by Estabrooks and Grondin (2008) and Bremault et al. (2008).

2.4 Finite Element Analysis of Combined Flexure and Torsion

Empirical flexure and torsion interaction information is traditionally obtained through costly and time-consuming full scale testing. Recently, finite element analysis has proved to be beneficial,

and can reduce the experimental results needed for understanding interactions. In the following sections, recent advances in FE modeling techniques in the areas of combined action are reviewed.

Finite Element Models Presented in Bremault et. al. (2008)

The following theoretical (not used to approximate empirical results) finite element models have been summarized and referenced by Bremault et al. (2008):

Bathe and Wiener (1983) modeled fixed-end cantilever I-sections that included warping effects. Kanok-Nukulchai and Sivakumar (1988) modeled several cases of pure torsion and combined flexure and torsion using a degeneration process (developing finite elements from 3D equations) in which warping was allowed. Bild et al.(1992) developed a model similar to the formulations of Hancock and Trahair (1978) for simply supported beams with an eccentrically applied load at mid-span; the model can approximate effects of nonlinear material properties, buckling, initial imperfections, residual stresses, and nonlinear geometric effects in the transverse direction (but not in the rotational direction).

Driver (2000) produced models of the test specimens used in his earlier empirical work (Driver and Kennedy 1987) using 3D brick elements with non-linear material and geometric properties. The fillets were also modeled to take into consideration their effect in increasing pure torsional resistance, as described by Driver and Kennedy (1987). The material model was isotropic elastic-strain hardening, and used the von Mises yield criterion to model stress interaction. An approximate residual stress was considered in two cases. The third case did not consider residual stress effects. The FEM results agreed well with testing data. It was also found that residual stress distribution had little effect on overall results. Furthermore, the cross-section was able to achieve stresses beyond those of yielding.

Pi and Trahair(1993a,1994c)

Pi and Trahair (1993a, 1994c) used FEM analysis to investigate the behavior of I-shaped beams under combined loadings, while considering the LTB slenderness pertaining to flexural effects. A non-linear (large rotation) inelastic (non-linear constitutive relationship) finite element analysis approach was used. This approach is considered to be more accurate than the traditional approach of linear (small rotation assumptions) inelastic models for combined action of flexure and torsion. The latter approach generally overestimates the resistance when the primary behavior is

flexural, and underestimates the resistance when the primary action is torsion (Pi and Trahair 1994c).

The effects of strain hardening, typical residual stress distribution, and initial imperfections were considered. Residual stress assumptions are as shown in . Initial imperfections included crookedness and initial rotations. For each of the three bracing configurations analyzed, three sets of analyses with different lateral torsional buckling slenderness values of 0.5, 1.0, and 1.41 were investigated. For each of the nine scenarios analyzed, the eccentricity of the applied load was varied from pure flexure to torsion-dominant cases for each configuration. It was found that the maximum bending moment and the maximum torque are related to the slenderness of the beam. It was also found that bracing can affect the interaction between flexure, torsion, and flexural torsional buckling.

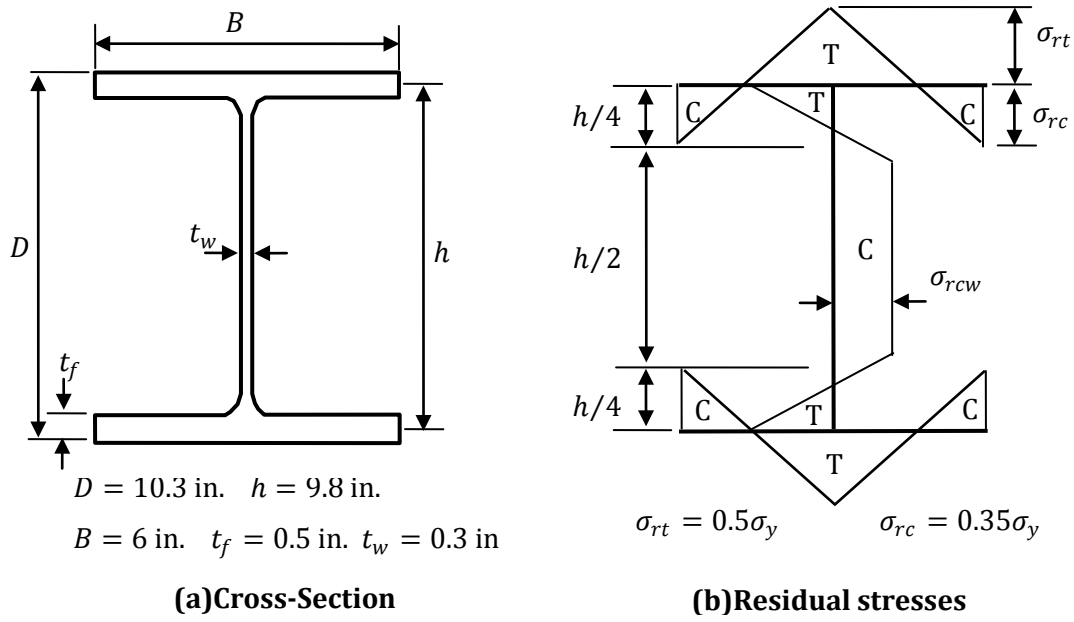

Figure 11 Cross-section and residual stress distribution, Pi and Trahair (1994c).

Estabrooks and Grondin (2008)

Estabrooks and Grondin (2008) performed experimental tests on six specimens with idealized boundary conditions in an attempt to produce lower bound resistances; the idealized end

condition attempted to provide pinned action for both flexure and torsion. These idealized conditions also provided ideal means for validating empirical results using finite element models that employed the same boundary conditions

The models were developed using ABAQUS software, where the SR4 shell element was used. A mesh refinement study was performed to reduce dependence upon mesh size and computational effort; the three meshes considered are shown in Figure 12. An intermediate mesh size, containing 960 elements was selected based upon its convergence (within 0.8%) to the finest mesh used.

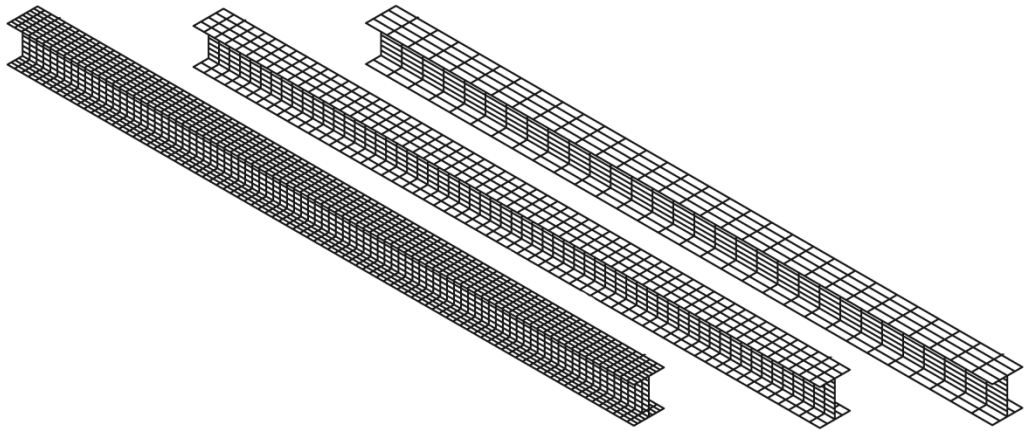

Figure 12 Mesh study in Estabrooks and Grondin (2008)

The model incorporated assumptions such as elastic-plastic strain hardening constitutive behavior, residual stress, and initial imperfections. In particular, the constitutive behavior was modeled to approximate the coupon tests of the steel used in the experimental work. The residual stress of the hot rolled I-shape was approximated with a certain temperature gradient and the resulting stress distribution. The initial imperfection was assumed to be a sin wave with amplitude of l/500, which closely resembled the measurements taken of the test specimens. Initial imperfections of the flanges being non-parallel, as measured in the test specimens, were also included in the model development.

As compared to empirical findings, the FE model produced from errors ranging from 2 - 26% compared to the empirical results. The FE model produced a “softer” mid-span moment ratio vs. mid-span deflection response, with a more gradual transition to the plateau region; the difference in slope ranged from 0.4 - 8%. Meanwhile, the FE model produced a “stiffer” mid-span torsion ratio vs. mid-span rotation response, with a more abrupt transition to the plateau region.

The sensitivity to material strength was also investigated. It was found that a 16.8% increase in yield strength produced a 9.9% increase in overall torsional capacity.

The impact to the maximum moment (mid-span) ratios vs. mid-span deflection and maximum torsion (mid-span) ratios vs. mid-span rotation due to the sensitivity parameters was also investigated. The sensitivity study showed that the end condition assumptions were the most likely sources of the discrepancies observed between the empirical and FE model results.

Bremault, Driver, and Grondin (2008)

Bremault al. (2008) produced finite element models which were developed through validation of the empirical results of Driver and Kennedy (1987). Then, these modeling techniques were extended for use in parametric studies of combined loading cases. In total, 180 different cases were analyzed in ABAQUS with varying cross-sections, boundary conditions, beam slenderness loading conditions, and the moment-torsion ratio.

As in the experimental test, the FE combined flexure and torsion load was produced by an eccentric concentrated force acting on a loading bracket. For example, the following figure shows the mesh and loading bracket of the finite element model for beam 3 in (Driver and Kennedy, 1987)

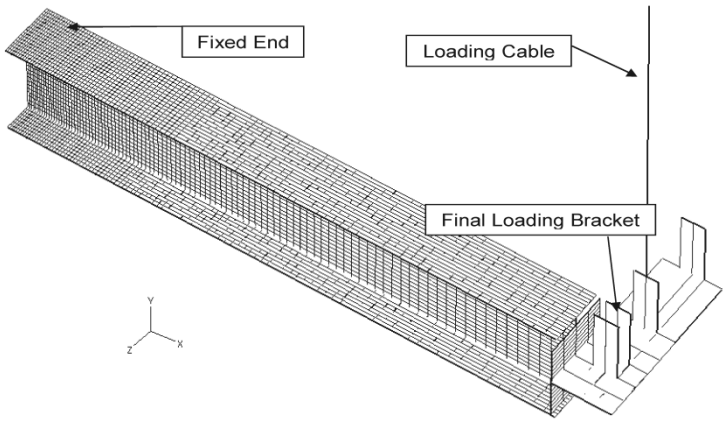

Figure 13 FEM model for beam 3 in (Driver and Kennedy, 1987)

Similar to(Estabrooks and Grondin, 2008), the S4R shell element was selected. Meshing size was reduced in areas where large strains were expected in order to observe local buckling and yielding, such as the area close to the fixed end of the cantilever beam in Figure 13.

A mesh refinement study was performed with three different mesh configurations, utilizing 1300, 5400, and 11700 nodes, respectively, in order to ensure the convergence of solutions. The

difference between the initial mesh size (1300 nodes) and the first alternative mesh size was fairly significant. However, further decrease of mesh size to the second alternative mesh size (11700 nodes) caused negligible difference in results; therefore, the first alternative mesh, consisting of 5400 nodes, was selected based upon the meshing trials to optimize solution efficiency.

The material and geometric behavior was modeled as non-linear. In particular, the geometric non-linearity (large rotation) effects were modeled using the geometric nonlinearity option of ABAQUS, which enables the consideration of alternate load paths (instability due to bifurcation) caused by buckling, allowing the FE model to better predict the beam's post-yielding and post-buckling behavior.

The cases of combined flexure and torsion loading (E1, E2, and E3) in Bremault et al. (2008) showed a variation in behavior, with some specimens yielding due to warping hinges and others yielding due to flexural hinges. It is difficult to distinctly qualify the occurrence of each, as exceptions were encountered. In general, the lower eccentricities (E1) caused flexural response to control while the large eccentricity (E3) caused torsional response to control. These effects were highly dependent upon the boundary conditions used. Especially, for simply supported beams, the hinge formation determined the collapse mechanism, hence had a strong influence on the beams' behavior.

2.5 AISC Design Provisions

In the (AISC, 2010), the design of I-shaped beams is categorized as Non-HSS members with other shapes. The interaction of the combined effects of the required strengths (torsion, bending moment, shear force, and/or axial force) must satisfy the requirement of AISC Specification Section H3, which states :the design torsional strength, $\phi_T F_n$ and the allowable torsional strength, F_n / Ω_T, for non-HSS members shall be the lowest value obtained according to the limit states of yielding under normal stress, shear yielding under shear stress, or buckling, determined as follows:

$$\phi_T = 0.90 \ (LRFD) \quad \Omega_T = 1.67 \ (ASD) \tag{2.28}$$

For the limit state of yielding under normal stress:

$$F_n = F_y \tag{2.29}$$

For the limit sate of shear yielding under shear stress:

$$F_n = 0.6F_y \tag{2.30}$$

For the limit state of buckling:

$$F_n = F_{cr} \tag{2.31}$$

where F_{cr} =buckling stress for the section as determined by analysis.

The required stresses can be computed by elastic stress analysis using theories of structural mechanics. According to the AISC design code, it is usually sufficient to consider normal stresses and shear stresses separately, because maximum values rarely occur in the same place in the cross section or at the same place in the span, AISC (2010). The reader may refer to AISC (2010) for more details regarding the I-shaped section. Summary

In this chapter, previous theoretical results and design methods for beams subject to combined flexure and torsion awere reviewed. Although considerable empirical and analytical research have been conducted in this area, the empirical study is still incomplete, and the various design methods addressing the interaction between flexure and torsion in the plastic phase remain to be studied. FEM is a powerful tool for performing more complete parametric studies regarding parameters affecting the behavior and ultimate strength of beam members, and good agreement between FEM results and empirical results have been achieved. The current AISC design provisions were also reviewed.

Chapter 3 Finite Element Model Development and Verification

3.1. Overview

As stated in the previous chapters, FEM is the main tool in this effort used to study the behavior as well as to determine the load capacity of the I-shaped beams subject to combined flexural and torsional loading. Hence, it is important to ensure that the modeling techniques can produce reasonably accurate results. The validity of a more comprehensive investigation can be justified only if a close agreement can be achieved between FEM model simulation results and other reliable results provided in previous research, which include theoretical predictions, experimental results, and FEM results.

In this Chapter, an FE model created for the purpose of verification is described. The loading process can often be divided into two stages—the elastic stage and the inelastic stage, and the structure exhibited different behavior in each stage. Correspondingly, the main objective of for the verification were two-fold: the first was to verify the elastic response of the FE model using theoretical results for elastic response, which have been well-established. The second objective was to verify the inelastic response of the FE model using physical experiment results and FEM results presented in (Estabrooks and Grondin, 2008).

This chapter is organized as follows: the elastic analysis theory is introduced, the modeling information is described, the elastic response of the beam is analyzed theoretically, and then verification the elastic response of the FE model is described. Next the theory for inelastic analysis is introduced, and the inelastic response analysis of a beam subject to different types of loads is described. The inelastic response is verified using experimental results and FEM results from previous research. Finally, this chapter is concluded with a brief summary.

3.1. Elastic Response

An I-shaped steel beam in the interstate 59 bridge is considered for the verification of elastic response. In the following section, the theory for the elastic response is first introduced, then the details of the model are described, and then simulated elastic response is verified using theoretical results.

3.1.1. Theoretical Analysis of Elastic Response

For elastic analysis, the combined stress is calculated by adding the elastic stresses obtained for flexure and torsion using the principle of superposition. The theories regarding the flexural behavior and the torsional behavior, which includes both pure torsion and warping torsion behaviors, are introduced in this section. In particular, the magnitude and the location of the maximum normal stress and maximum shear stress, which can be computed as described below are of interest:

3.1.1.1 Flexural behavior

Henceforth, a global coordinate x-y-z is used with the x axis perpendicular to the web of the beam, the y axis in the vertical direction, and the z axis perpendicular to the x-y plane. The flexural moment vector lies in the cross section of the beam, as shown in Figure 14. For the I-59 beam considered in this research, the flexural moment M is directed along the x direction only, i.e., $M_y = 0$.

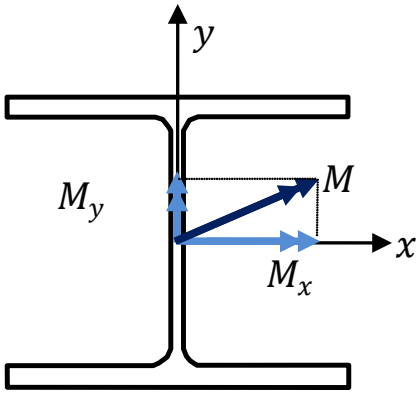

Figure 14 Flexure moment in the cross section

The normal stress due to flexure is given by

$$\sigma_b = \frac{M_x y}{I_x} - \frac{M_y x}{I_y} = \frac{M_x y}{I_x} \tag{3.1}$$

where

σ_b = the normal stress caused by the flexural effect, ksi.

M = flexure moment about either the x or y axis, $kip - in$, and

I = the area moment of inertia, I_x or I_y, in^4.

For the loading condition considered, the maximum σ_b occurs at mid-span, where the moments in each direction are maximum. This maximum moment value can be computed as:

$$(M_x)_{\max} = \frac{qL^2}{8} + \frac{P_y L}{4} = \frac{qL^2}{8} + \frac{PL}{4} \qquad (3.2)$$

Where

S_x = elastic section modulus, in^3. $S_x = \frac{I_x}{y}$

q = uniform distributed load, lb/in.

P = a concentrated load at midspan, lb, and

P_y = a concentrated load along Y axis, lb

L = the length of the steel beam or bridge, in.

Therefore, we have $(\sigma_b)_{\max} = \frac{qL^2/8 + PL/4}{S_x}$

The distribution of the bending stress, σ_b , across the I-shaped beam section is shown in Figure 15.

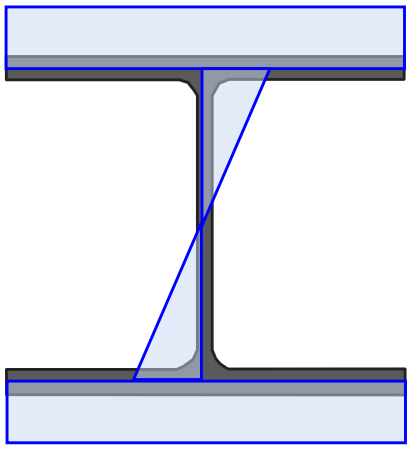

Figure 15 σ_b distribution.

The shear stress due to flexure is given by the following expression

$$\tau_b = \frac{-V_x \int_0^s xtds}{tI_y} + \frac{-V_y \int_0^s ytds}{tI_x} \tag{3.3}$$

where

τ_b = the shear stress caused by the flexural effect, ksi ,

V = shear force acting parallel to the x or y axis through the shear center S, lb.

t = the thickness of the web or the flange, in, and

s = curvilinear coordinate system along the middle surface of the cross sectional elements.

The maximum V_x and V_y forces for the I-59 beam at the mid-span are given by

$\left(V_y\right)_{\max} = \frac{P}{2}$ and $\left(V_x\right)_{\max} = 0$ Hence, the distribution of τ_b follows the distribution of $\int_0^s ytds$, and is shown in Figure 16.

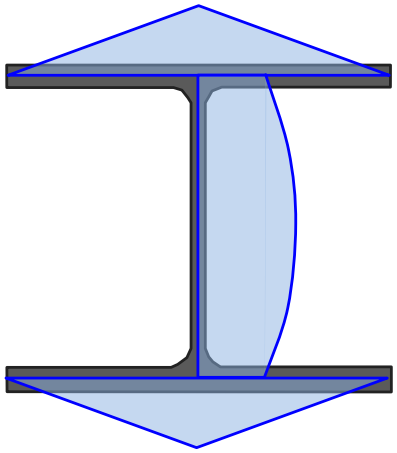

Figure 16 τ_b distribution

In the above figure, the maximum shear stress value in the flange is given by

$$(\tau_{bf})_{\max} = \frac{\frac{P}{2} \cdot \frac{hb_f t_f}{4}}{t_f I_x} \tag{3.4}$$

where

$(\tau_{bf})_{\max}$ = the maximum value of shear stress in the flanges, ksi ,

t_f = the thickness of the flange, in ,

b_f = the width of the flange, in , and

h = the distance between the centroids of both flanges, in .

t_w = the thickness of the web, in .

3.1.1.2 Pure torsion behavior

The shear stress caused by pure torsion, or the St. Venant shear, is expressed as:

$$\tau_{sv} = Gt\theta' \tag{3.5}$$

where

τ_{sv} = shear stress caused by St. Venant shear, ksi ,

G = shear modulus of rigidity of steel, 11200 ksi ,

t = the thickness of investigated beam, and

θ' = rate of change of angle of rotation θ , i.e., the first derivative of θ with respect to z . When the beam is subject to a concentrated torque load located at z , the twist angle θ is given by

$$\theta = \begin{cases} \dfrac{Tl}{GJ}\left[(1-\alpha)\dfrac{z}{l} + \dfrac{a}{l}\left(\dfrac{\sinh\dfrac{\alpha l}{a}}{\tanh\dfrac{l}{a}} - \cosh\dfrac{\alpha l}{a}\right)\times\sinh\dfrac{z}{a}\right], & 0 \le z \le \alpha l, \\ \dfrac{Tl}{GJ}\left[(1-z)\dfrac{\alpha}{l} + \dfrac{a}{l}\left(\dfrac{\sinh\dfrac{\alpha l}{a}}{\tanh\dfrac{l}{a}}\times\sinh\dfrac{z}{a} - \sinh\dfrac{\alpha l}{a}\times\cosh\dfrac{z}{a}\right)\right], & \alpha l \le z \le l. \end{cases} \tag{3.6}$$

where a is the torsional resistance given by $a = \sqrt{\dfrac{EC_w}{GJ}}$, E is Young's modulus, C_w is the wraping constant of the cross-section (in.^{4}), and J is the torsional constant of the cross section (in.^{4}). When the beam is subject to a uniformly distributed torque load,

$$\theta = \frac{t_q a^2}{GJ}\left[\frac{l^2}{2a^2}\left(\frac{z}{l}-\frac{z^2}{l^2}\right)+\cosh\frac{z}{a}-\tanh\frac{l}{2a}\times\sinh\frac{z}{a}-1\right] \tag{3.7}$$

where t_q is the distributed torque (kip-in./in.).

The distribution of St. Venant shear stress corresponds to the distribution of θ' given the fact that G and t are constants. The location of maximum θ' varies according to different boundary condition and load cases in general. The maximum St. Venant shear stress $(\tau_{sv})_{\max}$ occurs at the end of the beam because θ' achieves its maximum value when $z = 0$ for simple supported boundary conditions The values are different on the flanges from those on the web since the thicknesses of those two plates differ. The maximum shear stress in the flanges due to pure torsion is given by

$$(\tau_{svf})_{\max} = Gt_f\left|\theta'(0)\right| \tag{3.8}$$

where

$(\tau_{svf})_{\max}$ =the maximum shear stress in the flange, ksi.

For webs:

$$(\tau_{svw})_{\max} = Gt_w\left|\theta'(0)\right| \tag{3.9}$$

where

$(\tau_{svw})_{\max}$ = the maximum shear stress in the web due to pure torsion, ksi.

Note that $\tau_{sv}(L/2) = 0$ because $\theta'(L/2) = 0$ for the present loading condition

3.1.1.3 Warping torsion behavior

For a cross section subject to pure torsion, the normal stress due to the warping effect is given by:

$$\sigma_w = E\omega_n\theta'' \tag{3.10}$$

where

E = the modulus of elasticity of steel, ksi,

ω_n = the normalized unit warping of the cross section, in.^{2}

$\theta''(z)$ = the second derivative of the angle of twist with respect to the distance along the length of the beam.

For the present loading condition, the maximum warping normal stress $(\sigma_w)_{\max}$ occurs at the mid-span at the flange tips, and is given by the following expression

$$(\sigma_w)_{\max} = E(\omega_n)_{\max}\left|\theta''\left(\frac{L}{2}\right)\right| \tag{3.11}$$

The warping normal stress σ_w follows the distribution of ω_n as shown in Figure 17.

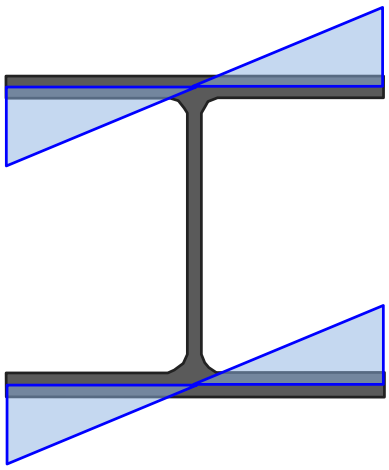

Figure 17 σ_w distribution

The warping shear stress is given by

$$\tau_w = \frac{-ES_w\theta'''}{t} \tag{3.12}$$

where

$\theta'''(z)$ = the third derivative of the twist angle with respect to the beam length,

S_w is the warping static moment, in^4 ,which is given by

$$S_w = \int_0^s \omega_n t ds$$

The maximum warping shear stress $(\tau_w)_{\max}$ occurs at the mid-span at the mid-width of the flange. τ_w conforms to the distribution of S_w, and is shown in the figure below.

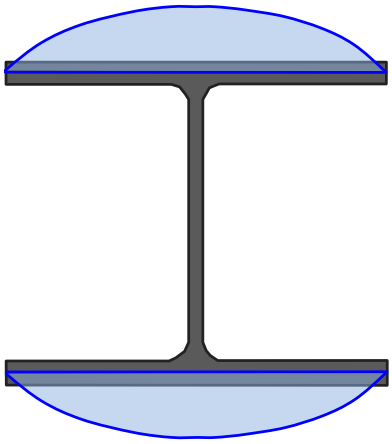

Figure 18 τ_w distribution

The maximum warping shear stress at the end of the beam is given by

$$(\tau_w)_{\max} = \frac{E(S_w)_{\max}\left|\theta'''(0)\right|}{t_f} \tag{3.13}$$

The maximum warping shear stress at the mid-span of the beam can be computed by

$$(\tau_w)_{\max} = \frac{E(S_w)_{\max}\left|\theta'''(L/2)\right|}{t_f} \tag{3.14}$$

The total normal stress is computed as a summation of all normal stresses computed previously as:

$$\sigma = \frac{P_z}{A} + \frac{M_x y}{I_x} - \frac{M_y x}{I_y} + E\omega_n\phi'' \tag{3.15}$$

where

A = the area of cross section, in.^{2}.

The normal stress at the mid-span ($z = L/2$) is given by

$$\sigma_{bx} + \sigma_w = \frac{M_x y}{I_x} + E\omega_n \left|\theta''\right| \tag{3.16}$$

Similarly, the total shear stress is computed by the following expression

$$\tau = \frac{-V_y \int_0^s ytds}{tI_x} - \frac{ES_w\theta''}{t} + Gt\theta' \qquad 1 \tag{3.17}$$

3.1.1.4 Summary of elastic stresses due to flexure and torsion

The stress in the cross-section subject to combined bending and torsion is computed by adding the stresses caused by flexure, pure torsion, and warping, based on the principle of superposition. Specifically, on the flanges at the mid-span, the flexural normal stress is given by

$$\sigma_f = \frac{wl^2/8 + Pl/4}{S_x} \tag{3.18}$$

and the warping normal stress is

$$\sigma_w = E(\omega_n)_{\max} \left|\theta''\left(\frac{L}{2}\right)\right| \tag{3.19}$$

Hence, the maximum normal stress is given by the superposition of σ_b and σ_w:

$$\sigma = \sigma_w + \sigma_f = E(\omega_n)_{\max} \left|\theta''\left(\frac{L}{2}\right)\right| + \frac{wl^2/8 + Pl/4}{S_x} \tag{3.20}$$

The maximum flexure-induced shear stress on the flanges at the mid-span is given by (3.4), and the maximum flexure-induced shear stress on the web at mid-span is

$$(\tau_{bw})_{\max} = \frac{\frac{P_y}{2} \times \left(\frac{hb_f t_f}{4} + \frac{t_w h^2}{8}\right)}{t_w I_x} \tag{3.21}$$

The warping-related shear stress on the flanges at the mid-span is given by

$$(\tau_w)_{\max} = \frac{E(S_w)_{\max} \left|\theta'''\left(\frac{L}{2}\right)\right|}{t_f} \tag{3.22}$$

The shear stress on the web caused by the warping effect is negligible. Hence the maximum shear stress on the flanges is

$$(\tau_f)_{\max} = (\tau_{bf})_{\max} + (\tau_w)_{\max} = \frac{\frac{P_y}{2} \times \frac{hb_f t_f}{4}}{t_f I_x} + \frac{E(S_w)_{\max} \left| \theta'''\left(\frac{L}{2}\right) \right|}{t_f} \qquad (3.23)$$

and the maximum shear stress on the web is $(\tau_w)_{\max}$.

3.1.2. Elastic Model Information

The I-59 beam finite element model shares the same geometry information as a bridge on Interstate 59, which is an interstate highway connecting Birmingham, Alabama to Chattanooga, Tennessee and New Orleans, Louisiana. The total length of the beam is 658 in, and its cross section is that of an I-shape 36×150. The beam is simply supported at two ends, as shown in Figure 19.

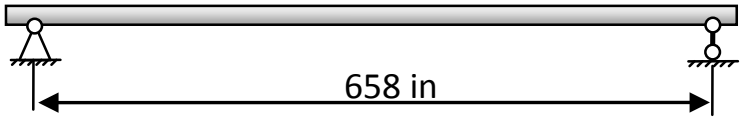

Figure 19 Simply supported I-59 bridge beam

3.1.3. Loading Condition

The applied load on the I-59 beam consists of two components; one is the distributed load caused by the self weight of the deck slab and the self weight of the temporary, and the other one is a concentrated force which corresponds to the maximum live load induced by an HS-20 truck. By the principal of superposition for elastic analysis, the response of the beam to these two types of loads is considered separately, and the results are added together to obtain the overall response to the combination of these two types of loads.

In the elastic analysis of the I-59 beam, two loading cases are considered with the torsion introduced into the model via different means as shown in Figure 20. In the first case, in order to avoid the load concentration on the upper flange of the beam, two pairs of concentrated forces are applied at the ends of a loading bracket at the mid-span to produce the combined flexure and torsion caused by the truck. In particular, P_1=P_2=-10 lbf, T1=T2= 0.679 lbf. In the second case, the torsion is generated by a uniform pressure load of 0.02 psi on half of the upper surface of the top

flange over the whole length of the beam. These loads were calculated from dead and live bridge loads according to the AASHTO LRFD Bridge Design Specifications (AASHTO 2010).

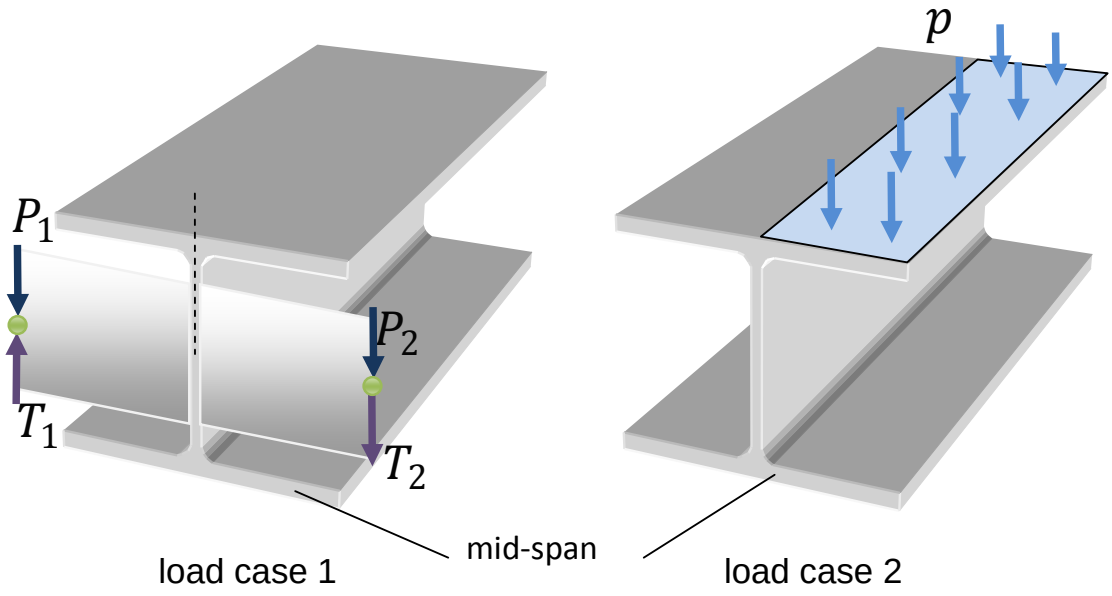

Figure 20 I-59 Loading cases

3.1.4. Material Model

For the elastic analysis of I-59 beam, only two properties of the steel material need to be specified: the young's modulus is set as 29000 ksi, and the Poisson's ratio is chosen as 0.3.

3.1.5. I-59 Beam Model Mesh

The I-59 bridge beam was modeled using a very fine mesh with 18000 S4R shell elements for the beam and the loading bracket together. The aspect ratio of the mesh is approximately 1. For each cross-section, there are 8 elements across the flanges and 24 elements in the web. The final mesh of the beam is shown in Figure 21.

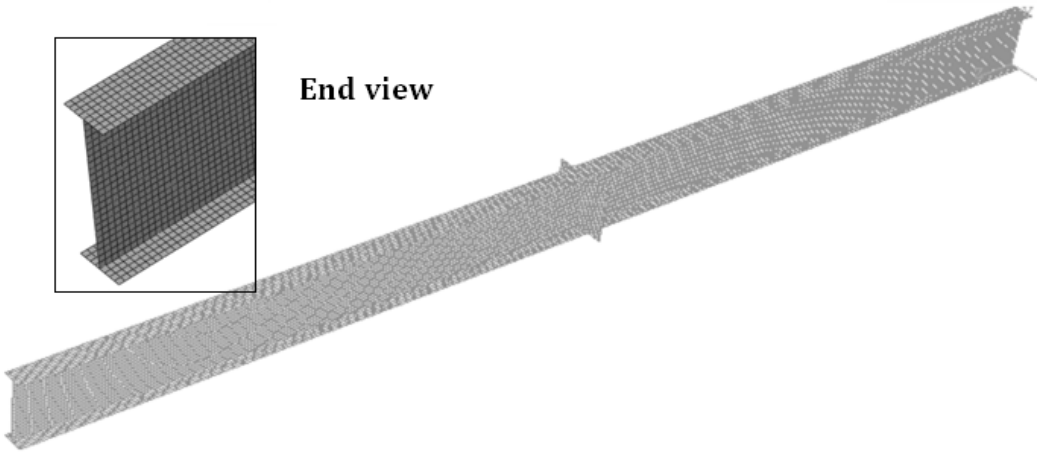

Figure 21 I-59 Beam finite element model

3.1.6. Element Properties

The S4R elements were used in the FEM study of Estabrooks and Grodin (2008) and Bremault, et al. (2008). This shell element is a four-node, doubly curved shell element that accounts for finite membrane strains and allows for changes in element thickness. It has six degree of freedom at each node including three translation components and three rotation components.

According to (Bremault et al. 2008), the S4R element is able to perform under a wide range of conditions without failure, and is in general accurate enough as long as an appropriate mesh is used. Furthermore, the accuracy of the S4R element is also verified by FEM simulation models in this research. It was found that the difference between the S4R and S4 element in terms of both elastic and inelastic response was negligible for the large mesh sizes in this study. Hence, throughout this thesis, the S4R element is used in all models to increase the efficiency of the computation.

3.1.7. Boundary Conditions

In this study, simple support boundary conditions were considered for all beam models, as shown in Figure 22. The four end points of the two intersection lines between the web and the flanges were pinned in the lateral direction (X direction). The center of the whole beam was restrained from any movement along the axis of the beam (Z direction). The centroid of the beam sections at the two ends were fixed to prevent any movement in the vertical direction (Y direction). No lateral bracing was applied. Similar boundary conditions have been used in other research on I-shaped section beams such as (Estabrooks and Grondin, 2008).

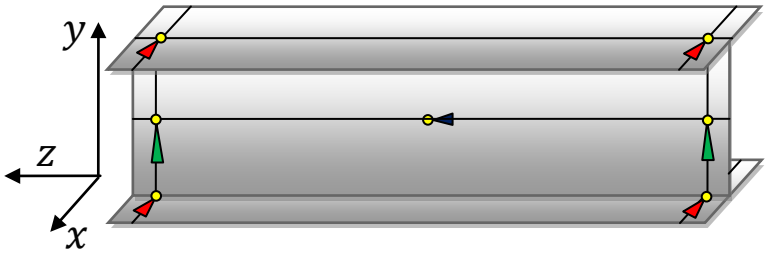

Figure 22 Simple support boundary conditions

3.1.8. FEM Analysis

The I-59 beam FE models were analyzed with ABAQUS's general static analysis using the Newton's method, which is a numerical technique for solving equilibrium equations.

3.1.9. Verification of Model Results

The deformation plots of the I-59 beam for the two loading cases are shown Figure 23 and Figure 24, respectively. The theoretical results for these two loading cases are calculated using the method introduced in Section 3.1.1. For long beams such as the I-59 beam subject to a mid-span concentrated load or pressure load, the normal stress asociated with the flexural moment at the mid-span is critical, hence, a comparison was made for the critical section for normal stress only.

Ideally, such a comparison should be made for the normal stress at the mid-span. However, because the loading bracket was introduced to avoide local stress concentration and web distortion, the critical section in the FE model deviates from the mid-span. Therefore, the comparison is made for a section with one inch offset from the midspan, and the theoretical results were computed for the same section for the comparison.

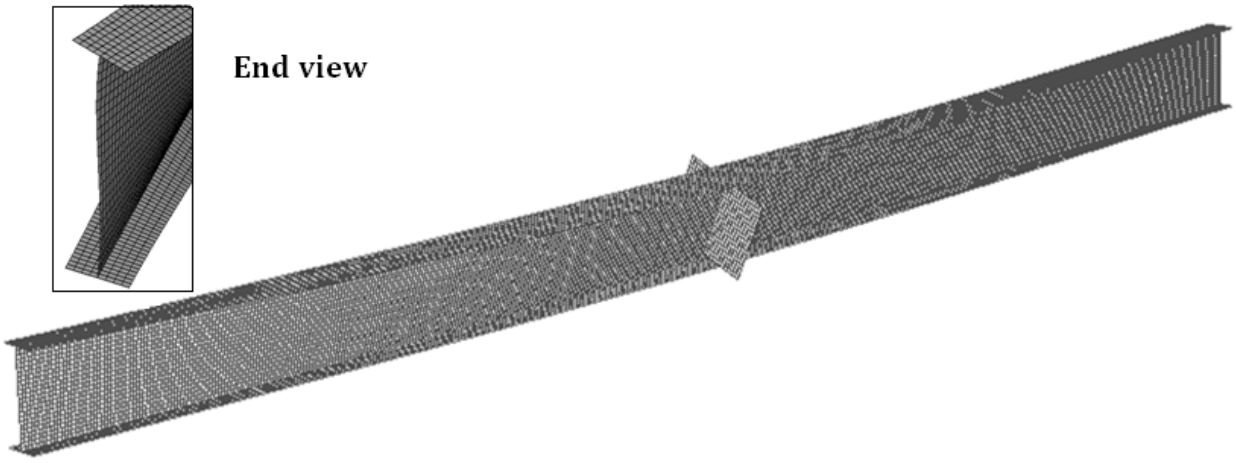

Figure 23 I-59 model deformation concentrated load

The normal stress at the critical section of the FEM results were compared with the theoretical values, as illustrated by Figure 25 and Figure 26. In these figures, the green, blue, and red lines represent the theoretical normal stress results on the top flange, web, and bottom flange respectively. The green, blue, and red circles correspond to the FEM normal stress results at the integration points of the element at the same location on the beam section. As shown in these figures, the FE results matched the theoretical predictions quite well.

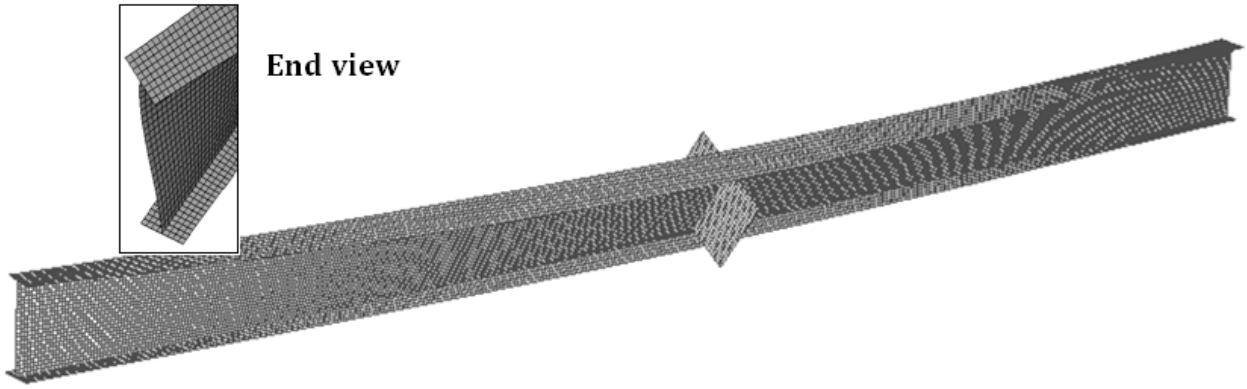

Figure 24 I-59 model deformation, pressure load

The details of the FEM and theoretical results comparison are listed in Table 1 to Table 6. In these tables, the stress values are extracted at the centroid of the elements. The relative error for elements on the upper flange is computed by dividing the difference between the FEM and theoretical results by the maximum stress on the flange as predicted by elastic analysis. One reason for computing the error in such a way is that the theoretically-predicted normal stress at the centroid of the section is zero, in which case the standard definition of the relative error does not work. The relative errors for elements on the other parts of the section are defined in a similar manner.

For case 1, the maximum relative errors of the FEM results occurat the flange elements with largest stress (both positive and negative). For case 2, the maximum errors occur at the top elements on the web. Overall, the FEM results provided a good approximation to the theoretical solution.

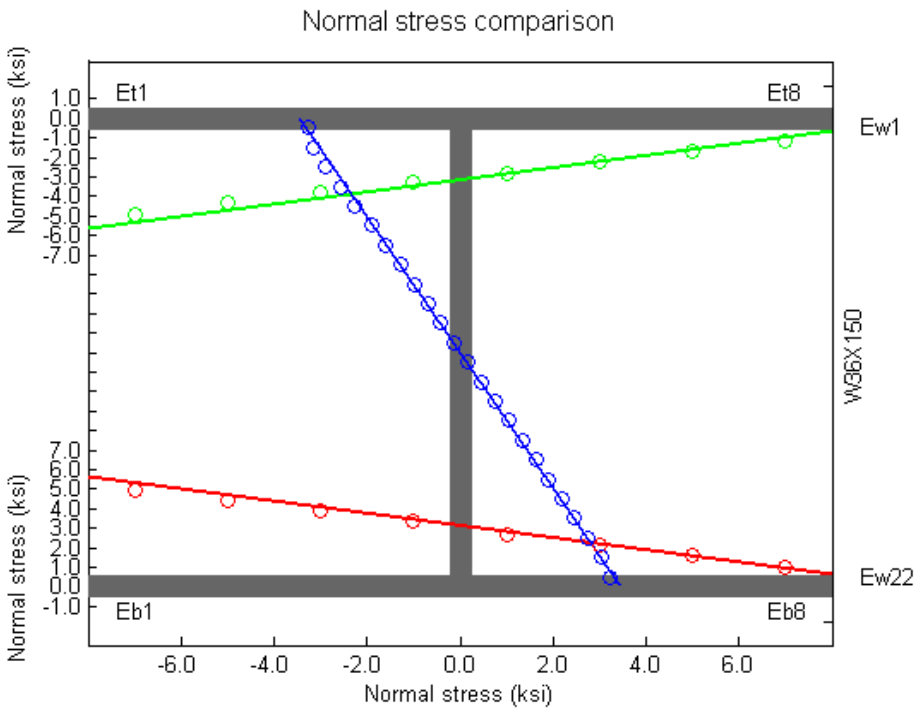

Figure 25 I-59 beam normal stress comparison, concentrated force load.

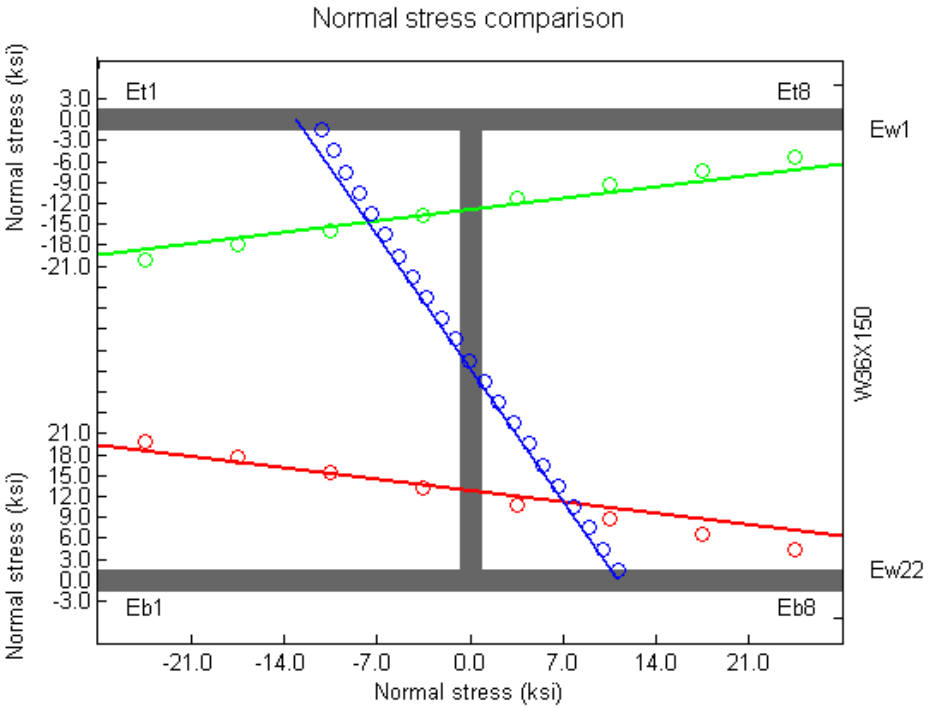

Figure 26 I-59 beam normal stress comparison, pressure load

Table 1. Top flange node FEM results, concentrated force loading

Top flange element #	Normal stress		Relative error (%)
	Theoretical results(ksi)	FEM results(ksi)	
Et1	-5.30	-4.93	7.06
Et2	-4.68	-4.37	5.97
Et3	-4.07	-3.79	5.15
Et4	-3.45	-3.25	3.80
Et5	-2.83	-2.79	0.76
Et6	-2.21	-2.24	0.55
Et7	-1.60	-1.71	2.23
Et8	-0.98	-1.16	3.44

Table 2. Bottom flange node FEM results, concentrated force loading

Bottom flange element #	Normal stress		Relative error (%)
	Theoretical results(ksi)	FEM results(ksi)	
Eb1	5.30	4.98	6.11
Eb2	4.68	4.43	4.79
Eb3	4.07	3.89	3.31
Eb4	3.45	3.33	2.15
Eb5	2.83	2.69	2.62
Eb6	2.21	2.14	1.40
Eb7	1.60	1.58	0.36
Eb8	0.98	1.02	0.79

Table 3. Web node FEM results, concentrated force loading

Web element #	Normal stress		Relative error (%)
	Theoretical results(ksi)	FEM results(ksi)	
Ew1	-3.30	-3.25	1.30
Ew2	-3.01	-3.15	4.21
Ew3	-2.72	-2.91	5.76
Ew4	-2.44	-2.57	4.05
Ew5	-2.15	-2.26	3.37
Ew6	-1.86	-1.90	1.18
Ew7	-1.58	-1.61	0.88
Ew8	-1.29	-1.29	0.06
Ew9	-1.00	-0.99	0.27
Ew10	-0.72	-0.70	0.64
Ew11	-0.43	-0.41	0.59
Ew12	-0.14	-0.12	0.71
Ew13	0.14	0.16	0.56
Ew14	0.43	0.45	0.67
Ew15	0.72	0.74	0.68
Ew16	1.00	1.04	0.97
Ew17	1.29	1.33	1.19
Ew18	1.58	1.63	1.68
Ew19	1.86	1.91	1.41
Ew20	2.15	2.19	1.14
Ew21	2.44	2.46	0.68
Ew22	2.72	2.74	0.62
Ew23	3.01	3.03	0.54
Ew24	3.30	3.23	1.93

Table 4. Top flange node FEM results, pressure loading

Top flange element	Normal stress		Relative error (%)
	Theoretical results(ksi)	FEM results(ksi)	
Et1	-19.45	-20.10	3.34
Et2	-17.57	-17.96	2.01
Et3	-15.70	-15.83	0.70
Et4	-13.82	-13.71	0.59
Et5	-11.95	-11.14	4.14
Et6	-10.07	-9.28	4.06
Et7	-8.20	-7.33	4.45
Et8	-6.32	-5.28	5.33

Table 5. Bottom flange node FEM results, pressure loading

Bottom flange element #	Normal stress		Relative error
	Theoretical results(ksi)	FEM results(ksi)	
Eb1	19.45	19.84	2.02
Eb2	17.57	17.68	0.53
Eb3	15.70	15.50	1.04
Eb4	13.82	13.32	2.60
Eb5	11.95	10.85	5.65
Eb6	10.07	8.69	7.12
Eb7	8.20	6.52	8.63
Eb8	6.32	4.36	10.06

Table 6. Web node FEM results, pressure loading

Web element #	Normal stress		Relative error
	Theoretical results (ksi)	FEM results (ksi)	
Ew1	-12.94	-11.12	14.06
Ew2	-11.81	-10.30	11.70
Ew3	-10.69	-9.38	10.10
Ew4	-9.56	-8.37	9.20
Ew5	-8.44	-7.36	8.30
Ew6	-7.31	-6.33	7.58
Ew7	-6.19	-5.32	6.69
Ew8	-5.06	-4.28	6.05
Ew9	-3.94	-3.26	5.27
Ew10	-2.81	-2.19	4.78
Ew11	-1.69	-1.14	4.23
Ew12	-0.56	-0.05	3.95
Ew13	0.56	1.04	3.66
Ew14	1.69	2.15	3.61
Ew15	2.81	3.27	3.55
Ew16	3.94	4.41	3.65
Ew17	5.06	5.54	3.69
Ew18	6.19	6.67	3.76
Ew19	7.31	7.80	3.78
Ew20	8.44	8.91	3.68
Ew21	9.56	10.02	3.58
Ew22	10.69	11.12	3.34

3.2. Inelastic Response

In this section, a beam in (Estabrooks and Grondin, 2008) is used to investigate the validity of the inelastic response of the FE model. The experimental data of the beam was recorded in the report. Similar to Section 3.2,the theoretical results for the inelastic analysis are first introduced,

then the details of the model are described, and finally the model simulation results are verifed using the experimental data in (Estabrooks and Grondin, 2008).

3.2.1. Theoretical Analysis of Inelastic Response

Next, theoretical results on the inelastic response of beam sections in the pure flexure and pure torsion cases are introduced, and are then used in the analysis of the inelastic response FEM results.

3.2.1.1 Flexural plastic yielding

It is assumed that for I-shape beams, which have a doubly symmetric section, the neutral axis is located at the geometric centroid even after developing inelastic behavior. Figure 27 shows the development of the plasticity process at the cross section from the yield limit state to the ultimate limit state. After the tips of the web reach the yield stress, which would be considered failure according to the yield limit state criterion, the stress on the web still develops along the length of the web beside the tips of the web. Eventually, the upper half of the web develops a uniform tensile stress equal to the yield stress, and the lower half of the web develops a uniform compressive stress equal to the yield stress. The plastic moment can be calculated directly using the resulting forces and lever-arm principle. Taking the web as an example, the flexural moment can be computed as

$$M_p = 2[\sigma_y (h/2) t_w](h/4) = \frac{t_w h^2}{4}\sigma_y = Z\sigma_y \qquad (3.24)$$

where

Z = the plastic section modulus, a geometrical property for the given cross section, in^4,

h = the height of the web, in, and

t_w = the width of the web, in.

The shape factor k, which is given by

$$k = \frac{M_p}{M_y} = \frac{Z}{S} \qquad (3.25)$$

which is another useful section property. It is expressed as the ratio of the plastic moment to the elastic moment, and is also the ratio of plastic section modulus to the elastic section modulus. k

accounts for the strength of the section that remains after the first yield until the full plastification of the section. In AISC, the value of flexural shape factor k varies from 1.0 to 2.0 for different cross sections. For rectangular cross sections, it is 1.5; for a solid circular cross section, it is 1.7; for I-shaped cross sections, its range is typically from 1.12 to 1.16, with an average of 1.14. Once the plasticity spreads along the entire cross section, a plastic hinge is formed at that location.

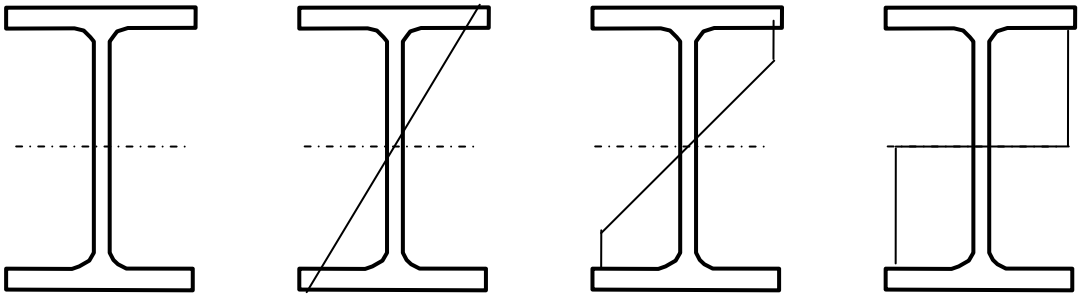

(a) Elastic (b) Elastic-plastic (c) Plastic

Figure 27 Plastification of I-shape cross section subject to flexure.

The moment to curvature relation during the plastification process is shown in Figure 28.

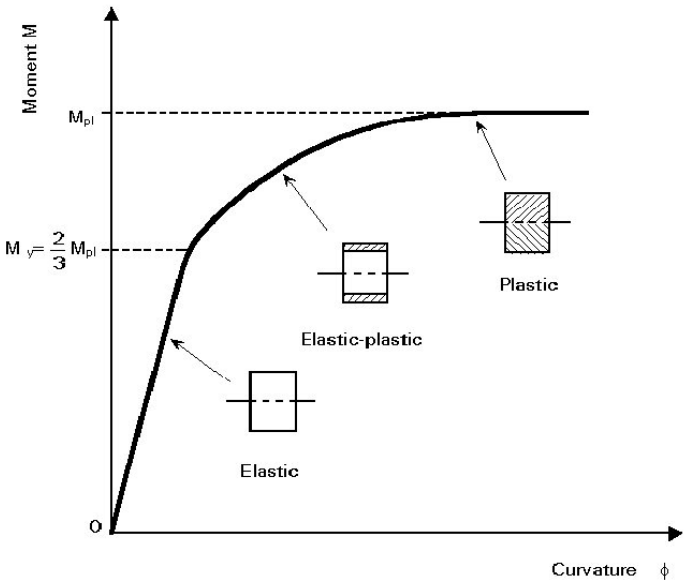

Figure 28 Moment-curvature relation for a rectangular cross section (ESDEP, 2012)

3.2.1.2 Pure plastic torsion

For an I-shaped cross-section, the plastic uniform torsion T_{up} is calculated as

$$T_{up} = \tau_y \left[t_f^2 \left(b_f - \frac{t_f}{3} \right) + \frac{t_w^2 h}{2} + \frac{t_w^3}{6} \right] \quad (3.26)$$

t_f = the thickness of the flange, in,

t_w = the thickness of the web, in,

b_f = the width of the flange, in, and

h = the clear distance between flanges, in.

The warping plastic torque is calculated as:

$$T_{wp} = \frac{2M_{fp}(h + t_f)}{L} \quad (3.27)$$

where L = the span of the beam,

M_{fp} = the flange plastic moment of the beam equal to: $M_{fp} = \frac{f_y b_f^2 t_f}{4}$

The combined plastic torque capacity of the section is:

$$T_p = T_{up} + T_{wp} \quad (3.28)$$

More details about these equations can be found in Chapter 2.

3.2.2. Inelastic FE Model Information

Estabrooks and Grondin (2008) performed an experimental study with six test cases of simply supported I-shaped section beams for examining the influence of combined flexural and torsional loading. For this research effort, FE models were also built and simulation results were compared to the experimental results reported in (Estabrooks and Grondin, 2008). Only present here the basic information of the compact beam used in (Estabrooks and Grondin, 2008) is presented here, which was used in this research effor for FE modeling and result verification. This beam is referred to as the Alberta beam throughout this thesis because it is the same beam as in the short report (Estabrooks and Grondin, 2008) from University of Alberta.

The section of the Alberta beam is W250×67 (SI), or equivalently, W10×45(U.S.). The beam was simply supported with a span of 4m(157.48 in) and free warping conditions at the ends. The

beam was braced laterally at the shear center of the mid-span of the beam to limit the lateral distortion of the beam while allowing the torsional rotation as well as the vertical deflection of the beam at the mid-span. A combined flexural and torsional loading was applied to the beam at the mid-span. Three types of initial loading were considered with initial flexural moment-to-torque ratios of 5:1, 10:1, and 20:1.

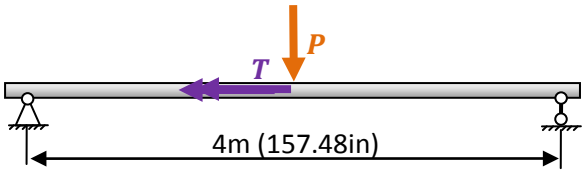

Figure 29 Weight load and concentrated force load

3.2.3. Loading Condition

In the simulations of Alberta beams, we used a different loading method from the one used in the previous experiments. In (Estabrooks and Grondin, 2008), the desired flexural moment was generated by a vertical concentrated force passing through the shear center of the I-shaped cross section at the mid-span, and the torsion was generated by applying a concentrated torque at the same point. Such a concentrated force and torque loading with thickened central flanges and web regions is illustrated in Figure 30. Both the upper and lower flanges and the web were thickened near the mid-span, which simulated the presence of a loading bracket, and helped avoid local distortion according to (Estabrooks and Grondin, 2008). When the thickness of the mid-span web was not increased, the flexural moment capacity was reduced by about 17 to 23%, as reported by Estabrooks and Grondin (2008). For a fair comparison, in the Alberta beam models in this research, the web and flange within five elements from both sides of the mid-span were also thickened by 50 mm(1.97 in) in the same way.

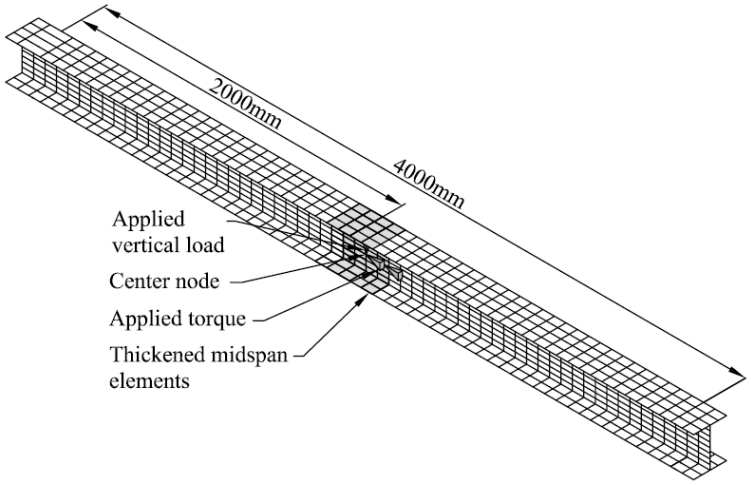

Figure 30 Loading method in Estabrooks and Grondin (2008)

The loading method in this study was inspired by the loading method discussed in (Bremault et al. 2008). In this report, the desired combination of flexural and torsional loading was produced by a concentrated force at the mid-span with an eccentricity to the shear center. The force acted on a loading bracket, as illustrated by Figure 31. Three load locations E1 E2 E3 on the bracket with different eccentricities were selected such that the moment-to-torque ratio can be changed by applying the same force to different load locations.

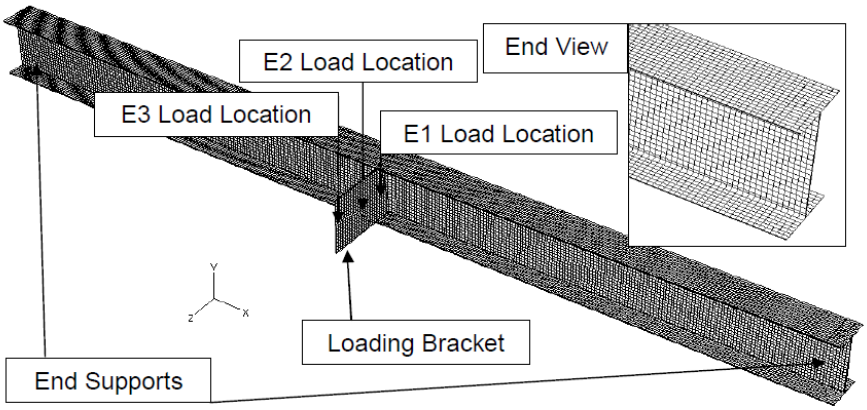

Figure 31 Loading method in (Bremault et al. 2008)

Because the flexural moment is usually generated by the gravity force, which does not change direction in the loading process, it is desirable to maintain the vertical direction of the force generating the flexural moment in the loading process of our FEM study. The loading method in (Bremault et al. 2008) could not provide a constant moment-to-torque ratio and maintain a vertical direction of the load force in the mean time. If a constant moment-to-torque ratio was to be maintained in the loading process, the force had to rotate with the bracket, and the force would

have a small vertical component and a large horizontal component when the deformation of the beam was large, which is not a realistic loading scenario. On the other hand, if the force remained vertical, the moment-to-torque ratio would change as the beam rotates.

As a comparison, the loading method in (Estabrooks and Grondin, 2008) maintains a constant moment-to-torque ratio and the vertical direction of the load throughout the whole loading process. It was found in the parametric study of the present effort that the concentrated torque load may still induce local distortion of the web for some test cases if the thickness of the web elements around the mid-span was not chosen properly. However, such distortions could be avoided by introducing a loading bracket similar to those in (Bremault et al. 2008).

In this research, the loading methods in (Estabrooks and Grondin, 2008) and (Bremault et al. 2008) were modified to generate the desired moment-to-torque ratio while maintaining the vertical direction of the forces generating the flexural moment. The details of this loading method are illustrated in Figure 32 to Figure 34. Specifically, a loading bracket was added to the mid-span as in (Bremault et al. 2008). The bracket extended to both sides of the web, but did not intersect the flanges in order to allow free development of buckling in the flanges. The flexural moment was generated by two vertical forces P_1 and P_2 on two end points, E_1 and E_2, of the bracket, as shown in Figure 32. P_1 and P_2 had the same magnitude. The torsional load was generated by T_1 and T_2 applied at E_1 and E_2 respectively. T_1 and T_2 were parallel to the intersection line of the bracket with the web. They had opposite directions and rotated with the bracket in the loading process.

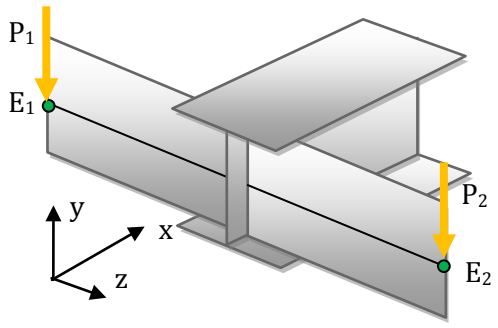

Figure 32 Flexure moment load forces

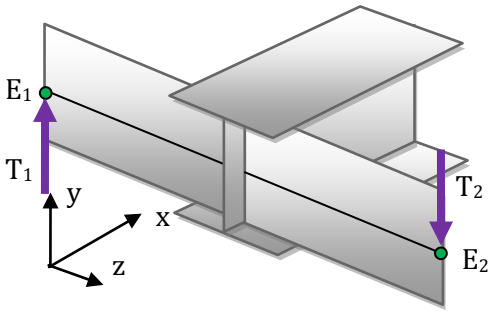

Figure 33 Torsional moment load forces

The moment-to-torque ratio was changed by choosing the magnitudes of P_1 and T_1, and applying P_1, P_2, T_1, T_2 to the bracket at the same time, as shown in Figure 34. With such a loading method, P_1 and P_2 remained vertical in the loading process such that the direction and magnitude of the flexure moment was kept constant. Meanwhile, T_1 and T_2 followed the rotation of nodes E_1, E_2 such that the magnitude of the torque was constant. Hence, the moment-to-torque ratio was constant in the loading process.

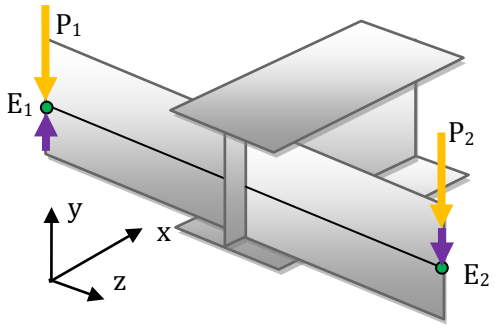

Figure 34 Combined flexure and torsional loading

3.2.4. Material Model

For the inelastic analysis of the Alberta beam, the steel plasticity data in (Estabrooks and Grondin, 2008) was used to allow a fair comparison with the experimental results in the same reference. The details of the plasticity data are given in Table 7. The Young's modulus was chosen as 29000 ksi, and the Poisson's ratio was 0.3. The plasticity data in Table 7 was take from from (Estabrooks and Grondin, 2008). These data consider the strain-hardening effect, and which was employed in the Alberta beam model. In the Alberta beam model, the Young's modulus of the loading bracket was set as 1000 times that of steel such that the bracket could be considered a rigid body, and its deformation would not affect the FEM results during the loading process.

Table 7. Steel plasticity data

True Stress (ksi)	True Plastic Strain
43.13	0
43.87	0.0172
52.18	0.0317
62.26	0.0786
65.02	0.0871
71.05	0.1474

3.2.5. Element Properties

For the same reason they were chosen when modeling the I-59 beam, the S4R element was used in the Alberta beam model.

3.2.6. Alberta Beam Model Mesh

In general, the finer the finite element mesh, the more accurate the results are. However, mesh refinement is also accompanied by longer computation time. Therefore it is convenient to find a balance between the computation time and the accuracy. In order to find the proper mesh size for the I-shaped steel beam inelastic response study, the Alberta beam was modeled using three different mesh sizes in this research, which are shown in Figure 35 to Figure 37. The coarse mesh contained 876 S4R elements in total for both the beam and the bracket with an aspect ratio below 1.3. For each cross-section, the coarse mesh corresponded to 4 elements on the flanges, with four elements on the web. The medium mesh contained 4912 S4R elements with an aspect ratio of approximately 1. For each cross-section, 6 elements were located on each flange, and 10 elements were located on the web. The fine mesh contained 7624 elements with an aspect ratio approximately 1. At each cross-section, each flange contained 8 elements, and the web contained 10 elements.

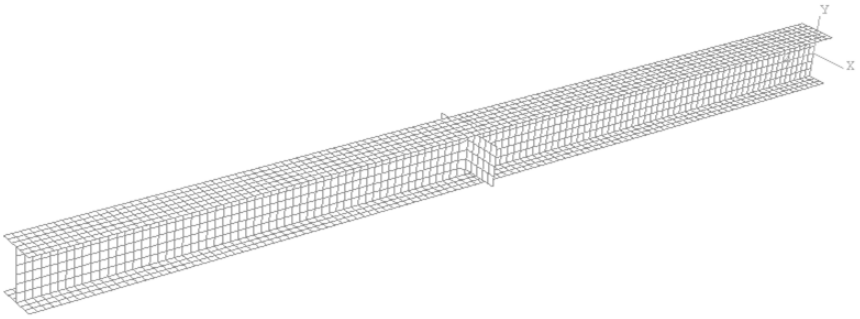

Figure 35 Alberta beam mesh-coarse

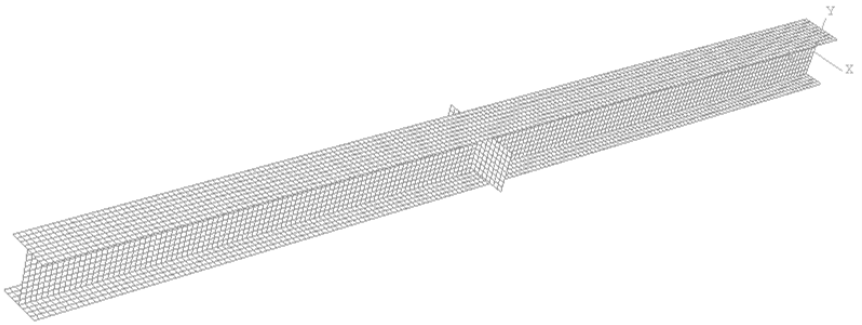

Figure 36 Alberta beam mesh-medium

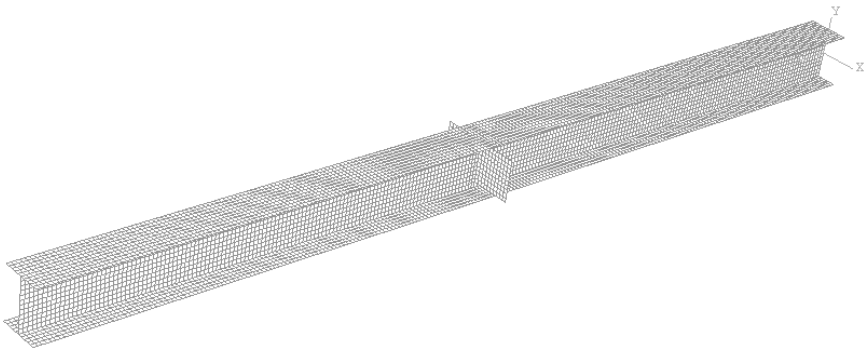

Figure 37 Alberta beam mesh-fine

All three meshes were used to compute the inelastic response of the beam subjected to case-1, case-2, and case-3 loading cases with 5:1, 10:1, and 20:1 moment-to-torque ratios, respectively. The results are shown in Figure 38 to Figure 40. It is clear that, for all three cases, the elastic and inelastic responses obtained using different meshes were very close. Hence, all three meshes were considered to be fine enough for the Alberta beam model. The simulation results obtained using the medium size mesh was used for FE model verification.

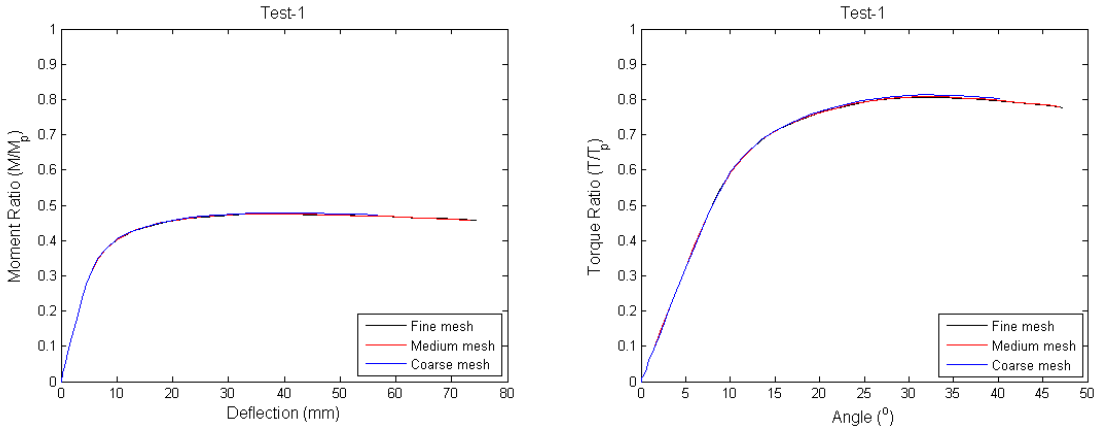

Figure 38 Alberta beam mesh refinement study case-1

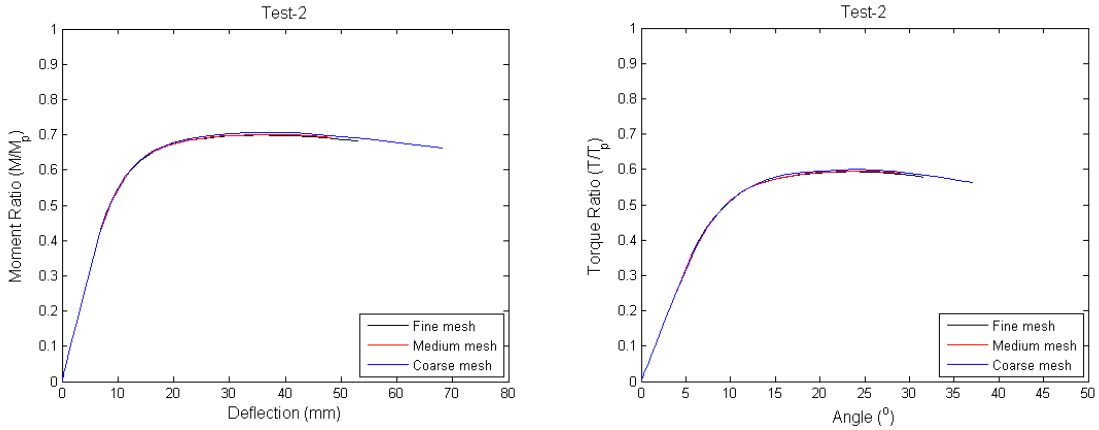

Figure 39 Alberta beam mesh refinement study case-2

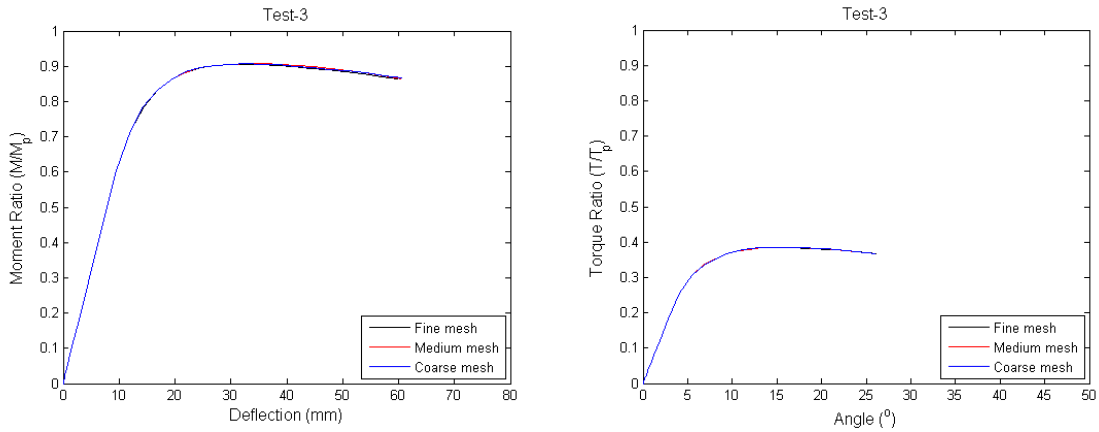

Figure 40 Alberta beam mesh refinement study case-3

3.2.7. Boundary Conditions

The boundary conditions for the Alberta beams are illustrated in Figure 41. Similarly to (Estabrooks and Grondin, 2008) and (Bremault et al. 2008), an additional 8 elements were added beyond the end supports to prevent local distortion of the web at the end supports.

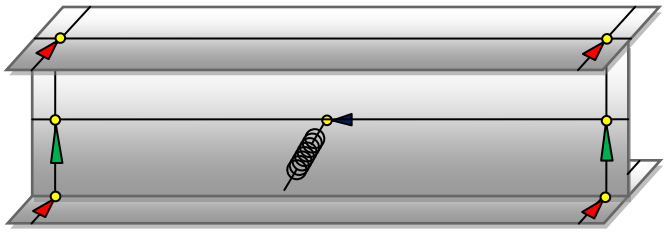

Figure 41 Boundary conditions

In (Estabrooks and Grondin, 2008), a spring element was introduced to model the lateral bracing used in the physical experiment. The spring restricted the displacement of the node along the x direction, and followed the center node as it deflected vertically to provide partial lateral restraint. Such a treatment of lateral bracing was also adopted in the Alberta beam models in this chapter. The stiffness of the spring was taken from (Estabrooks and Grondin, 2008).

3.2.8. FEM analysis

The Alberta beam FE models were analyzed in ABAQUS using the Riks method. Both geometric and material nonlinearities were considered in the FEM analysis. The Riks method treats the load magnitude as an unknown and solves for loads and displacements at the same time. Hence, another variable should be used to monitor the progress of the solution. Abaqus/Standard uses the "arc length" along the static equilibrium path in load-displacement space as this additional quantity. Such an approach provides solutions regardless of whether the response is stable or unstable. Throughout this thesis, the Riks method was used to solve the inelastic responses of all FE models.

3.2.9. Results Verification

For the Alberta beam model, the values of P_1, P_2, T_1, T_2 were selected to produce the moment-to-torque ratios used in the physical experiments of (Estabrooks and Grondin, 2008). All three cases, with moment-to-torque ratios of 20:1, 10:1, and 5:1 were reproduced in this simulation.

Similar to (Estabrooks and Grondin, 2008), the moment-displacement diagram and the torque-twist angle diagram were used to verify the FE results in this study. Both the moment and

torque were normalized with the value of M_p and T_p, which come from Table 4.3 in (Estabrooks and Grondin, 2008). Three cases were solved, and the inelastic response results from the present FE model were compared with the physical experimental results and FEM results documented in Figure 5-9 and Figure 5-11 in (Estabrooks and Grondin, 2008). The only difference between these three cases was the initial moment-to-torque ratio M_0/T_0: for case-1, $M_0/T_0 = 5$; for case-2, $M_0/T_0 = 10$; and for case-3, $M_0/T_0 = 20$.

The results of the comparison are shown in Figure 42 to Figure 44. As shown by these figures, in general, the FEM model provided a good approximation of the behavior of the beam subjected to different moment-to-torque ratios, and the error of the flexural resistance predicted by our FEM model was within 10% of the experiment result in (Estabrooks and Grondin, 2008). Hence, the performance of the FEM for predicting the inelastic behavior of class 1 I-shaped beams was considered to be satisfactory.

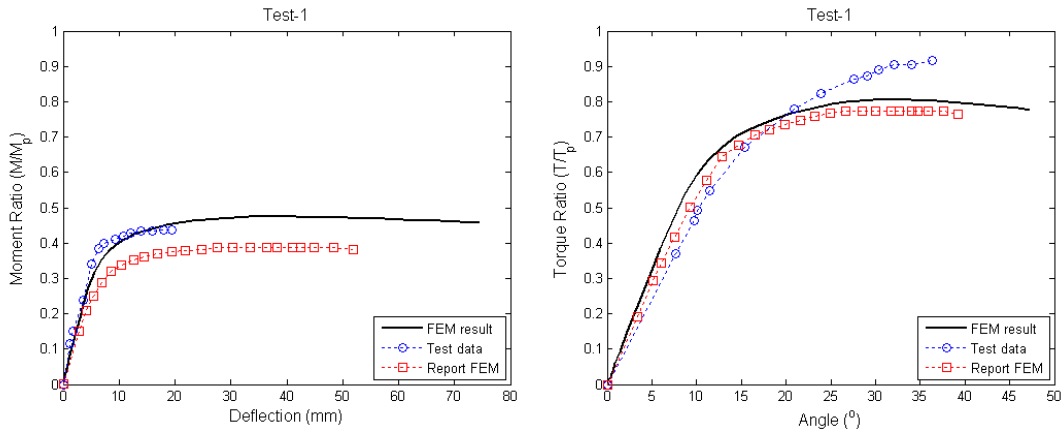

Figure 42 Alberta beam case-1 results verification, initial M/T=5:1

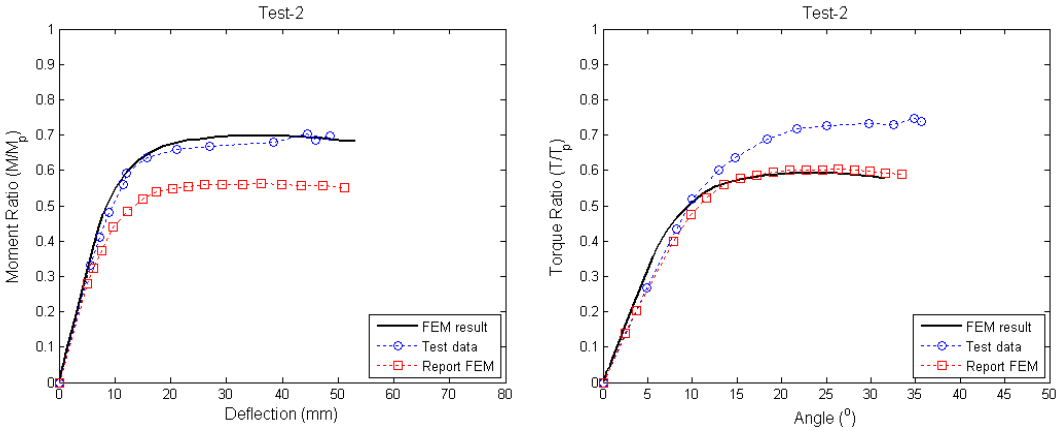

Figure 43 Alberta beam case-2 results verification, initial M/T=10:1

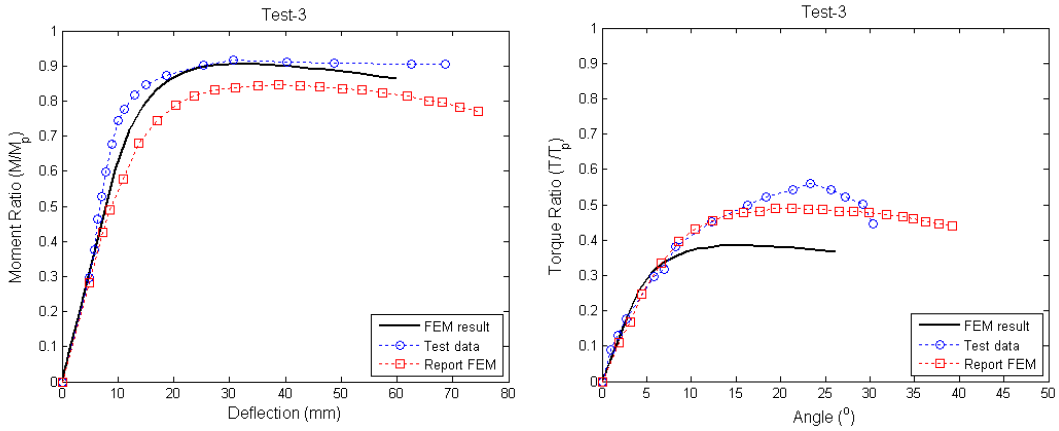

Figure 44 Alberta beam case-3 results verification, initial M/T=20:1

The comparison of the maximum flexural moment and torque indicated in the FE model and those given in the report are listed in Table 8. In general, the FE model developed in this research provided a good approximation to the ultimate strength of the beam for all three different cases with different moment-to-torque ratios. The largest error of the present FEM model occurred for the torsional resistance in case 3. However, because case 3 corresponded to an M/T ratio of 20:1, the failure of the beam was controlled by the flexure resistance of the beam. Hence, for this case the error in the torsional resistance of the beam would be of much less concern when determining the ultimate strength.

Table 8. Error comparison with report results

case #	maximum normalized internal force	Estabrooks and Grondin, 08			Current investigation	
		Experiment	FEM	Error (%)	FEM	Error (%)
1	$(M/M_p)_{\max}$	0.4383	0.3862	11.89	0.4745	8.26
	$(T/T_p)_{\max}$	0.9180	0.7746	15.62	0.2015	7.81
2	$(M/M_p)_{\max}$	0.7023	0.5632	19.81	0.6990	0.47
	$(T/T_p)_{\max}$	0.7459	0.6036	19.08	0.5936	20.42
3	$(M/M_p)_{\max}$	0.9153	0.8456	7.61	0.9057	1.05
	$(T/T_p)_{\max}$	0.5594	0.4896	12.48	0.3846	31.25

3.3. Summary

In this chapter, the FE models that were developed for both elastic and inelastic analysis of beams subject to different combinations of flexure and torsional loads were described. The simulation results obtained using the FE models were verified using both theoretical results, experimental results, and FEM results from previous research. It was shown that the elastic analysis results of the FE model were very close to those given by theoretical analysis, while the inelastic analysis results of the models matched the experimental results and FE simulation results of (Estabrooks and Grondin, 2008). The verified FE models were then used for the parametric study discussed in the next chapter.

Chapter 4 Parametric Study

4.1. Overview

In this chapter, the parametric study involving the inelastic behavior of I-shaped beam members subject to combined flexure and torsion is presented. Instead of performing a comprehensive study, a focus was placed on several key parameters which have major influence on the ultimate capacity and serviceability of the beams. The current ultimate strength design methods for beams subject to combined torsion and flexure were also evaluated using the FE analysis results.

4.2. Parameter Selection

The beams considered in this study were compact, I-shaped, simply supported, and unbraced. No loading history was considered. The residual stress pattern and initial imperfections were also ignored in this analysis, and perfect elastic-plastic steel yielding at 50 ksi was assumed. The strain-hardening property of the steel was not considered, since the strain-hardening region is rarely entered for beams subject to these combined loads (Pi and Trahair, 1994a,1994b) and (Trahair and Pi ,1997).

The following factors were considered in this parametric study.

Beam slenderness

The slenderness ratio is an important criterion for determining whether lateral torsional buckling will occur in a beam. The slenderness ratio of the beam is commonly defined as L / r_y, where L is the distance between points of lateral supports and r_y is the radius of gyration about the weak axis. Flexural members bent about their strong axis are classified according to the length of the beam as follows (AISC, 2010):

1) If $L < L_p$, the flexural member is considered to have adequate lateral support and is not subject to lateral-torsional buckling.
2) If $L_p < L \le L_r$, the flexural member is considered to be laterally unsupported and subject to inelastic lateral-torsional buckling.
3) If $L > L_r$, the flexural member is considered to be laterally unsupported and subject to lateral-torsional buckling.

The limiting values of L_r, L_p are specified in AISC (2010) as:

$$L_r = 1.95 r_{ts} \frac{E}{0.7F_y} \sqrt{\frac{J}{S_x d}} \sqrt{1+\sqrt{1+6.76\left(\frac{0.7F_y}{E}\frac{S_x d}{J}\right)^2}} \tag{4.1}$$

$$L_p = 1.76 r_y \sqrt{\frac{E}{F_y}} \tag{4.2}$$

where d = distance between the flange centroids, in.

Note that the development of inelastic lateral-torsional buckling in a type 2) beam is strongly affected by the residual stress in the beam, which is out of scope of this thesis. In this study, the emphasis was type 1) and type 3) beam members for which the effect of residual stress is negligible. Correspondingly, the lengths of the beams were selected according to the beam slenderness criterion such that either $L < L_p$, or $L > L_r$.

The moment resistance capability is an important quantity which was used for analyzing simulation results as discussed later in this chapter. The computation of this quantity depends on the failure mechanism of the beam, hence is also related to the beam slenderness. For compact sections with $L \le L_p$, the moment resistance capability is calculated as $M_n = M_p = Z_x \sigma_y$, where σ_y is the specified minimum yield stress of the type of the steel being used. For the present study, σ_y was chosen to equal to 50 ksi. Z_x is the plastic section modulus about the x-axis, with units of in^3. The Z_x value is also used for computing the flexural strength in the first yield theory.

When $L > L_r$, the moment resistance capacity is calculated as:

$$M_n = C_b \pi^2 E \left(\frac{r_{ts}}{L}\right)^2 \sqrt{1+0.078\frac{J}{S_x d}\left(\frac{L}{r_{ts}}\right)^2} S_x \le M_p \tag{4.3}$$

where C_b is the lateral-torsional buckling modification factor. Usually it is conservatively set as 1.0. For the simply supported boundary conditions considered in this study, it was taken as 1.32. J is

the torsional constant, in^4. S_x is the torsional constant, in^4. d is the distance between the flange centroid, in. $r_{ts} = \frac{\sqrt[4]{I_y C_w}}{\sqrt{S_x}}$, in^{-1}

Moment-to-torque ratio

Three values of moment-torque ratios were investigated to reveal the interaction between the moment and torque loadings. When the load applied has a small M/T ratio, the beam is subject to low flexural moment but high torque. When the load has a medium M/T ratio, the beam is subject to medium moment and medium torque. Similarly, when the load has a large M/T ratio, the beam undergoes high moment and low torque.

4.3. Selected Cases

For the 30 cases considered in the parametric study, a naming convention was followed which describes both the length of the member and its section shape. The name of a beam starts with either the letter "L" or the letter "S", followed by a number representing the shape of the section. "L" stands for long beams with large slenderness ratios, and "S" stands for short beams with small slenderness ratios.

In order to enrich the diversity of the beam sections considered in our simulation, we also considered two additional variables for section selection, which are the ratio of warping-to-pure-torsional resistance, and the torsional-to-flexural stiffness ratio. The ratio of warping-to-pure-torsional resistance is a measure of the ratio of torque carried by warping and pure torsion in the elastic range, which can be expressed as:

$$\lambda_{wp} = \sqrt{GJ \big/ EC_w} \tag{4.4}$$

In this equation, G and E depend on the material property, and are assumed to be constant. The other two variables vary with different cross sections. For an I-shaped cross section, $J = \frac{1}{3}\left(2bt_f^3 + (d - t_f)w^3\right)$ and $C_w = \frac{1}{4}(d - t_f)^2 I_y$ where t_f is the thickness of the flanges.

The torsional-to-flexural stiffness ratio is given by

$$\lambda_{tf} = \sqrt{C_w / I} \tag{4.5}$$

where the flexural stiffness EI_x is the slope of the moment-to-displacement curve when the beam is fully plastic. The torsional stiffness GJ is the slope of the torque-to-rotation angle curve in the elastic region. The flexural stiffness depends on I_x, and the torsional stiffness is related to J. Those two values are also associated with the material properties E and G, which are assumed to be constants.

The numbers 1-5 denote the five beam sections considered, the details of which are described in Table 9. For example, a long beam with section shape 12×53 would be referred as "L5" beam.

Table 9. Section number assignment

Section number	1	2	3	4	5
Section size	10×45	10×33	21×93	16×57	12×53

The warping-to-pure torsion stiffness ratio and the torsional-to-flexural stiffness ratio of the sections selected in this research are shown in Table 10. These cross sections were selected from 100 compact cross sections in AISC such that these two parameters could be studied independently, and could be classified into two groups. For the first group, sections were chosen to keep the λ_{pb} values as close as possible while having different λ_{wp} values. It was more difficult to choose members for the second group because the λ_{wp} values are more scattered in the steel manual. Hence only two sections were chosen for this group, as shown in Table 10. The first group (S1, S2, S3) have similar λ_{pb} values and different λ_{wp} values. The last two sections (S4, S5) have similar λ_{wp} values, and the λ_{pb} values are different. Pertinent additional properties of the selected I-shaped sections are shown in Table 10.

Table 10. Selected sections for the parametric study

Section number	$\sqrt{EC_w/GJ}$	$\sqrt{C_w/I}$	r_{ts} (in)	D (in)	J (in^4)	C_w (in^6)
1	67.60	2.20	2.27	10.1	1.51	1200
2	34.10	2.15	2.2	9.37	0.58	791
3	388.78	2.19	2.24	21.6	6.03	9940
4	122.04	1.87	1.92	16.4	2.22	2660
5	112.21	2.73	2.79	12.1	1.58	3160

Table 11 lists the beam lengths selected for different sections to incorporate two different values of slenderness ratio. In this table, L_s is the selected length of the short beam, and L_l is the length of the long beam. The values of L_s and L_l were selected such that all short beams share the same slenderness ratio L_s/r_y value, and all long beams share the same L_l/r_y value.

Table 11. Selected beam lengths for the parametric study

Section number	L_p (in)	L_S (in)	L_s/r_y	L_l (in)	L_l/r_y	L_p / r_y	L_r / r_y
1	85.2	72	36	336	167	42.2	160.6
2	82.2	70	36	324	167	42.4	134.8
3	78	66	36	307	167	42.4	138.9
4	67.8	58	36	267	167	42.4	137.3
5	105.1	90	36	414	167	42.4	136.5

Table 12 lists some key characteristics of the beams used in the parametric study. In this table, M_p is the plastic flexural moment, T_{up} is the uniform torque, T_{wp} is the warping torque, T_p is the plastic torque capacity of the section, M_y is the flexural moment considering the first yield theory, T_y is the torque capacity considering the first yield theory, and M_{cr} is the flexural moment considering LTB.

Table 12. Beam properties

Beam	M_p (kip·in)	T_{up} (kip·in)	T_{wp} (kip·in)	T_p (kip·in)	M_y (kip·in)	T_y (kip·in)	M_{cr} (kip·in)
S1	2745	102.35	130.61	465.93	2455	211.1	b
L1	2166.57	102.35	27.99	260.68	a	a	2166.6
S2	1940	53.56	88.96	285.03	1750	136.6	b
L2	1227.54	53.56	19.77	146.66	a	a	1227.5
S3	11050	299.27	516.23	1631.00	9600	748.0	b
L3	6924.93	299.27	110.98	820.51	a	a	6924.9
S4	5250	141.89	229.24	742.27	4610	356.7	b
L4	3271.78	141.89	53.23	390.25	a	a	3271.8
S5	3895	112.6233	184.08	593.41	3530	276.0	b
L5	2524.04	112.6233	40.02	305.28	a	a	2524.0

a--- the limit state of yield does not apply to long beams, elastic LTB controls

b---the limit state of LTB does not apply to short beams, the limit state controls

Three loading conditions with different moment-to-torque ratios, includeing 'high', 'mid', and 'low', were considered. For the high cases, the applied moment-to-torque ratio $M/T = 16$; for the mid cases, $M/T = 8$, and for the low cases, $M/T = 4$.

As a brief summary, for each of the five cross sections, six cases were investigated using ABAQUS to cover the two different beam slenderness ratios ("long" and "short") and the 'high', 'mid' and 'low' loading case. Hence a total of 30 cases are studied. For each case, the combined flexural and torsional load was applied via a bracket using the loading method described in Chapter 3. The size of the bracket, the applied concentrated forces P_1, T_1, and the applied moment and torsion are listed in Table 13. M_0 and T_0 are the reference loads on the beam in ABAQUS. The actual applied moment and torque in the loading process of FE analysis were obtained by multiplying reference loads M_0 and T_0 by the load proportion factor (LPF), which is a solution variable used by the RIKS method of ABAQUS.

In Table 13, d (distance between load points E_1 and E_2 in Figure 34) is chosen arbitrarily for each beam. The concentrated force P_1 was selected such that the generated flexure moment was close to the ultimate strength of the section subject to pure flexure load. T_1 was calculated such that

the flexure moment to torque ratio generated by the forces P_1, T1, P_2, and T_2 matched the specified loading case (high, mid, or low).

Table 13. Loading parameters of short beams

		P_1(kips)	T_2(kips)	d(in)	M_0(kip·in)	T_0(kip·in)
S1	high	444.44	66.67	15	16000	1000
	mid	222.22	66.67	15	8000	1000
	low	111.11	66.67	15	4000	1000
S2	high	457.14	100	10	16000	1000
	mid	228.57	100	10	8000	1000
	low	114.29	100	10	4000	1000
S3	high	484.85	100	10	16000	1000
	mid	242.42	100	10	8000	1000
	low	121.21	100	10	4000	1000
S4	high	551.72	100	10	16000	1000
	mid	275.86	100	10	8000	1000
	low	137.93	100	10	4000	1000
S5	high	355.56	55.56	18	16000	1000
	mid	177.78	55.56	18	8000	1000
	low	88.89	55.56	18	4000	1000

Table 14. Loading parameters of long beams

		P_1(kips)	T_2(kips)	d(in)	M(kip·in)	T(kip·in)
L1	high	95.24	14.88	67.2	16000	1000
	mid	47.62	14.88	67.2	8000	1000
	low	23.81	14.88	67.2	4000	1000
L2	high	98.77	20	50	16000	1000
	mid	49.38	20	50	8000	1000
	low	24.69	20	50	4000	1000
L3	high	104.24	16.29	61.4	16000	1000
	mid	52.12	16.29	61.4	8000	1000
	low	26.06	16.29	61.4	4000	1000
L4	high	119.85	14.05	53.4	16000	1000
	mid	59.93	14.05	53.4	8000	1000
	low	29.96	14.05	53.4	4000	1000
L5	high	77.29	12.08	82.8	16000	1000
	mid	38.65	12.08	82.8	8000	1000
	low	19.32	12.08	82.8	4000	1000

4.4. Finite Element Models

The details of finite element models can be found in Chapter 3 since the models used for this parametric study were similar to those in Chapter 3. The difference is that no lateral bracing was applied to the beams for the parametric study, and the web was not thickened around the mid-span to allow the development of buckling in the web.

A mesh refinement study was performed to select the appropriate mesh sizes for the models. This study covered three loading conditions and three different mesh sizes for the S1 beam. The ultimate strength of the beam was used as the criterion for evaluating the convergence of the mesh study. The result was then used to choose the mesh size for other beam FE models.

Specifically, three FE models with different mesh sizes were built for S1 beam. In Mesh 1, 14 elements were distributed on both the upper and the lower flanges at each cross section. In Mesh 2, 10 elements were allocated across the flanges, and in Mesh 3, only 6 elements were located on each flange at every cross section. The element aspect ratios in all three meshes were very close to 1.

Both the high, mid, and low loading cases were computed using each of the three meshes, and the resulting ultimate strength ratio for each case is recorded in Table 15. As shown in the table, the results obtained using all three meshes agreed very well. Therefore, mesh 2 was used as a baseline for mesh generation in this chapter. Specifically, the meshes for all beams were generated such that 10 elements were located across both the top and the bottom flanges in the lateral direction, while keeping the aspect ratio of the elements approximately 1.

Table 15. Mesh study record, S1 beam

S1 beam	Mesh 1	Mesh 2		Mesh 3	
Load	$M_1 = M_{\max}/M_p$	$M_2 = M_{\max}/M_p$	$\lvert M_2 - M_1\rvert/M$	$M_3 = M_{\max}/M_p$	$\lvert M_3 - M_1\rvert/M_1$
Low	0.3788	0.3812	0.63%	0.3833	1.19%
Mid	0. 5938	0. 5960	0.39%	0. 6030	1.57%
High	0.7736	0.7747	0.14%	0.7819	1.07%

The total number of elements in each of the short beams was between 4500-8300, and the number of elements in the long beams was between 15800-28900. Because of extensive amount of computations required for the large mesh sizes, all the cases are computed on the computer cluster at the High Performance Computation Center at Auburn University.

4.5. Parametric Study Results

In this section, the influence of different parameters on the behavior and ultimate strength of different beams, which are represented by the circles in Figure 47 to Figure 66, are characterized.

Influence of beam slenderness

According to the FE analysis results, the influence of the slenderness ratio on the behavior and failure mechanism of beams subject to combined flexure and torsion loading is critical. For short beams, the plasticized region first develops along the edges of the flanges at the mid-span due to the high normal stresses induced by the combination of moment and torsion. This region then spreads across the flanges at the mid-span as the load increases. A plastic hinge is formed at the mid-span when the beam reaches the ultimate strength. Thereafter, the strength of the beam decreases, and the plasticized region spreads in the beam. Figure 45 shows a typical Mises stress contour plot of a short beam when the ultimate strength is reached. It is obvious that a plastic hinge is formed at the mid-span of the beam.

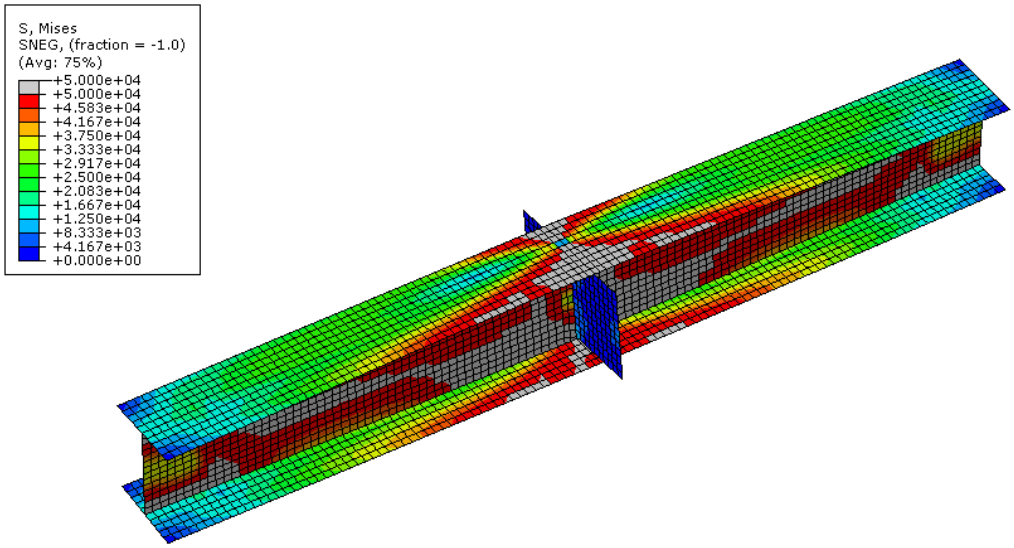

Figure 45 Mises stress plot of S1 beam at maximum strength subject to mid load

For long beams with large slenderness ratios, a plasticized region also develops at the mid-span as the load increases. However, as compared to the short beams, for the long beams, this region spreads quickly in the flanges and the web along the longitudinal direction to the two ends, and grows over the whole length of the beam by the time the ultimate strength is reached. Similar to the short beams, a plastic hinge also develops at the mid-span when the beam reaches the ultimate strength. After the ultimate strength is reached and a plastic hinge is formed, the vertical displacement of the mid-span section increases very quickly. Figure 46 shows a Mises stress contour plot of a long beam when the ultimate strength is reached.

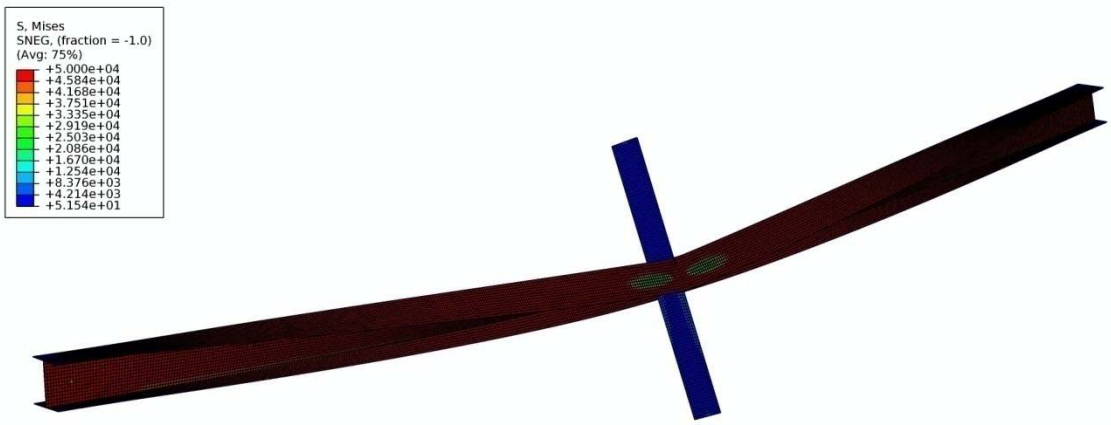

Figure 46 Mises stress plot of L1 beam at maximum strength subject to mid load

Effects of moment-to-torque ratio

The effect of moment-to-torque ratio is investigated via the moment-displacement diagrams and torque-rotation angle diagrams of all 30 cases, which are shown in Figure 47 to Figure 66. In these plots, the moment value is normalized by the plastic flexure moment M_p for short beams, and the lateral torsional buckling flexural moment capacity M_n for long beams. The torque value is normalized using plastic torsion capacity T_p for all beams. The displacement is the movement in the vertical direction of the shear center of the beam section at the mid-span. The rotation angle is the rotation of the mid-span section at the shear center around the global Z axis.

The influence of moment-to-torque ratio M/T to the ultimate strength of the beam can be easily observed from Figure 47 to Figure 66. It is noted that in each moment-displacement diagram, the curves almost overlap in the elastic region (straight lines at the beginning of the curve) regardless of the M/T ratios (high, mid, low). This suggests that in the elastic phase, the interference between flexure and torsion is not significant. Such an observation is also confirmed by the torque-rotation angle diagrams, for each of which the curves are also almost identical in the elastic region.

For each beam section, as the flexural load increases, plastic regions develop in the beam. When the M/T ratio is smaller, i.e., when the loading contains a larger portion of torsional load, the slope of the displacement-moment curve starts decreasing at a smaller moment value. A similar but opposite phenomena is observed for the torque-angle curves. Furthermore, as shown in these figures, for each beam section, the maximum moment decreases as M/T decreases, i.e., as there exists a larger portion of torsional load. Similarly, the maximum torque deceases as the flexural protion of the load increases. Hence, the torsion undermines the beam's capability of resisting flexural moment, and the flexural moment also causes a loss of the beam's torsional resistance. Note that such an observation on the interaction between flexural moment and torsional load holds for all beams.

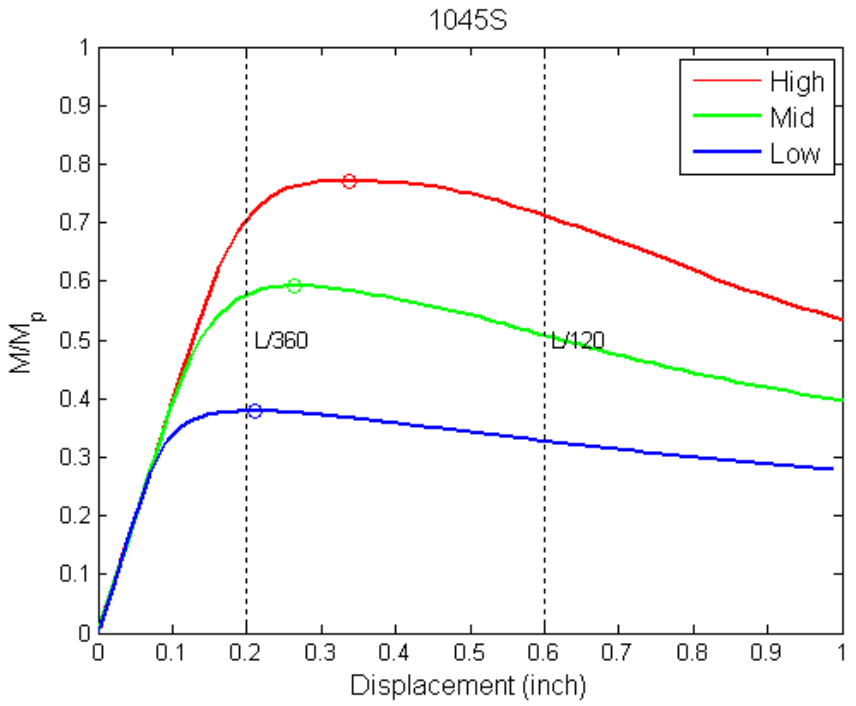

Figure 47 Moment-displacement diagram, S1 beam

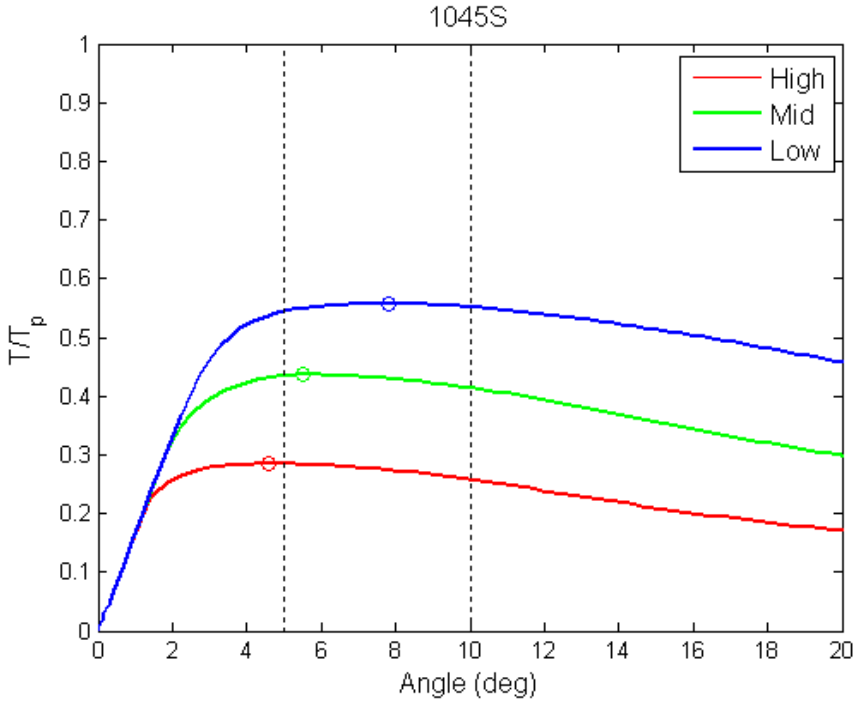

Figure 48 Torque-rotation diagram, S1 beam

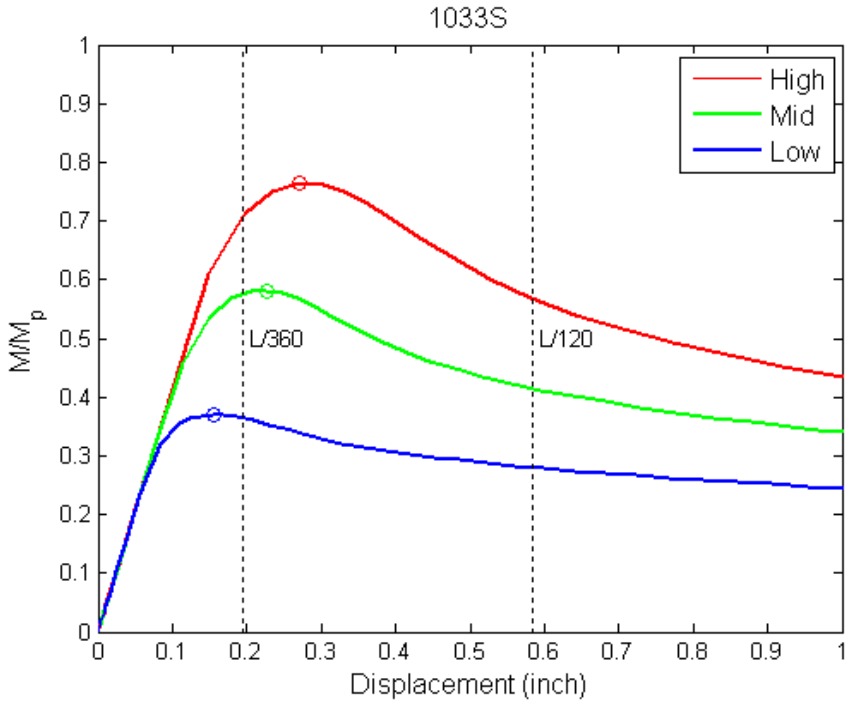

Figure 49 Moment-dispalcement diagram, S2 beam

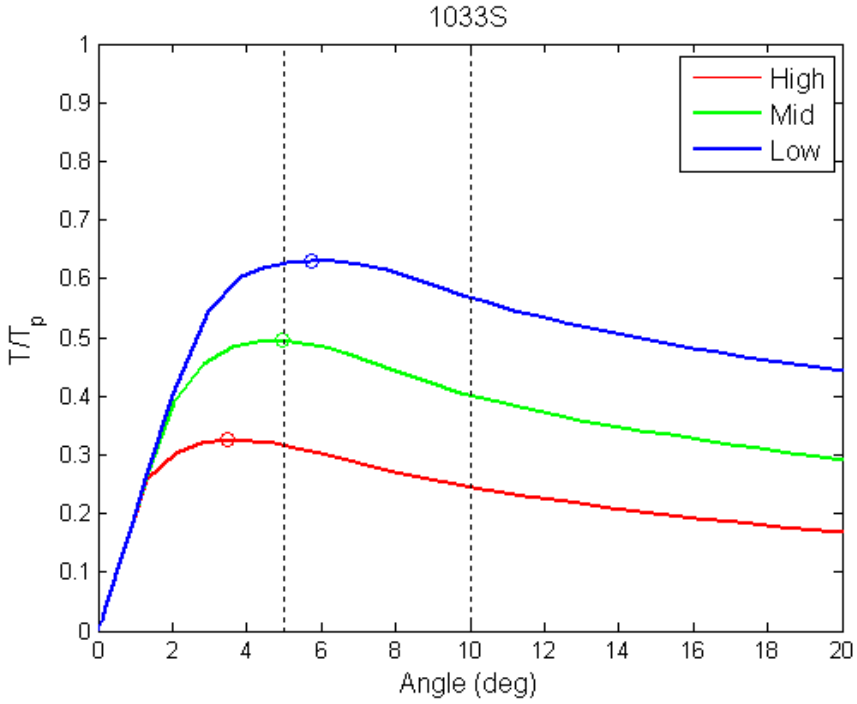

Figure 50 Torque-rotation angle diagram, S2 beam

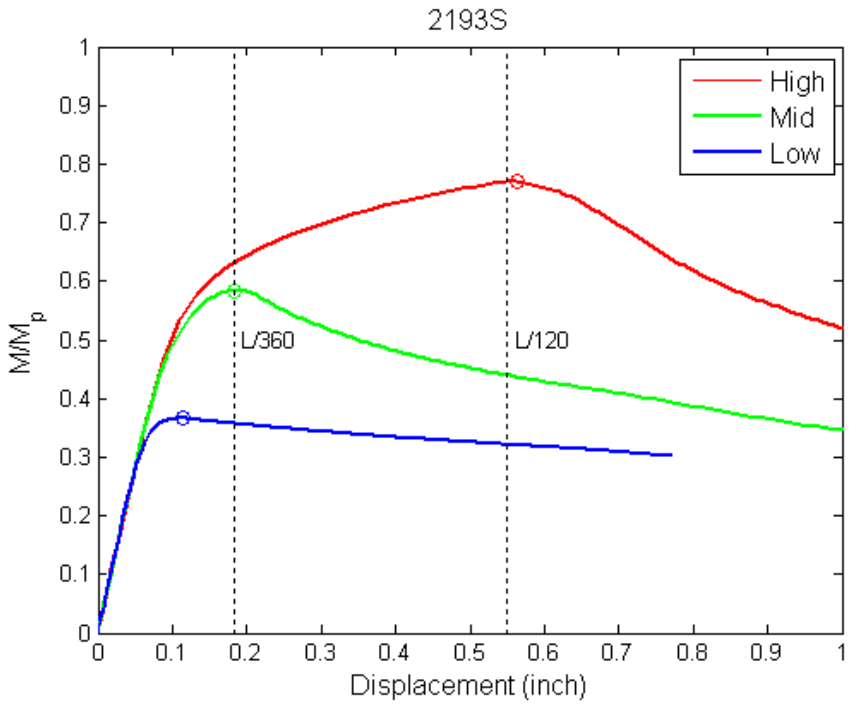

Figure 51 Moment-displacement diagram, S3 beam

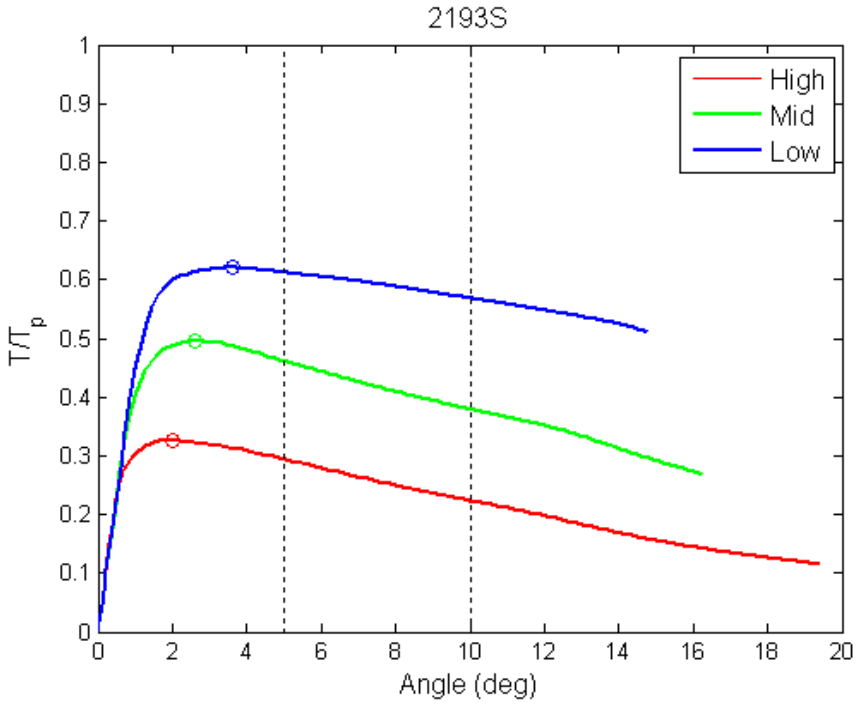

Figure 52 Torque-rotation angle diagram, S3 beam

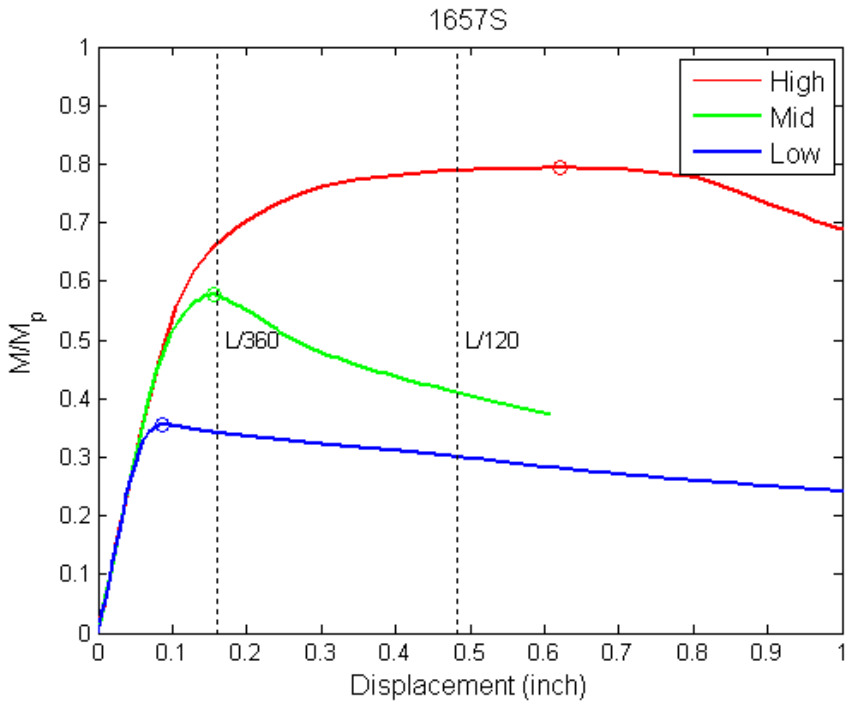

Figure 53 Moment-displacement diagram, S4 beam

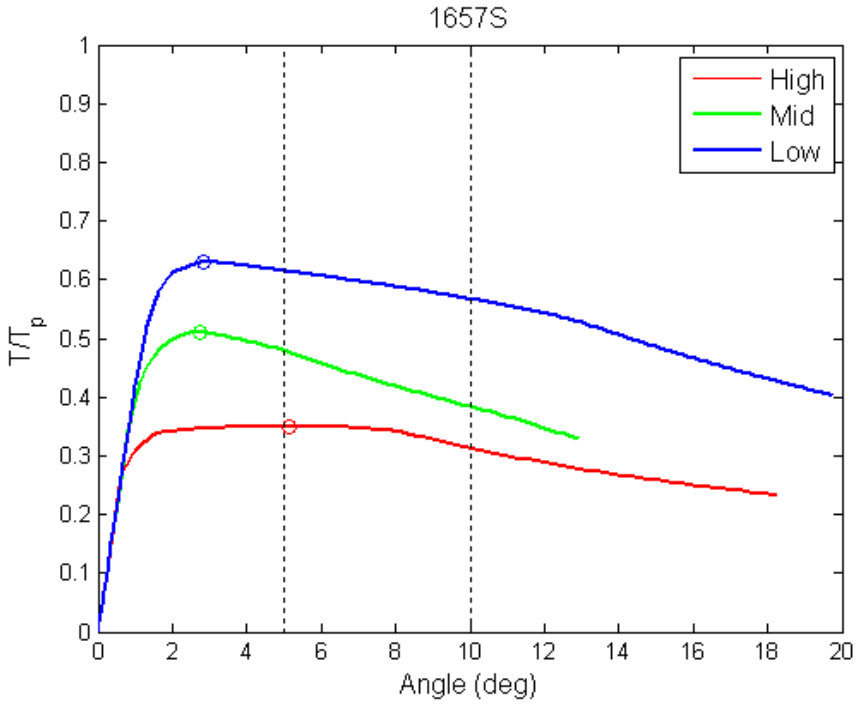

Figure 54 Torque- rotation angle diagram, S4 beam

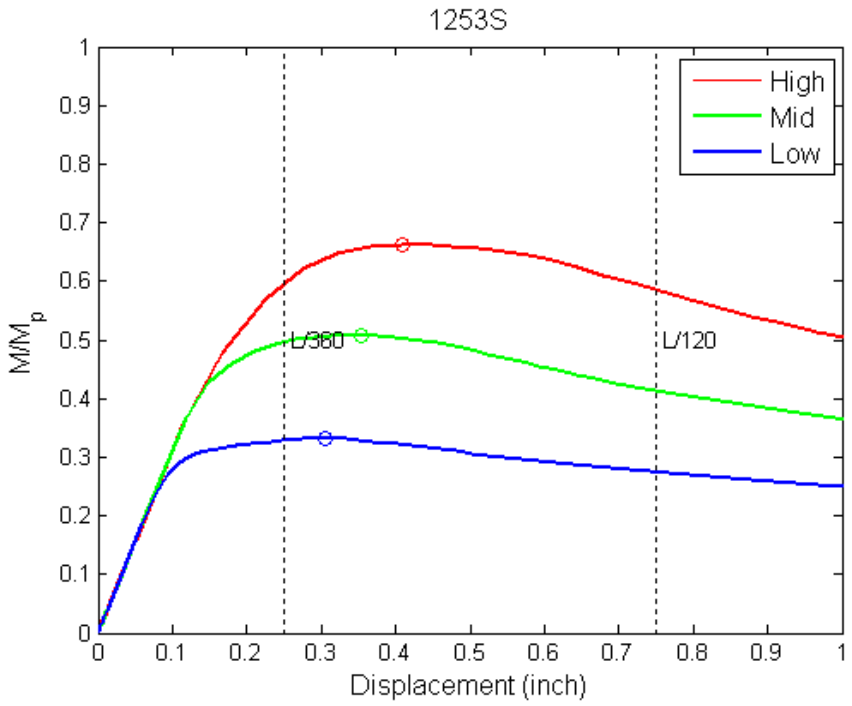

Figure 55 Moment-displacement diagram, S5 beam

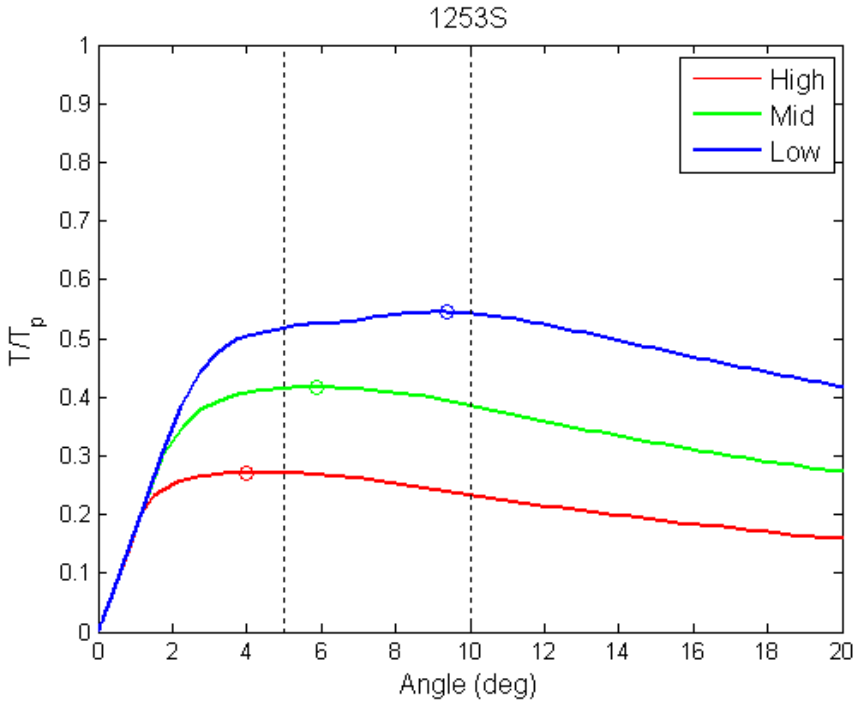

Figure 56 Torque-rotation angle diagram, S5 beam

The displacement-moment diagrams and rotation angle-torque diagrams for five long beams under different loading conditions are shown in Figure 57 to Figure 66. When the long beams reach the ultimate strength, the displacement and the rotation angle are very large, which are impractical. Hence, the ultimate strength analysis is not enough for analyzing all the behavior of long beams.

On the other hand, due to the large rotation angle of the long beams, the bending moment M cannot be considered approximately as aligned with the major axis of the cross-section. The actual moment along the major axis is actually smaller than M . This discrepancy is not considered in the moment-to-displacement plots for long beams. However, because the long beams are controlled by serviceability which happens when the rotation angle is small, such a discrepancy caused by large rotation angle will affect the conclusion of this thesis.

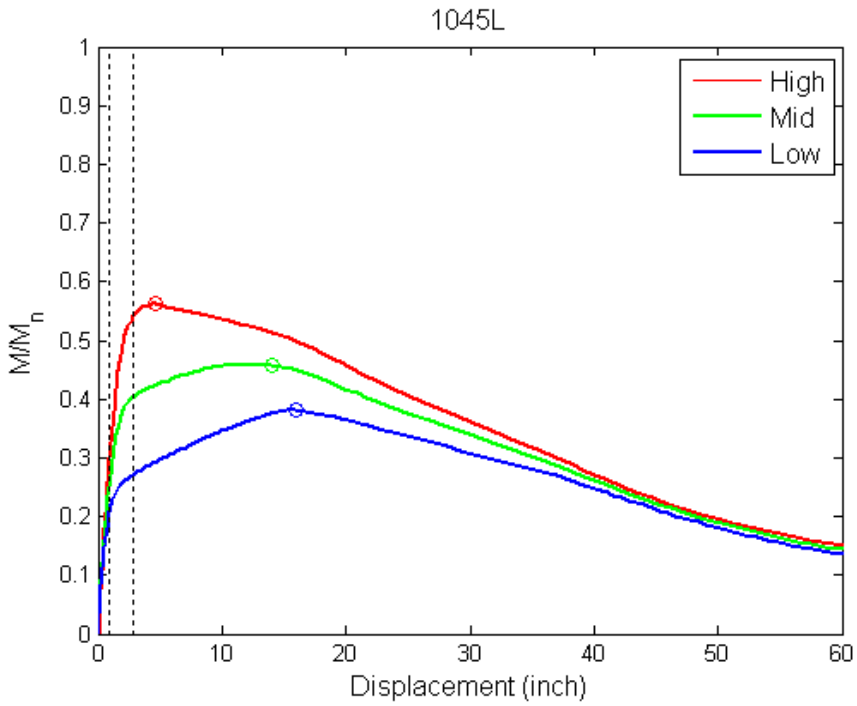

Figure 57 Moment-displacement diagram- L1 beam

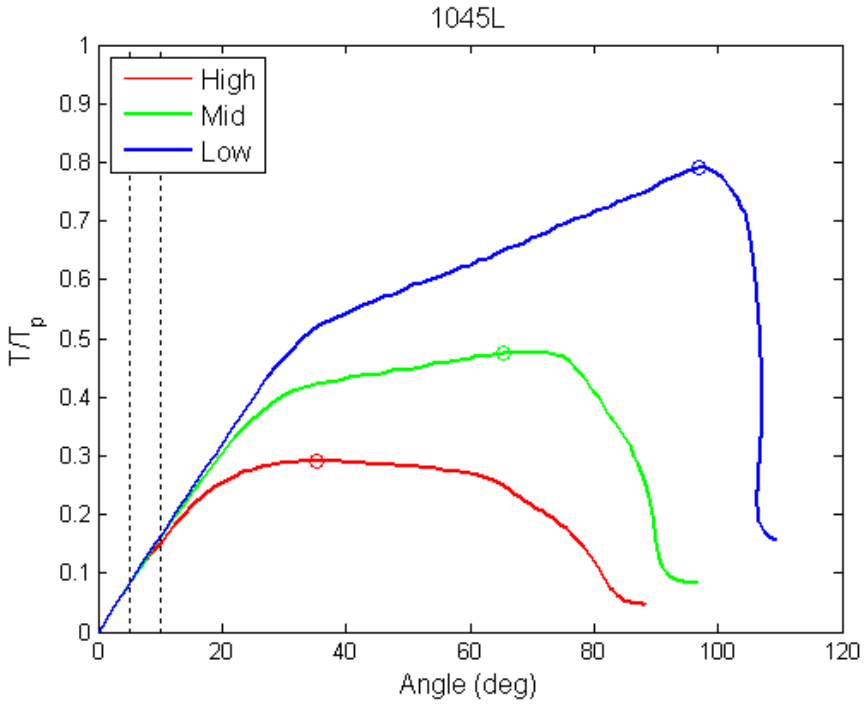

Figure 58 Torque-rotation angle diagram, L1 beam

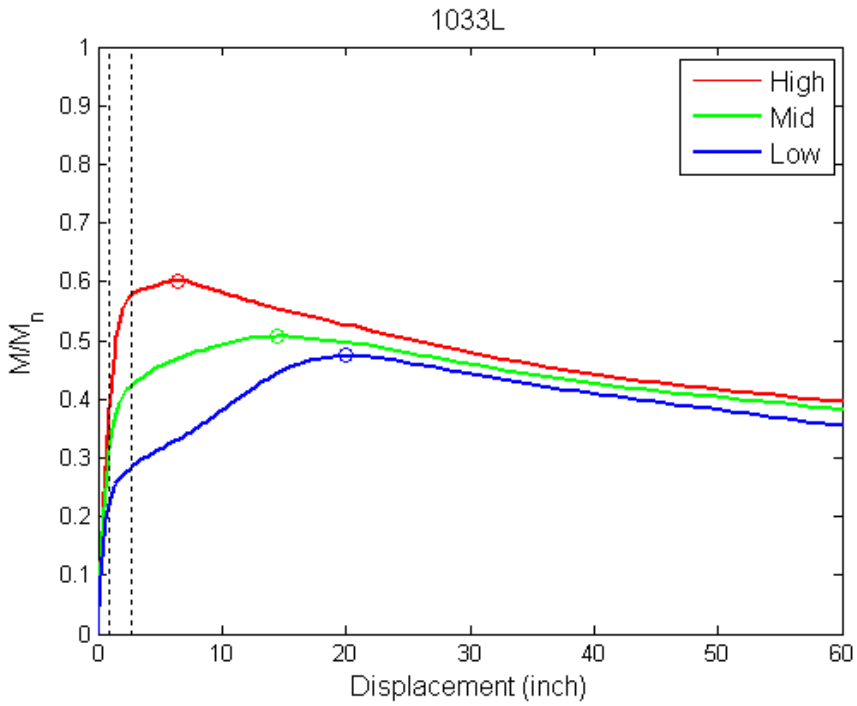

Figure 59 Moment-displacement diagram, L2 beam

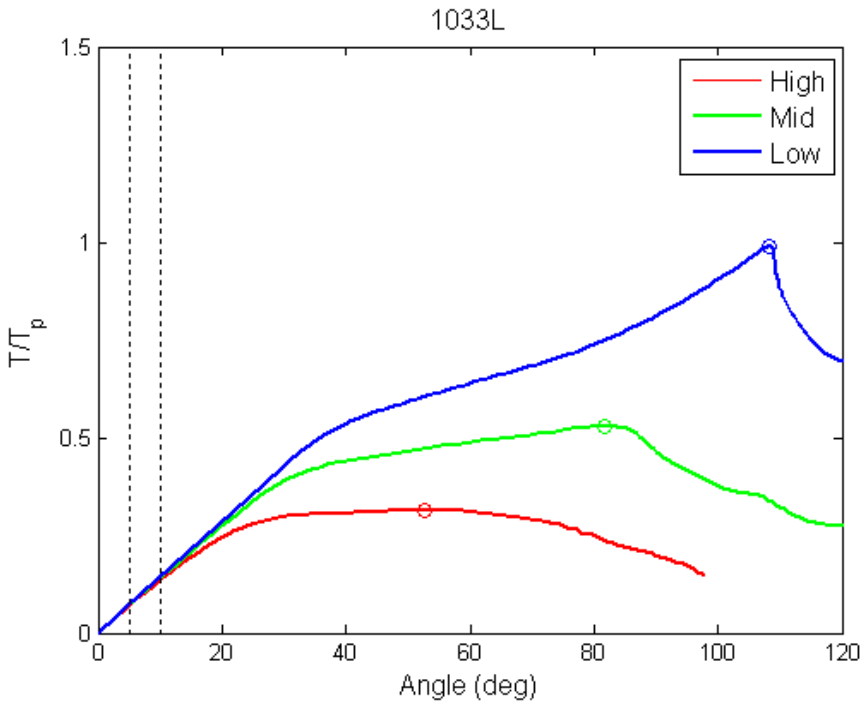

Figure 60 Torque-rotation angle diagram, L2 beam

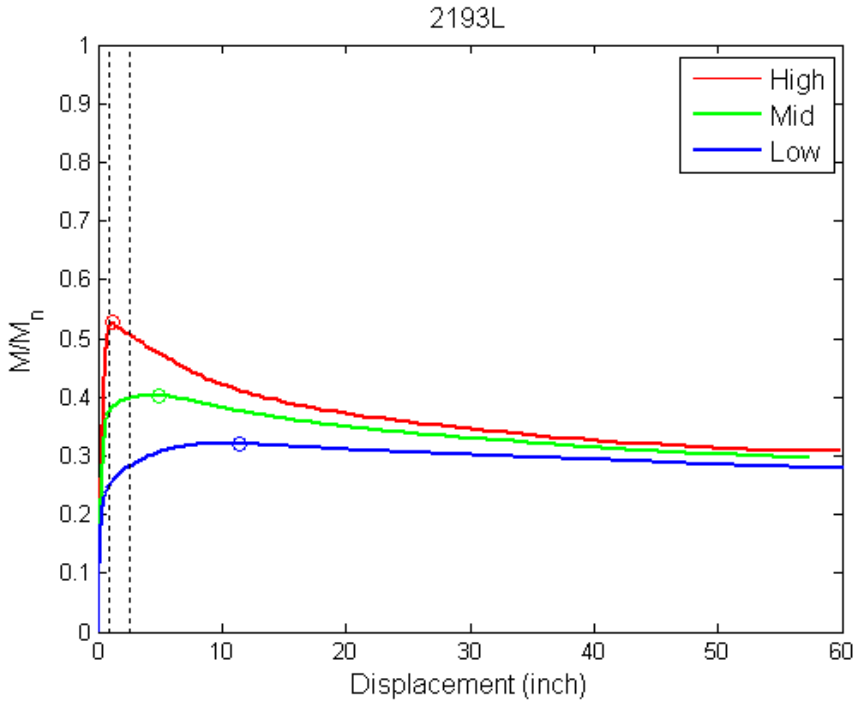

Figure 61 Moment-displacement diagram, L3 beam

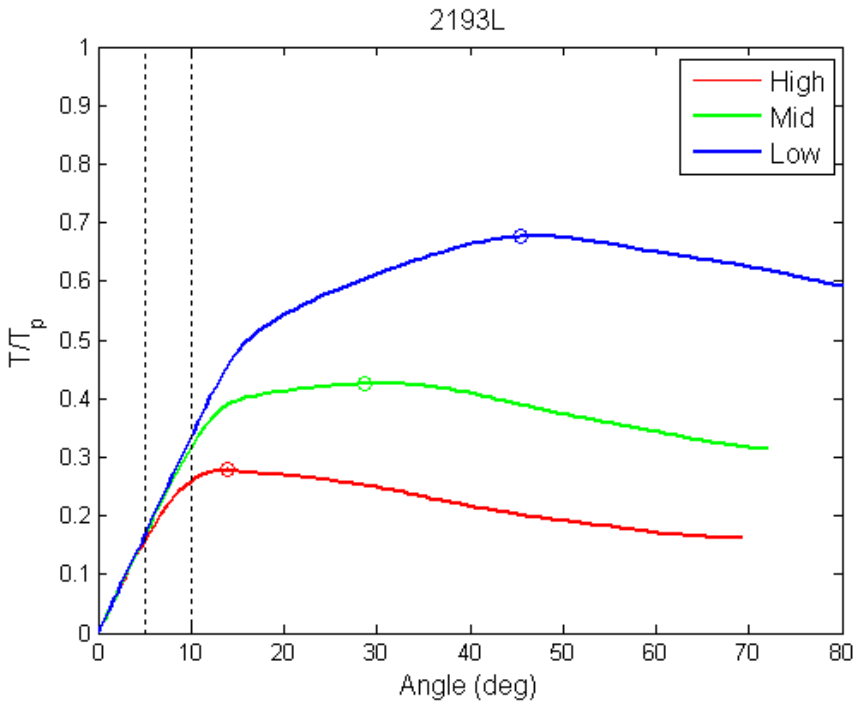

Figure 62 Torque-rotation angle diagram, L3 beam

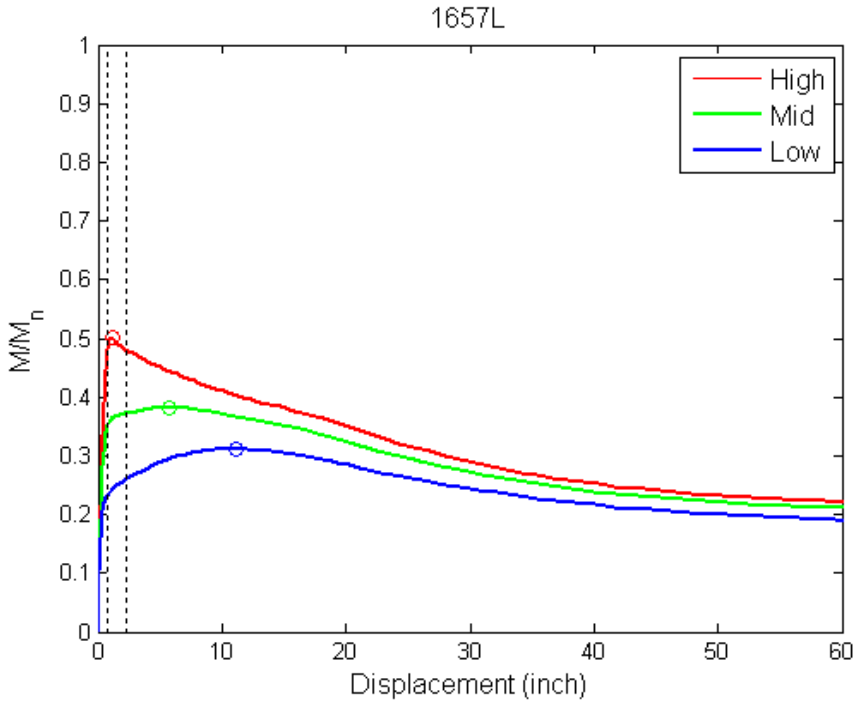

Figure 63 Moment-displacement diagram, L4 beam

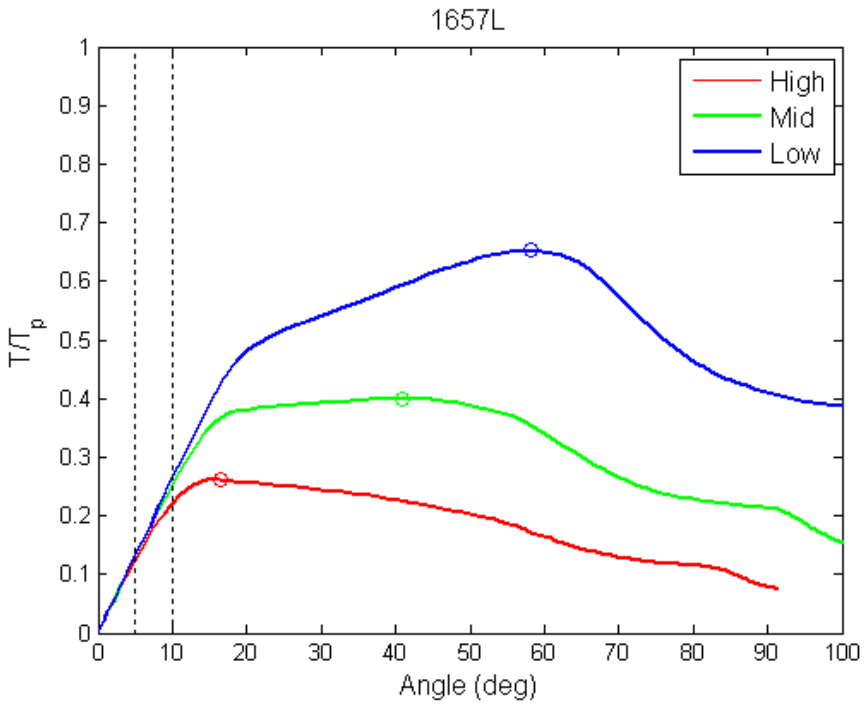

Figure 64 Torque-rotation angle diagram, L4 beam

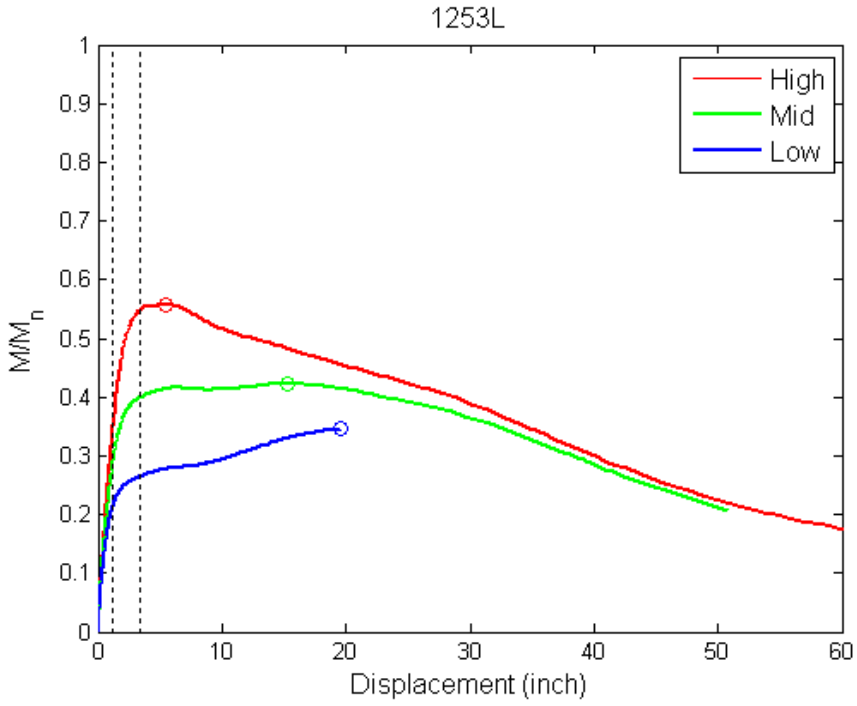

Figure 65 Moment-displacement diagram, S5 beam

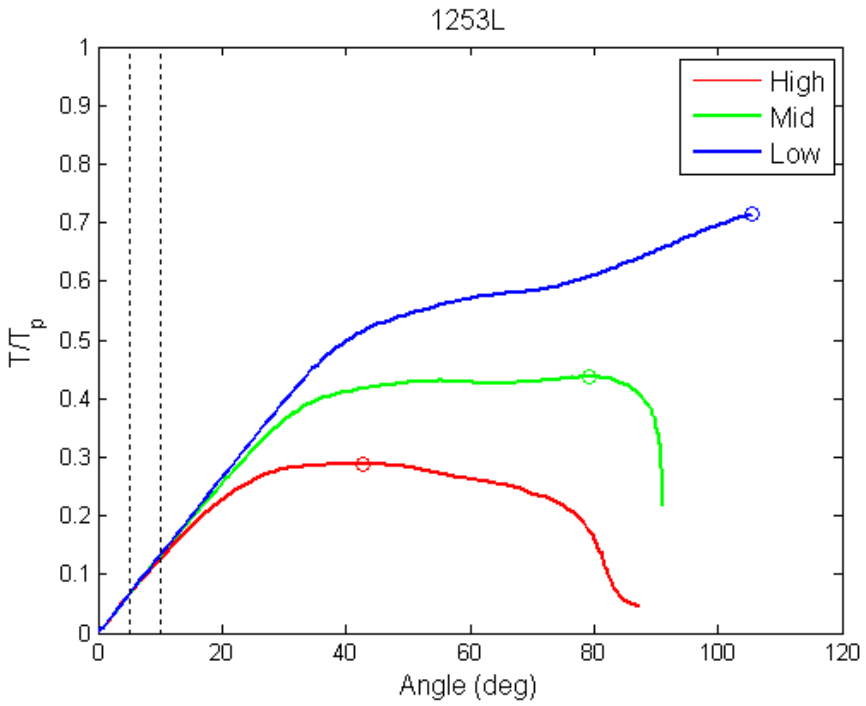

Figure 66 Torque-rotation angle diagram, L5 beam

Effects of other variables

The other two variables—ratio of warping-to-pure-torsional resistance, and torsional-to-flexural stiffness—were used to enrich the diversity of selections considered in the parametric study, and the FEM simulation results were analyzed to characterize the influence of these two variables. The moment-displacement and torque-rotation angle curves of different short beams are presented in Figure 67 to Figure 72. Recall that the first three sections (1045, 1033, and 2193) share a similar torsional-to-flexural stiffness, and have different warping-to-pure-torsional resistance. However, the FEM results do not exhibit any significant difference in the behavior or ultimate strength of these different sections. The other two sections (1657, 1253) share similar ratios of warping-to-pure-torsional resistance, and the fifth section (1253) has a larger torsional-to-flexural stiffness. As shown in Figure 67 to Figure 72, the 1253S beam behaves more rigidly for both flexure and torsion.

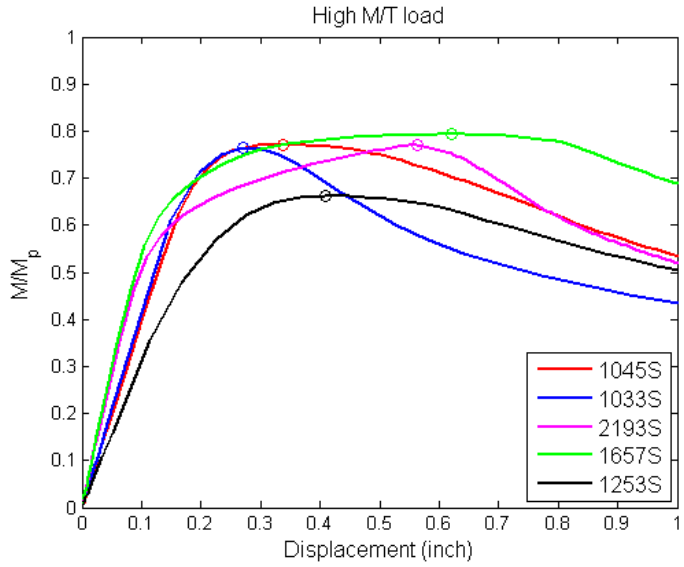

Figure 67 Moment-displacement diagram, short beams, high M/T load

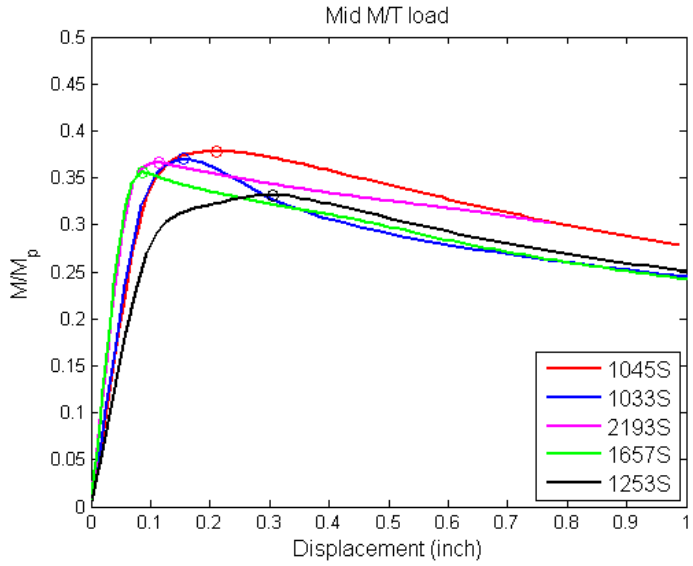

Figure 68 Moment-displacement diagram, short beams, mid M/T load

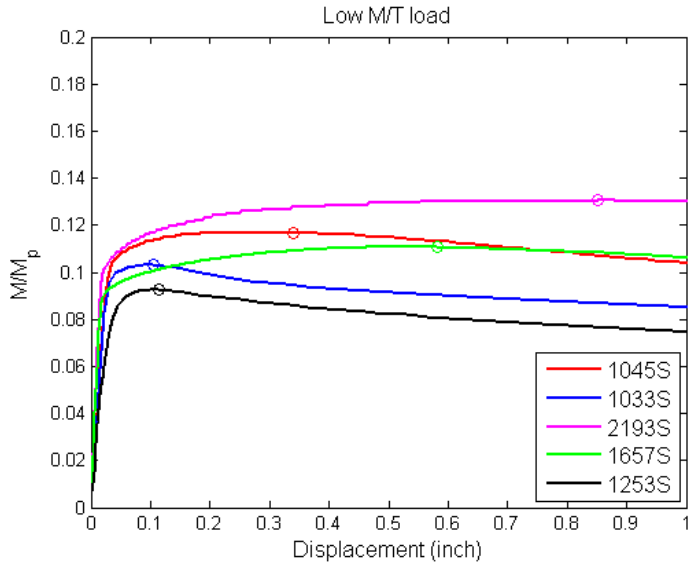

Figure 69 Moment-displacement diagram, short beams, low M/T load

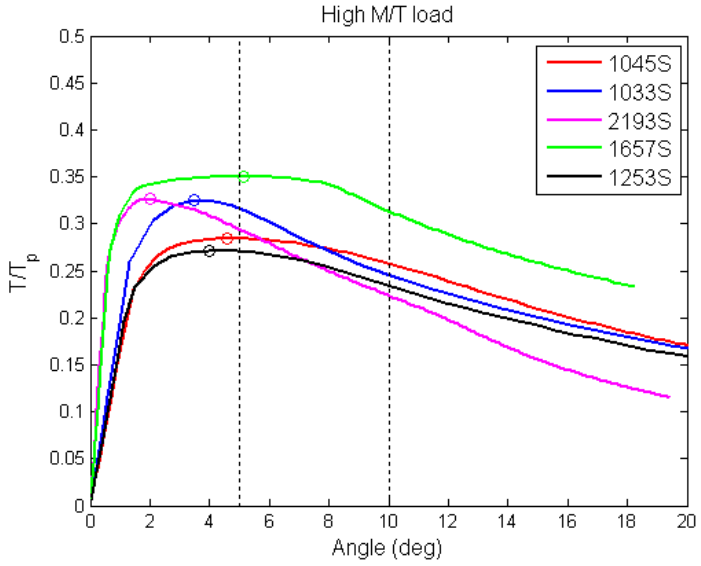

Figure 70 Torque-rotation angle diagram, short beams, high M/T load

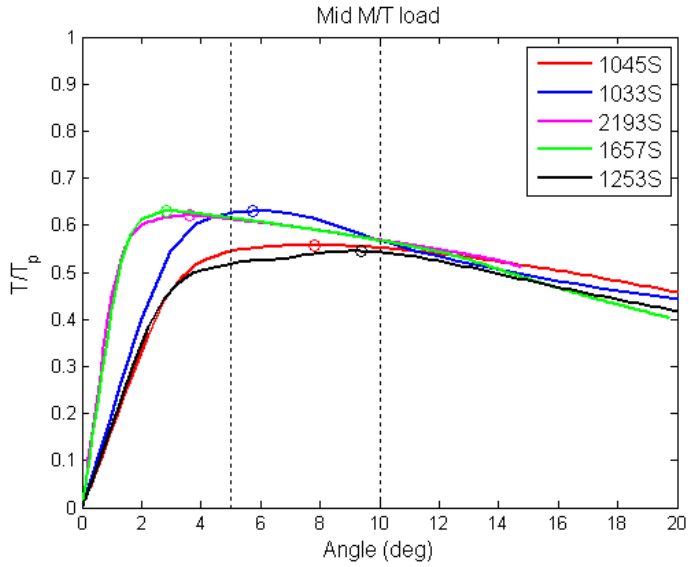

Figure 71 Torque-rotation angle diagram, short beams, mid M/T load

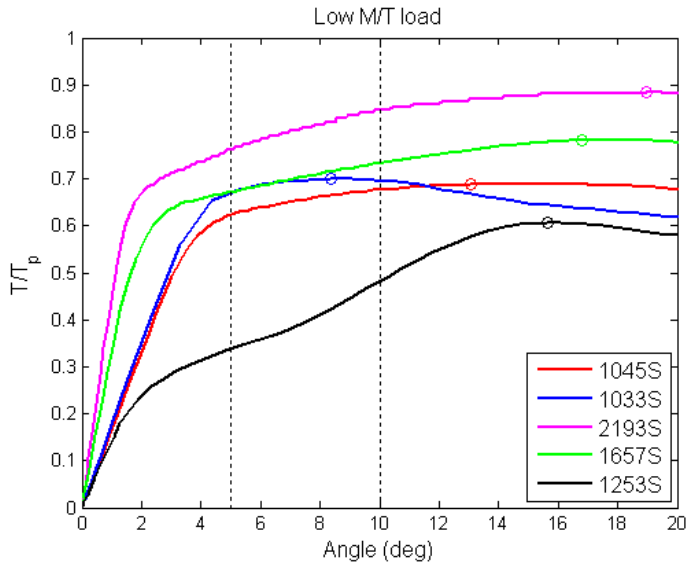

Figure 72 Torque-rotation angle diagram, short beams, low M/T load

4.6. Serviceability Check

Four serviceability criteria were examined for the FE simulation results, including two displacement criteria ($L/360$, $L/120$, where L is the length of the beam.) and two twist angle criteria (5 deg, 10 deg). The $L/360$ criterion was recommended by ASCE7-02 (2003). The less

restrictive $L/120$ criterion was introduced in this research for comparison. AISC (2010) requires checking the twist angle for serviceability, but does not provide any recommended value. Hence, the 5 deg, 10 deg are chosen based on the rule of thumb.

The serviceability check results for the short beams are shown in Table 16. In this table, the red color indicates the cases for which the corresponding serviceability criterion is violated when the beam reaches its ultimate strength (max load). For those regions marked by green color, the corresponding criterion is not violated when the beam achieves its ultimate strength. As shown in the table, the $L/360$ displacement serviceability criterion is violated by most of the short beams except for five out of the fifteen cases considered. Most of the short beams satisfy the 5 deg rotation angle serviceability criterion. Therefore, when designing beam members with a small slenderness ratio, checking the ultimate strength is as important as checking the serviceability.

Table 16 Serviceability results for short beams

	M/T	Max Load		U2=L/360		U2=L/120		UR3=5deg		UR3=10deg	
		M/M_p	T/T_p	M/M_p	T/T_p	M/M_p	T/T_p	M/M_p	T/T_p	M/M_p	T/T_p
S1	high	0.772	0.284	0.706	0.260	0.712	0.262	0.771	0.284	0.701	0.258
	mid	0.592	0.436	0.576	0.425	0.508	0.374	0.590	0.434	0.562	0.414
	low	0.378	0.557	0.378	0.557	0.328	0.482	0.370	0.545	0.375	0.552
S2	high	0.764	0.325	0.709	0.302	0.568	0.242	0.743	0.316	0.577	0.246
	mid	0.582	0.495	0.575	0.489	0.415	0.353	0.581	0.494	0.473	0.402
	low	0.370	0.630	0.365	0.621	0.281	0.478	0.368	0.626	0.334	0.569
S3	high	0.770	0.326	0.632	0.268	0.770	0.326	0.695	0.294	0.528	0.224
	mid	0.584	0.495	0.584	0.495	0.440	0.372	0.545	0.462	0.448	0.379
	low	0.366	0.620	0.357	0.605	0.322	0.545	0.361	0.612	0.335	0.568
S4	high	0.793	0.350	0.666	0.294	0.789	0.349	0.793	0.350	0.710	0.314
	mid	0.578	0.511	0.575	0.509	0.410	0.363	0.542	0.479	0.434	0.384
	low	0.356	0.630	0.341	0.603	0.301	0.531	0.348	0.615	0.321	0.567
S5	high	0.662	0.272	0.595	0.244	0.584	0.240	0.660	0.271	0.571	0.234
	mid	0.507	0.416	0.496	0.407	0.413	0.339	0.505	0.415	0.471	0.386
	low	0.332	0.544	0.329	0.539	0.275	0.451	0.316	0.518	0.331	0.543

The serviceability results of the long beams are shown in Table 17. Except for the L3 beam, all serviceability criteria are violated before the beam reaches the ultimate strength. For the L3

beam, the $L/120$ displacement serviceability criterion is not violated when the beam reaches its ultimate strength. Therefore, for beams with large slenderness ratios, serviceability is of more concern than ultimate strength.

The sequences at which different serviceability criteria and the ultimate strength are reached are shown in Figure 47 to Figure 66. In these figures, the $L/360$ and $L/120$ dashed lines in the moment-displacement diagrams represent the displacement serviceability criteria. The vertical dashed lines in the torque-rotation angle diagrams represent the 5 deg and 10 deg serviceability criteria. In these plots, the circles represent the ultimate strength of the beam. From these plots, it is easy to examine when the serviceability criteria are violated in the loading process. For each particular curve in these figures, if the circle is on the left of a dashed line, then the ultimate strength is reached before the serviceability criterion corresponding to the dashed line is violated. Otherwise, if a dashed line is on the left of the circle, then the serviceability is violated before the beam reaches its ultimate strength.

About 67% of the short beams considered in this research were controlled by the L/360 criterion, 7% were controlled by the L/120 criterion, 33% were controlled by the 5 degree twist angle criterion, and none of the short beams was controlled by the 10deg criterion. Hence, for the short beams it is necessary check both the deflection serviceability and the twist angle serviceability of the design result.

100% of the long beams considered in this research were controlled by the L/360, 5deg, and 10deg serviceability criterion, which suggests that serviceability is of major concern for the design of long beams. Furthermore, it is observed from Figure 57-66 that the loading curves intersect the 5deg serviceability dashed line at the beginning the loading process, much earlier than intersecting deflection serviceability lines or meeting the ultimate strength circles. This suggests that the long beams are mainly controlled by the twist angle serviceability.

Table 17 Serviceability Results of Long Beams

	M/T	Max Load		U2=L/360		U2=L/120		UR3=5deg		UR3=10deg	
		M/M_p	T/T_p	M/M_p	T/T_p	M/M_p	T/T_p	M/M_p	T/T_p	M/M_p	T/T_p
L1	high	0.562	0.292	0.297	0.154	0.541	0.281	0.153	0.080	0.292	0.151
	mid	0.458	0.476	0.260	0.270	0.404	0.420	0.078	0.081	0.154	0.160
	low	0.380	0.790	0.205	0.426	0.271	0.564	0.039	0.081	0.078	0.162
L2	high	0.602	0.315	0.370	0.194	0.578	0.302	0.134	0.070	0.260	0.136
	mid	0.506	0.529	0.304	0.318	0.423	0.442	0.068	0.071	0.135	0.141
	low	0.474	0.991	0.225	0.471	0.284	0.594	0.034	0.071	0.068	0.142
L3	high	0.527	0.278	0.514	0.271	0.506	0.267	0.297	0.157	0.490	0.258
	mid	0.403	0.425	0.375	0.395	0.399	0.421	0.157	0.166	0.299	0.315
	low	0.321	0.676	0.249	0.525	0.283	0.597	0.079	0.168	0.159	0.335
L4	high	0.501	0.263	0.475	0.249	0.482	0.252	0.239	0.125	0.421	0.221
	mid	0.382	0.400	0.350	0.367	0.372	0.390	0.125	0.131	0.242	0.254
	low	0.311	0.652	0.232	0.487	0.260	0.545	0.063	0.132	0.126	0.264
L5	high	0.557	0.288	0.335	0.173	0.547	0.283	0.127	0.066	0.246	0.127
	mid	0.422	0.436	0.279	0.288	0.401	0.414	0.064	0.066	0.127	0.132
	low	0.346	0.714	0.210	0.435	0.265	0.548	0.032	0.066	0.064	0.133

4.7. Discussion of Plastic Design Criteria for Combined Loading

In this section, based on the FEM simulation results of the parametric study, the strength limit state design approaches of Dinno and Merchant (1965) and Trahair and Pi (1994c) introduced in Chapter 2 are assessed in comparison with the AISC elastic design approach.

4.7.1. Ultimate Strength

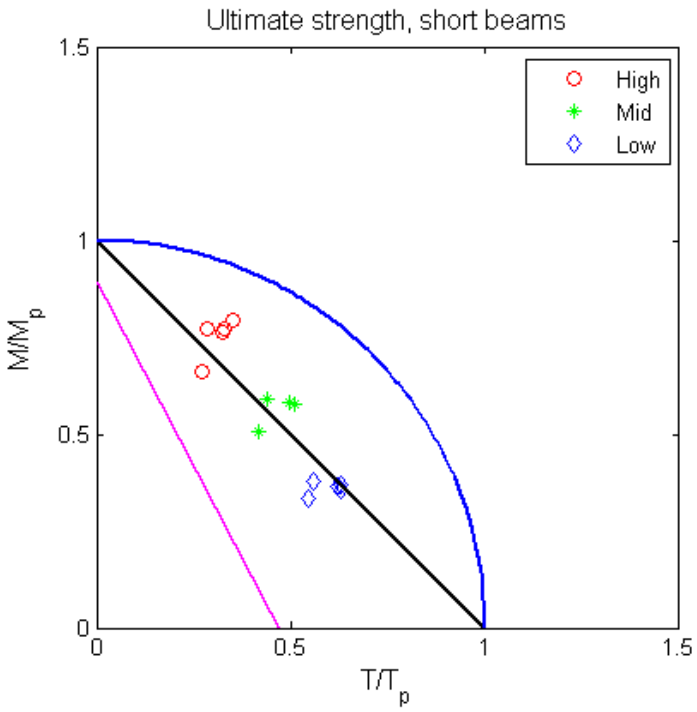

Figure 73 Design criterion comparison, ultimate strength, short beams

In Figure 73, the blue ¼ circle corresponds to the circle interaction criteria proposed by Dinno and Merchant (1965), and the black line is the design criteria by Trahair and Pi (1994c). The magenta line is the first yield criterion suggested by the current AISC design code which passes through two points $(0, M_y/M_p)$ and $(T_y/T_p, 0)$, where M_y/M_p and T_y/T_p are the average values for all short beams, since these values are very close for all short beams considered in this parametric study. These two points correspond to the first yield strength for the pure flexure and pure torsion cases, respectively. The ultimate strength results for the short beams are also plotted separately for each beam in Figures 74 to 78.

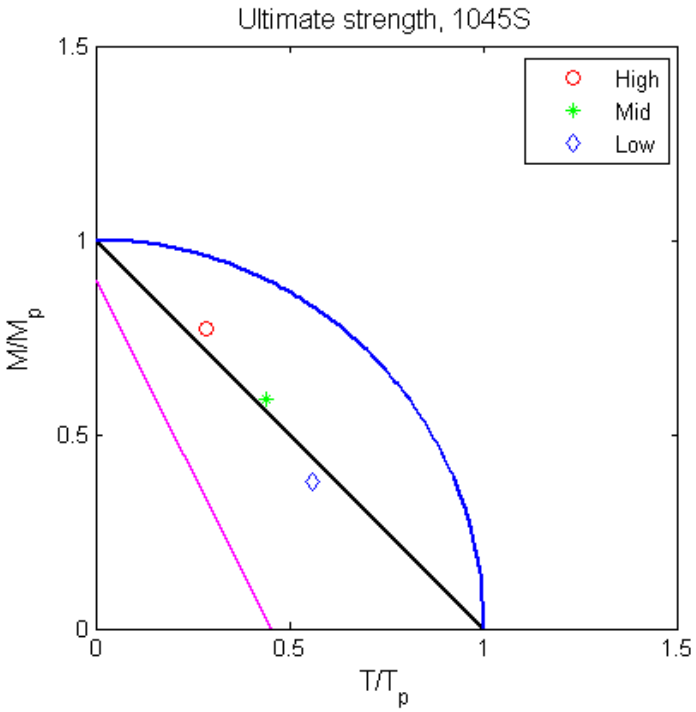

Figure 74 Design criteria comparison, ultimate strength, S1 beam

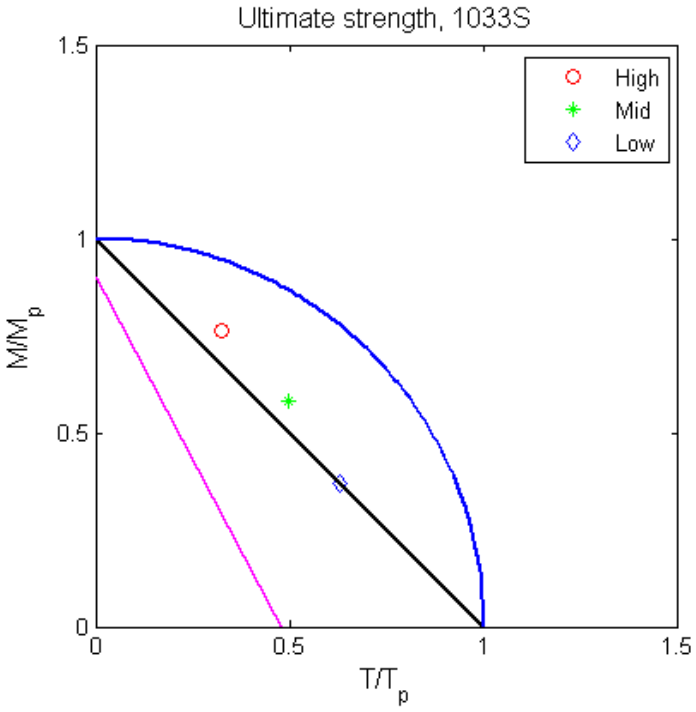

Figure 75 Design criteria comparison, ultimate strength, S2 beam

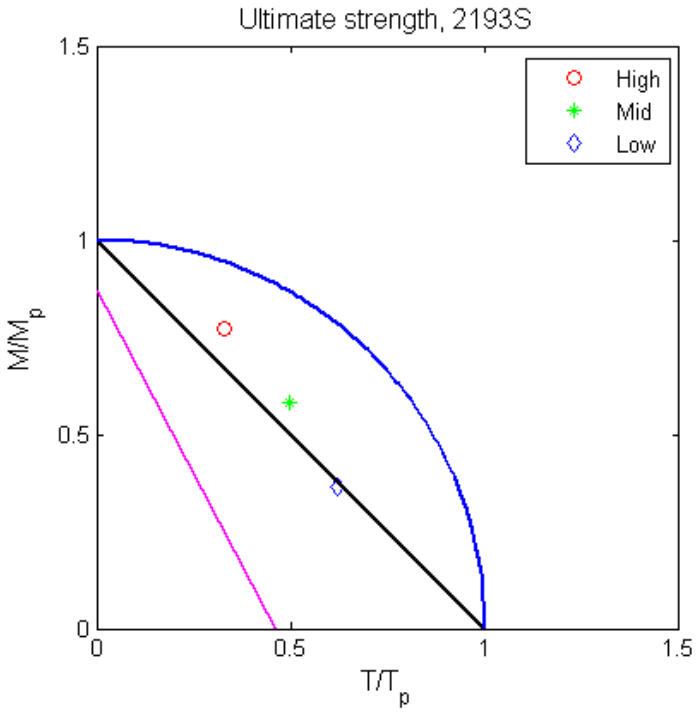

Figure 76 Design criteria comparison, ultimate strength, S3 beam

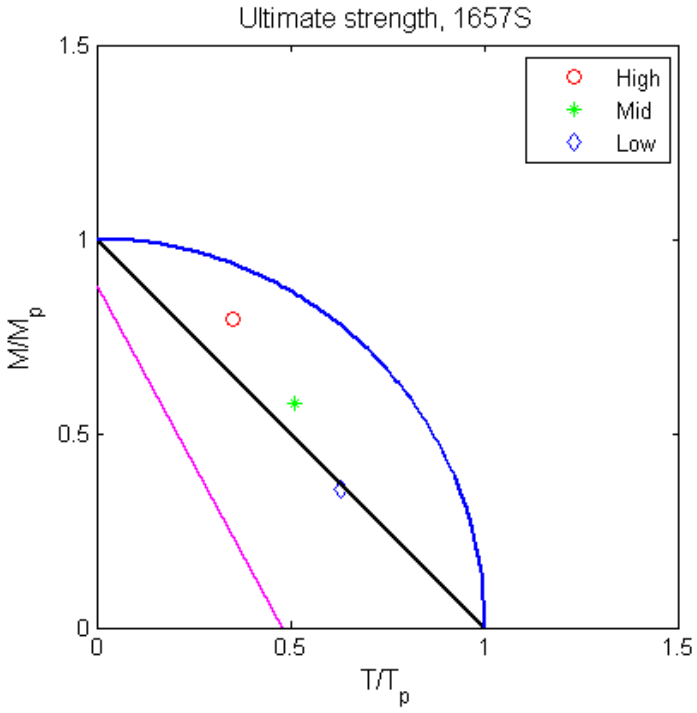

Figure 77 Design criteria comparison, ultimate strength, S4 beam

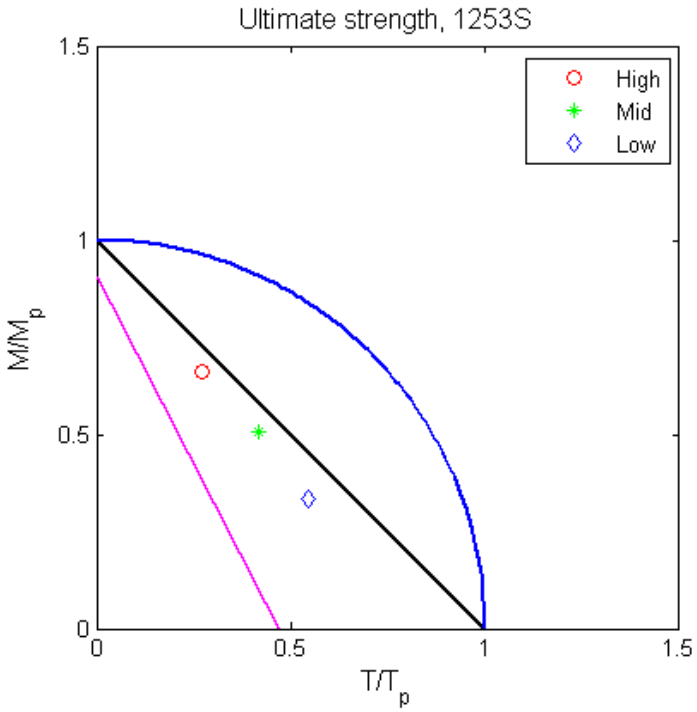

Figure 78 Design criteria comparison, ultimate strength, S5 beam

The ultimate strength FE simulation results for long beams are shown in Figures 79- 83. In these figures, the first yield criterion magenta line for long beams passes points (0,1) and $(T_y/T_p, 0)$. Because the values are very different for long beams, the ultimate strength results for each long beam are shown separately as shown separately in Figures 79- 83. The circle criterion is not plotted in these figures because they are not suitable for long beams which typically fail by lateral torsion buckling.

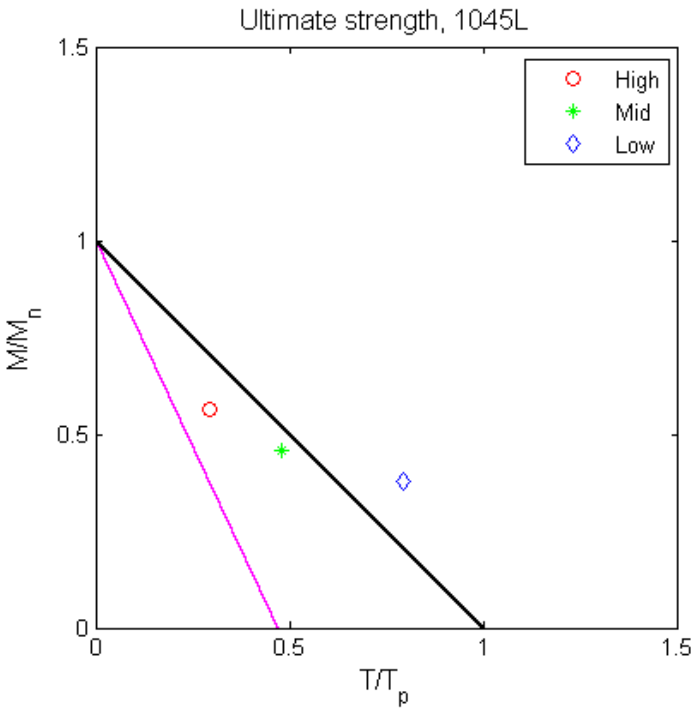

Figure 79 Design criteria comparison, ultimate strength, L1 beam

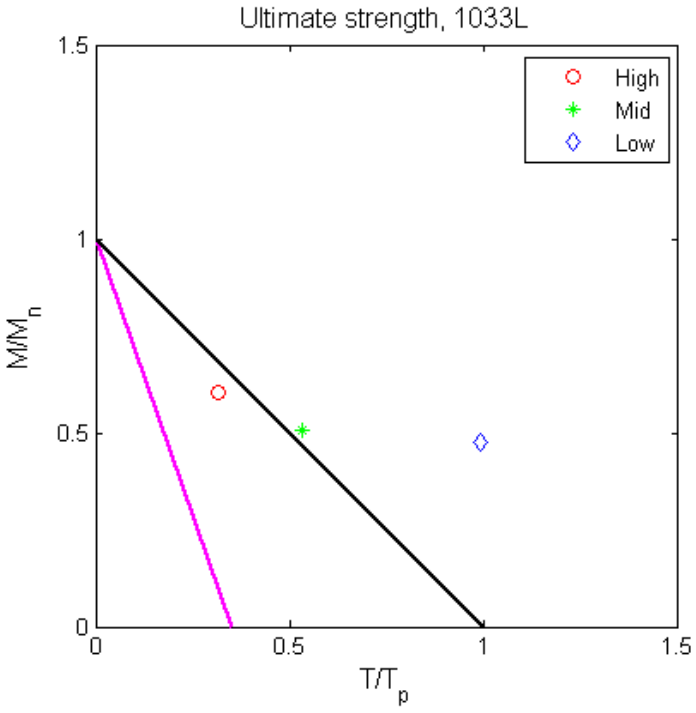

Figure 80 Design criteria comparison, ultimate strength, L2 beam

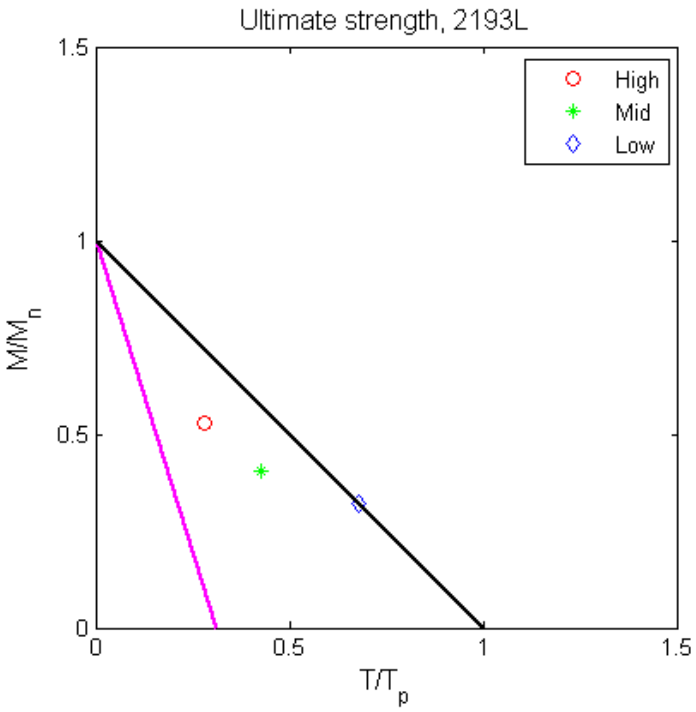

Figure 81 Design criteria comparison, ultimate strength, L3 beam

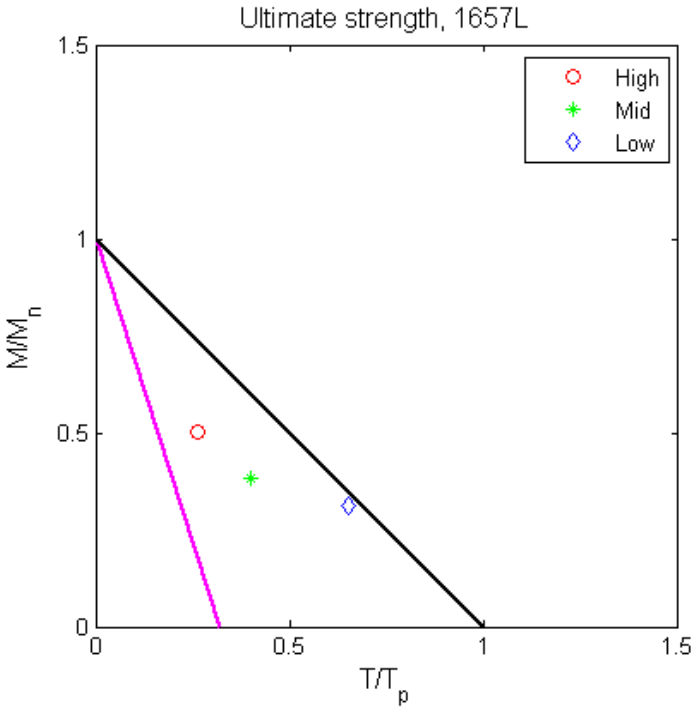

Figure 82 Design criteria comparison, ultimate strength, L4 beam

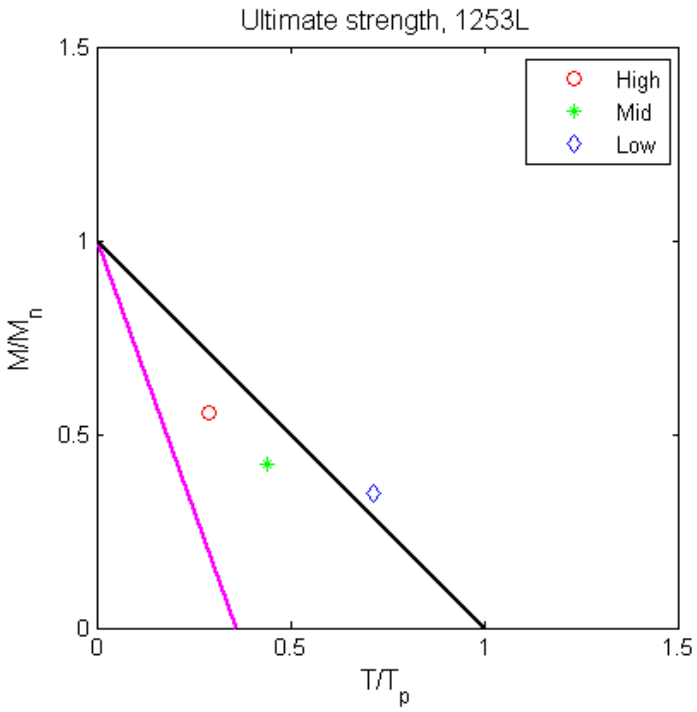

Figure 83 Design criteria comparison, ultimate strength, L5 beam

For short beams, as shown by Figures 74 to 78, all points, which correspond to the ultimate strength of different beam sections subject to loads with different moment-to-torque ratios, are located below the circular arc. Hence, as a design criterion, the circle criterion over-estimates the capacity of the beam subject to combined torsion and flexure, and is not safe for design purposes. The straight line criteria (black line) proposed by Trahair and Pi (1994c) provides a good match with the points. However, some points are slightly below this straight line, hence, this criterion also over estimates the strength of the beam in some cases. All ultimate strength points fall above the magenta line. Hence, for design purposes, the AISC design provision is conservative enough, and leads to safe design results. However, considering the distance between the ultimate strength points and this line, the design result could be over conservative.

For long beams, the ultimate strength points are again above the magenta lines. Most of these points fall between the magenta and the black lines. In some cases, such as the L2 beam results shown in Figure 80, the ultimate strength point for the low M/T ratio is much higher than the black line. These excessively large ultimate strength results are caused by severe deformation and distortion of the long beams. As will be shown in the next subsection, for the long beams, the serviceability would be more appropriate limit state rather than the ultimate strength.

4.7.2. Serviceability

Four serviceability criteria--including L/360, L/120 for deflection serviceability, and 5 degrees and 10 degrees for twist angle serviceability-- are used as the limit states. The results are used to assess the design criteria shown as straight lines in Figures 85- 87 for all short beams, and Figures 88-89 for a representative long beam. More serviceability plots are available in Appendix B.

From Figures 85- 87, it is obvious that the black line still provides a good estimation when these serviceability criteria are used as the limit state. For the long beam, as shown in Figure 89, the twist angle serviceability criterion is violated at a very early stage of the loading process. Specifically, the twist serviceability controlled strength is very close to the origin and the first yield elastic design provision by AISC considerably overestimates the strength of the long beam. A similar conclusion holds for other long beams.

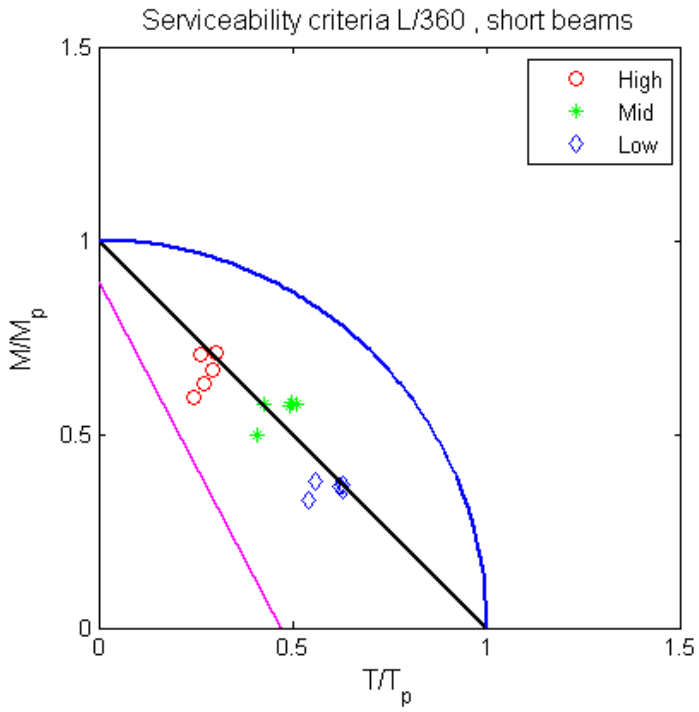

Figure 84 Design criterion comparison, L/360 displacement serviceability, short beams

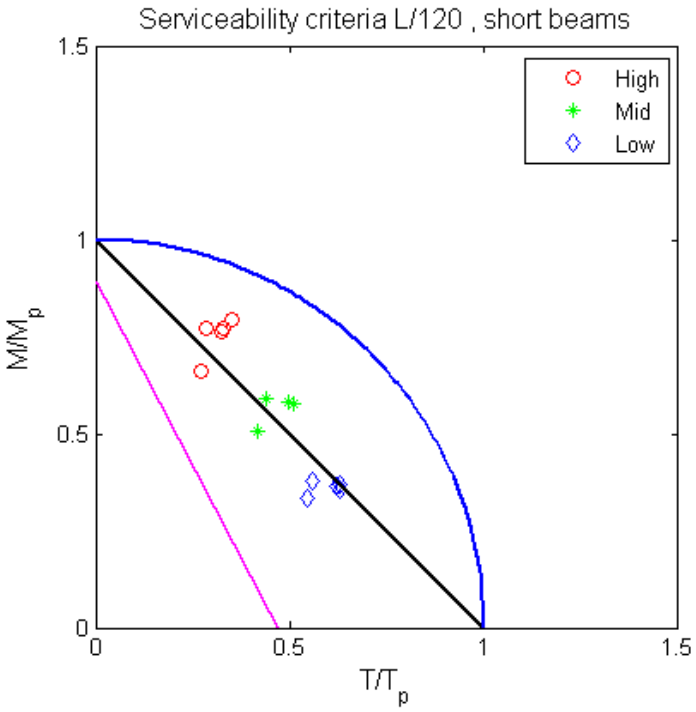

Figure 85 Design criterion comparison, L/120 serviceability, short beams

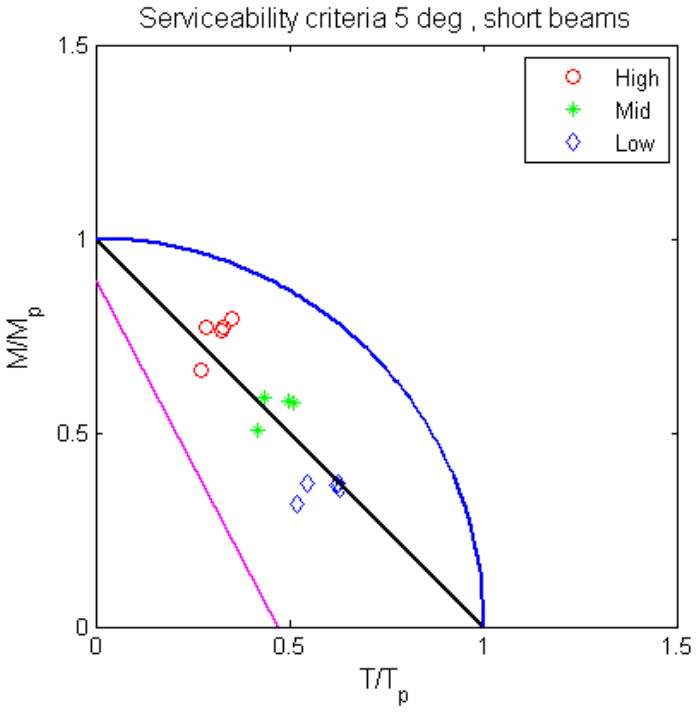

Figure 86 Design criterion comparison, 5deg serviceability, short beams

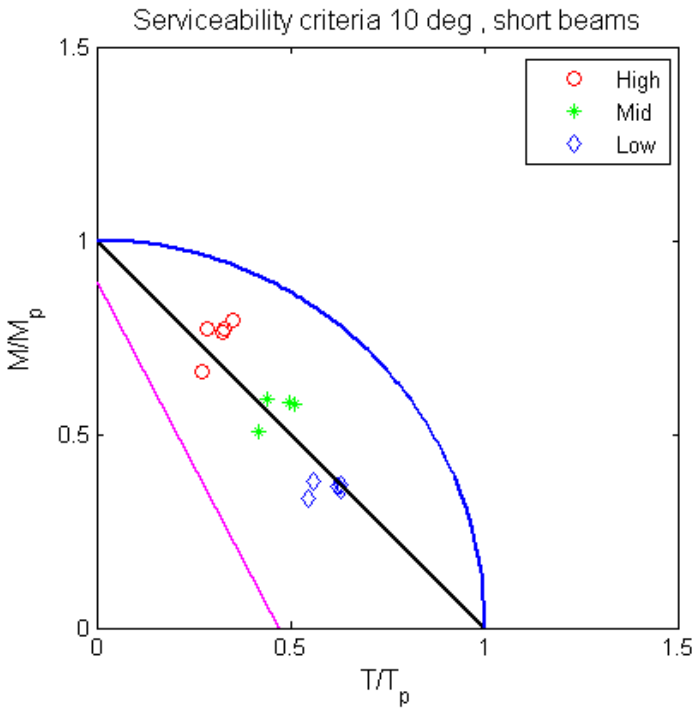

Figure 87 Design criterion comparison, 10deg serviceability, short beams

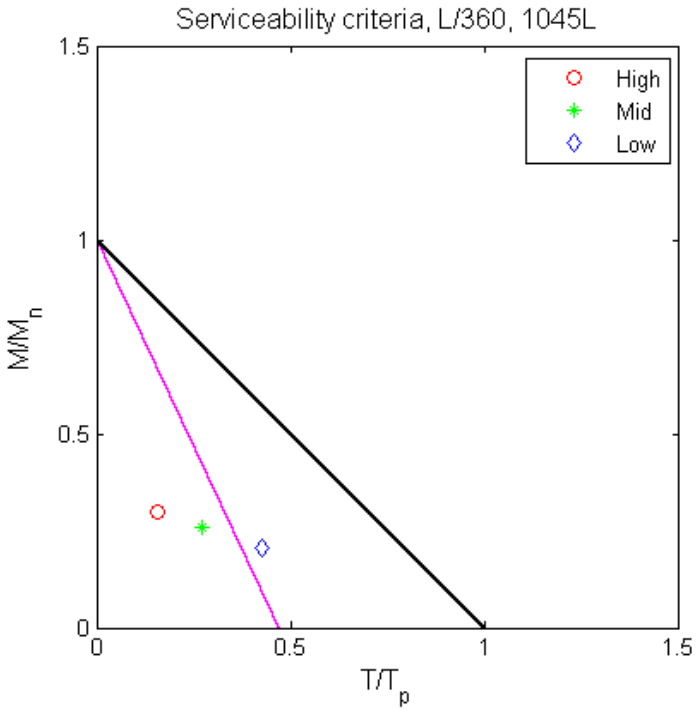

Figure 88 Design criteria comparison, L/360 serviceability, L1 beam

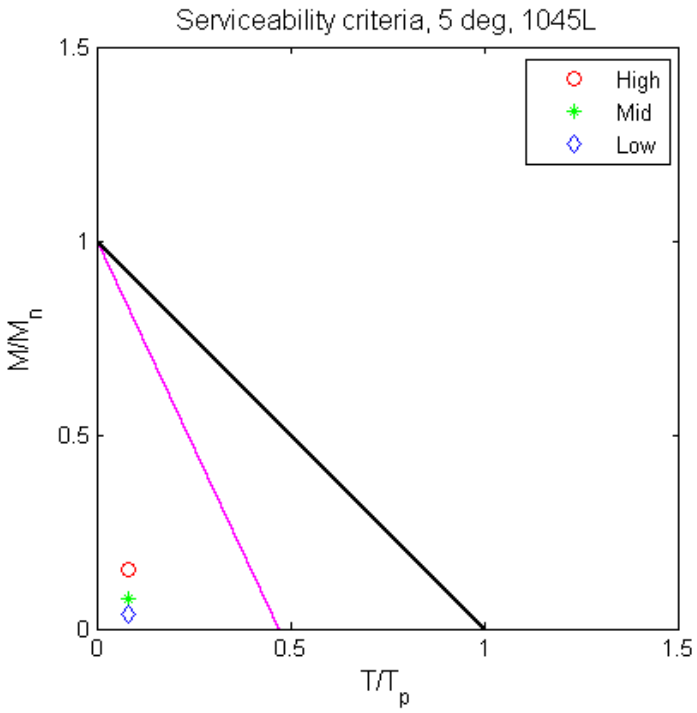

Figure 89 Design criteria comparison, 5 deg serviceability, L1 beam

4.8. Summary

In this chapter, a parametric study for the combined flexure and torsion of I-shaped beams using FE models verified in the previous chapter was presented. According to the FE analysis results, the moment-to-torque ratio affects the inelastic behavior and the ultimate strength of all I-shaped beams considered in this study. The slenderness ratio also has a strong influence on the failure mechanism of the I-shaped beams. It is noted that, for beams with a high slenderness ratio, the serviceability in terms of deflection and rotation are of major concern, since these quantities increase quickly to an unacceptable extent before the ultimate strength of the beams are reached.

Chapter 5 Summary, Conclusion, and Recommendations

5.1. Summary

In this thesis, a study of the behavior of I-shaped steel beams subject to a mixture of flexural and torsional load was studied via the FEM approach was described. For this purpose, FEM models were developed and verified using experimental results documented in previous research. A parametric study including a total of 30 ABAQUS simulation cases was performed to investigate the influence of key parameters on the capacity and behavior of selected I-shaped beam members. The simulation results were analyzed to reveal the influences of different parameters on the beams' behavior, ultimate strength, and serviceability. The FE simulation results were also compared with the major design methods currently available for combined flexure and torsion. Among all design methods, the criterion proposed by Trahair and Pi (1994c) provides the closest estimation of the ultimate strength of all short beams, although this criterion slightly over-estimates the ultimate strength for some beam members.

5.2. Conclusions

Both of the two parameters considered in the parametric study of this thesis, the flexure-to-torque ratio and the beam slenderness ratio, showed strong influence on the behavior of the beam:

- A low flexure-to-torque ratio can considerably reduce the maximum flexure capacity of the beam. Therefore, it is important to consider the interaction between flexure and torsion for plastic design.
- The beam slenderness ratio affects both the failure mechanism (hence the ultimate strength) and the serviceability of the beams.

It is found that the selection of limit state has strong influence on the assessment result of plastic design criteria.

When the ultimate strength is used as the limit state, for short beams with small slenderness:

- The circle criterion by Dinno and Merchant (1965) tends to overestimate the strength of the beam, leading to unconservative design results for both the short and long beams;
- The design method described by Trahair and Pi (1994c) provides a good estimation of the ultimate strength of the short beams;

- The AISC design provision underestimates the ultimate strength of the beams, hence might produce over-conservative design result.

For long beams with large slenderness, none of the three plastic design methods mentioned above accurately predicts the ultimate strength. However, this is not a major concern since the ultimate strength is not the controlling criterion for long beams.

When the serviceability criteria are used as the limit state, the following can be concluded for short beams:

- The circle criterion cannot ensure the satisfaction of flexure and/or twist angle serviceability criteria;
- The design result using the method by Trahair and Pi (1994c) may violate some serviceability criteria in some cases, hence, should always be checked for serviceability;
- The AISC design provision produces design results satisfying all serviceability criteria.

For long beams, none of the design methods can ensure serviceability. Therefore, these criteria are not suitable for designing long beams with large slenderness ratio.

5.3. Recommendations

It is suggested that future research explores the following directions:

- A detailed parametric study for establishing an upper bound of the slenderness ratio within which the interaction equation by Trahair and Pi (1994c) provides an acceptable estimation of the ultimate strength of the beam.
- A study of the plastic behavior of I-shaped beam members subject to axial force in tension or compression, and the mixture of different loading types.
- The investigation of the beams' behavior subject to other types of loading such as distributed torsion and pressure on the flanges of the beam.

References

American Institute of Steel Construction (AISC). *2010 Steel Construction Manual*. 13th Ed. American Institute of Steel Construction, New York, NY.

ASCE7-02 (2003), Minimum Design Loads for Buildings and Other Structures, American Society of Civil. Engineers/Structural Engineering Institute (ASCE/SEI), 2nd Edition.

Augusti, G. (1966). "Full plastic torque of I-beams." *International Journal of Mechanical Sciences*, 8(10), 641-649.

Bathe, K.J., and Wiener, P.M. 1983. "On Elastic-Plastic Analysis of I-beams in Bending and Torsion." *Computer & Structures*, 17 (5-6), 711-718.

Bild, S., Chen, G., and Trahair, N.S. 1992. "Out-of-Plane Strengths of Steel Beams". *Journal of Structure Engineering*, ASCE, 118(8), 1987-2003.

Billinghurst, A. and Williams, J.R.L and Chen, G. and Trahair, N.S (1992) "Inelastic Uniform Torsion of Steel Members." *Computers and Structures*. 42(6), 887-894.

Boulton, N.S. (1962). "Plastic Twisting and Bending of an I-beam in which the Warping is Restricted." *International Journal of Mechanical Sciences*, 4, 491-502.

Bremault, D. and Driver, R.G. and Grondin, G.Y. (2008)."Limit States Design Approach for Rolled Wide Flange Beams Subject to Combined Torsion and Flexure." Structural Engineering Report. University of Alberta.

Chen, G. and Trahair, N.S., (1993). "Inelastic Nonuniform Torsion of Steel I-beams" *Journal of Constr. Steel Res*. Vol. 23, 189-207.

Chu, and Johnson ,R.B (1974)."Torsion in Beams With Open Section". *Journal of Structural Division*, ASCI, Vol. 100, ST7, 1397-1419.

Christopherson, D.G. (1940), "A theoretical Investigation of Plastic Torsion in an I-beam." *J. App. Mech*. Vol.7, pp1-4.

Dinno , K.S. and Gill , S.S (1964). “The Plastic Torsion of I-section with Warping Restraint”. *International Journal of Mechanical Sciences*, Vol. 6, 27-43.

Dinno, K.S. and Merchant, W. (1965). “A procedure for Calculating the Plastic Collapse of I-sections Under Bending and Torsion.” *The Structural Engineer*, 43(7), 219-221.

Driver, R.,G., and Kennedy, D.J.L. (1987). “Combined Flexure and Torsion of I-Shape Steel Beams”. Structural Engineering Report 144. University of Alberta.

Driver, R.G., and Kennedy, D.J.L. (1989). “Combined Flexure and Torsion of I-Shaped Steel Beams”. *Canadian Journal of Civil Engineering*, 16(2), 124-139.

Driver, R.G. (2000). “Ultimate Strength Modeling of Wide Flange Beams Subjected to Torsion.” Proceeding-2000 Annual Technical Session, Structural Stability Research Council, 24-26 July 2000, Memphis, TN.

ESDEP. (2012). The European Steel Design Education Programme. 2 June 2012 ‹http://www.fgg.uni-lj.si/kmk/esdep/master/wg07/l0820.htm›.

Estabrooks, B.G. and Grondin, G.Y. (2008). “Combined Bending and Torsion of Steel I-Shaped Beams”. Structural Engineering Report 276. University of Alberta.

Farwell, Jr.,C.R. and Glalmbos, T.V., (1969). "Nonuniform Torsion of Steel Beams in Inelastic Range." *ASCE Journal of the Structural Division* 95(ST12), 2813-2829.

Galambos, T.V. (1968). Structural Members and Frames. Prentice-Hall Englewood Cliffs New Jersey, 373.

Hancock, G.J. and Trahair, N.S. (1978). “Finite Element Analysis of the Lateral Buckling of Continuously Restrained Beam-Columns”. *Transactions of the Institution of Engineers*, Australia: Civil Engineering, CE20(2), 120-127.

Heins, C.P. (1975) “Bending and Torsional Design in Structure Members”. Lexignton Brooks, Lexignton, Mass., 367.

Hibbeler R.C. (2008). Mechanics of Materials. McGraw-Hill Book Co. New York, 364.

Hodge, P.G. (1959). Plastic Analysis of Structures. McGraw-Hill Book Co. New York, 364.

Kubo, C.G. Johnston, B.G. and Eney, W.J. (1956). “Non-Uniform Torsion of Plate Girders". *ASCE Transactions*, V121, 759-785.

Kollbruner C.F, Coric, B. and Hajdin,N. (1978). Elastic-Plastic Thin-walled I-section Beam Subjected to Bending and Warping Torsion: Comparison Between Theoretical and Experimental Results

Lin, P.H (1977). “Simplified Design for Torsional Loading of Rolled Steel Members,” *Engineering Journal of the AISC*, 3rd quarter, 98-107.

Megson, T.H. G (2005). Structural and Stress Analysis, Boston, MA. Elsevier Butterworth Heineman.

Nadai, A. (1931), Plasticity. McGraw-Hill, New York, N.Y.

Nadai, A. (1954), Theory of Flow and Fracture of Solids. McGraw-Hill New York, N.Y.

Osterrieder, P. and Kretzschmar, P. (2006). "First-Hinge Analysis for Lateral Buckling Design of Open Thin-Walled Steel Members." *Journal of Constructional Steel Research*, 62(1-2), 35-43.

Pastor, T.P., and Dewolf, J.T. (1979). “Beams with Torsional and Flexural Loads .”Journal of the Structural Division, ASCE Vol.105, No. ST3, 527-538.

Pi, Y.L. and Trahair, N.S. (1993a). “Inelastic Bending and Torsion of Steel I-beam”. Research Report No. R683. The University of Sydney.

Pi, Y.L. and Trahair, N.S. (1993b). “Inelastic Torsion of Steel Beams”. Research Report No. R679. The University of Sydney.

Pi, Y.L. and Trahair, N.S. (1994a). “Plastic Collapse analysis of Torsion”. Research Report No. R685. The University of Sydney.

Pi, Y.L. and Trahair, N.S. (1994b). “Torsion and Bending Design of Steel Members”. Research Report No. R686. The University of Sydney.

Pi, Y.L. and Trahair, N.S. (1994c). “Inelastic Bending and Torsion of Steel I-Beams”. *ASCE Journal of Structural Engineering*, 120(12), 3397-3417.

Pi, Y.L. and Trahair, N.S.(1995a). “Inelastic Torsion of Steel I-Section Beams”. *ASCE Journal of Structural Engineering*, 121(4), 609-620.

Pi, Y.L. and Trahair, N.S. (1995b). “Plastic Collapse Analysis of Torsion”. *ASCE Journal of Structural Engineering*, 121(10), 1389-1395.

Salmon,C.G., and Johnson J.E. (1980). Structures. 2nd edition Harper and Row Publishers, New York, 946.

Seaburg, P.A. and Carter, C.J. (2003). “Torsional Analysis of Structural Steel Members.”American Institute of Steel Construction, Chicago, IL.

Timoshenko, S.P. and Goodier. J.N. (1970) Theory of Elasticity, 3rd Ed, McGraw-Hill, New York,N.Y.
Walker, A.C. (1975). "Design and Analysis of Cold-formed Sections." International Textbook Co. LTD. London. 174.

Appendix A. Nomenclature

a	torsional resistance, in.
A	area of the cross-section, in.^{2}
b_f	the width of the flange, in.
B	flange bimoment, kip-in.^{2}
B_p	plastic flange bimoment, kip-in.^{2}
C_b	lateral-torsional buckling modification factor
C_w	cross-section wrapping constant, in.^{4}
d	distance between flange centroids, in.
E	young's modulus of steel, ksi
F_{cr}	buckling stress, ksi
G	shear modulus of elasticity, ksi
h	the height of the web, in.
I_w	warping section constant, in.^{4}
I_x	moment of inertial about the x axis, in.^{4}
I_y	moment of inertial about the y axis, in.^{4}
J	torsional constant, in.^{4}
k	shape factor
K	warping factor
l	length of the steel beam, in
L	distance between points of support
M	flexure moment, kip-in.
$M_{applied}$	applied flexure moment, kip-in.
M_{bx}	flexure-torsional buckling strength, kip-in.
M_{fp}	flange plastic moment, kip-in.
M_{ipc}	critical flexure moment, kip-in.
M_n	moment resistance capacity, kip-in.
M_{wp}	web plastic bending moment, kip-in.
M_p	flexure capacity, kip-in.
M_y	flexure moment about the y axis, kip-in.
P	concentrated load, lb.
q	distributed load, lb/in.
r_y	radius of gyration about weak axis, in.
S_w	warping static moment, in.^{4}
S_x	elastic section modulus
t_f	flange thickness, in.
T_{sv}	pure torsion, kip-in.
T_{up}	pure torsion plastic capacity, kip-in.
T_{wp}	warping torsion resistance, kip-in.
T_p	cross-sectional plastic capacity, kip-in.
t_q	distributed torque, kip
T_{shu}	pure torsion resistance, kip-in.
t_w	web thickness, in.
V	shear force, lb.
W_n	normalized warping function, in.^{2}
Z	plastic section modulus, in.^{2}
α_m	moment modification factor
α_s	slenderness reduction factor
ϕ_t	performance factor for torsion
$(\tau_{bf})_{\max}$	maximum shear stress in the flanges, ksi

τ_{sv} St. Venant shear stress, ksi

λ_{tp} normalized plastic collapse load factor

λ_{up} uniform torsion collapse load factor

λ_{wp} warping torsion collapse load factor

θ' rate of change of angle of rotation

$\theta''(z)$ the second derivative of the twist angle

$\theta'''(z)$ the third derivative of the twist angle

$(\tau_{svf})_{\max}$ maximum shear stress in the flange due to pure torsion, ksi

$(\tau_{svw})_{\max}$ maximum shear stress in the web due to pure torsion, ksi

$(\tau_f)_{\max}$ maximum shear stress in the flange, ksi

$(\tau_w)_{\max}$ maximum shear stress in the web, ksi

σ_w normal stress due to warping, ksi

σ_u ultimate tensile stress, ksi

σ_y minimum yield stress, ksi

ω_n normalized unit warping

Appendix B. Plots of Design Criteria Comparison

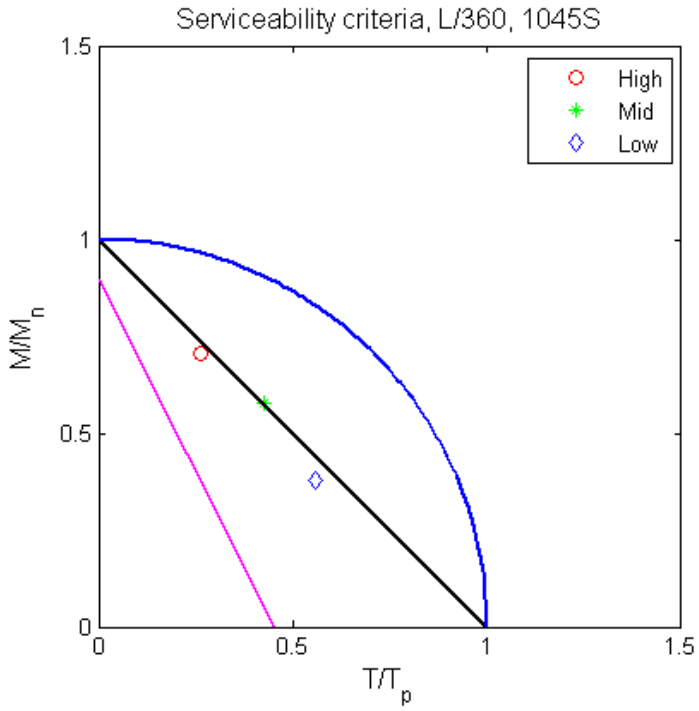

Figure 90 Design criteria comparison, L/360 serviceability, S1 beam

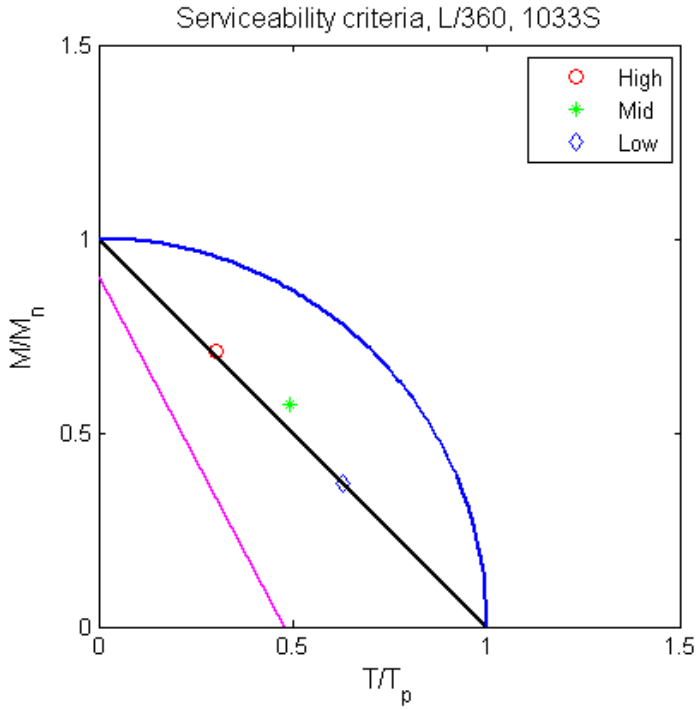

Figure 91 Design criteria comparison, L/360 serviceability, S2 beam

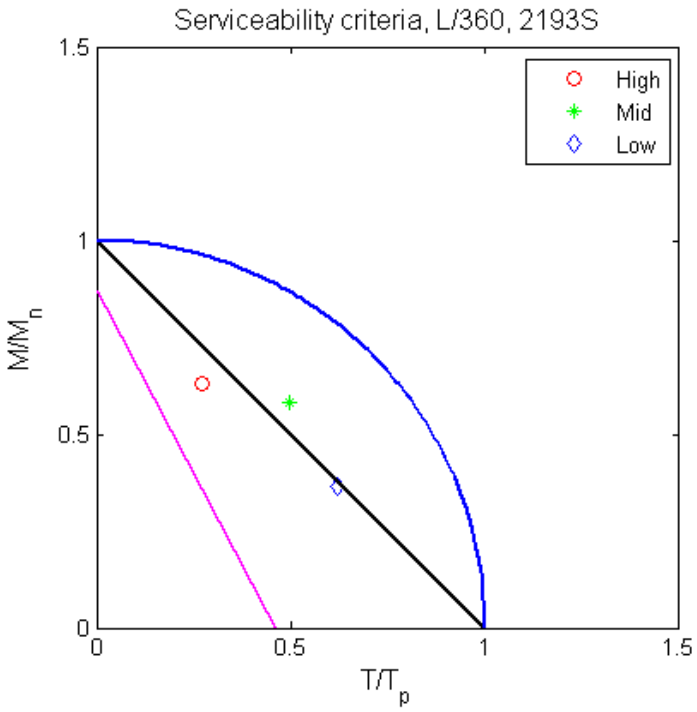

Figure 92 Design criteria comparison, L/360 serviceability, S3 beam

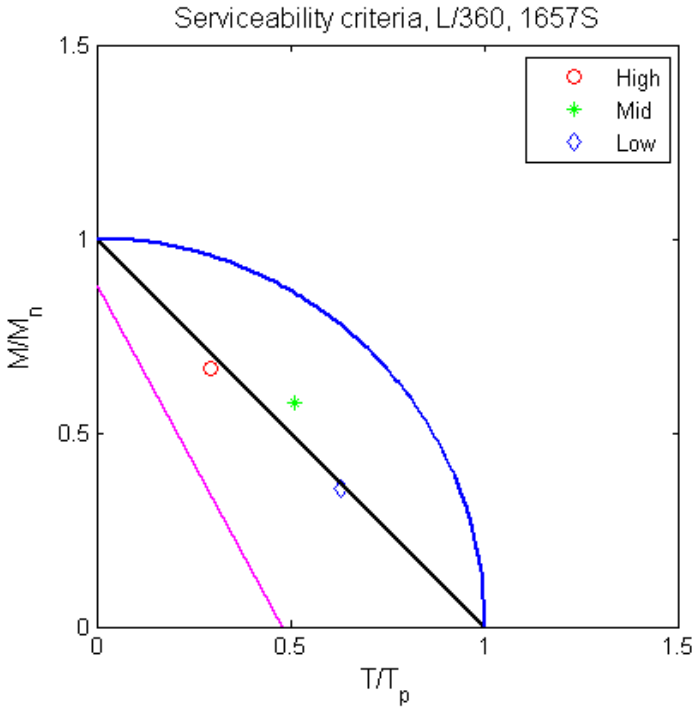

Figure 93 Design criteria comparison, L/360 serviceability, S4 beam

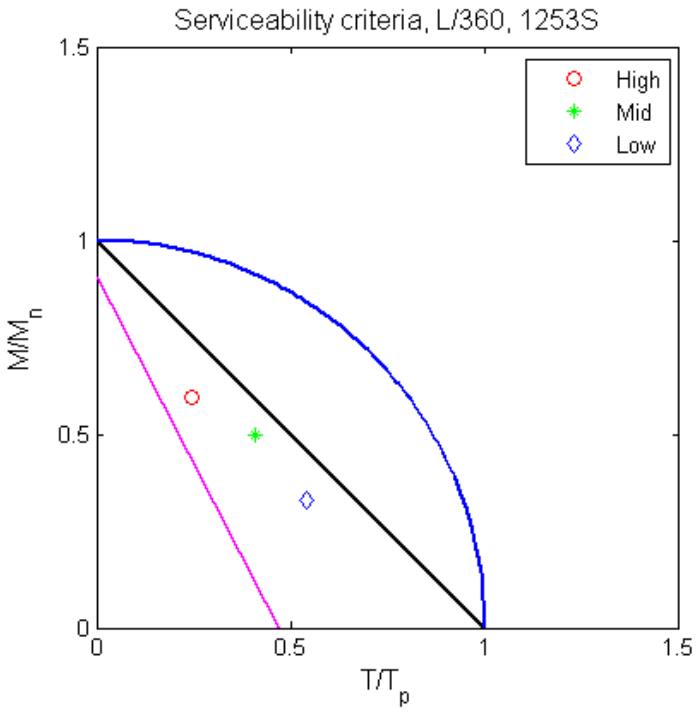

Figure 94 Design criteria comparison, L/360 serviceability, S5 beam

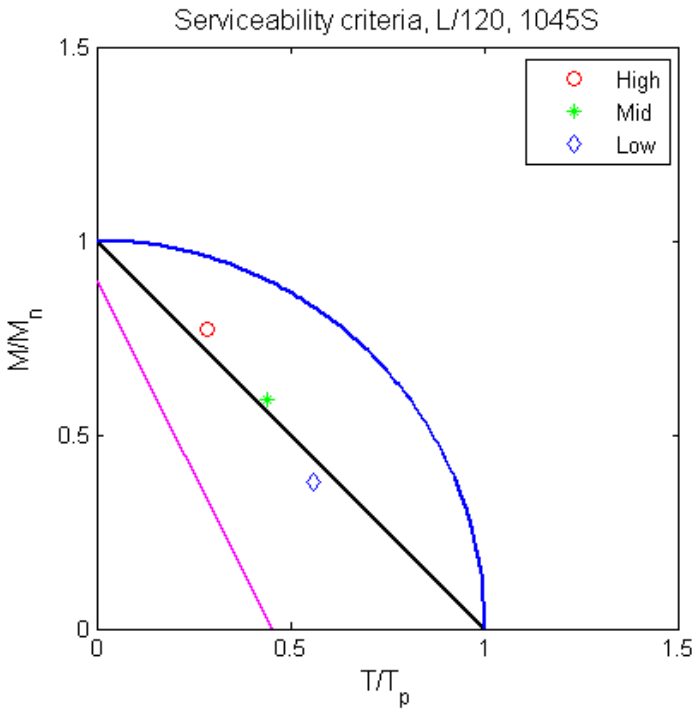

Figure 95 Design criteria comparison, L/120 serviceability, S1 beam

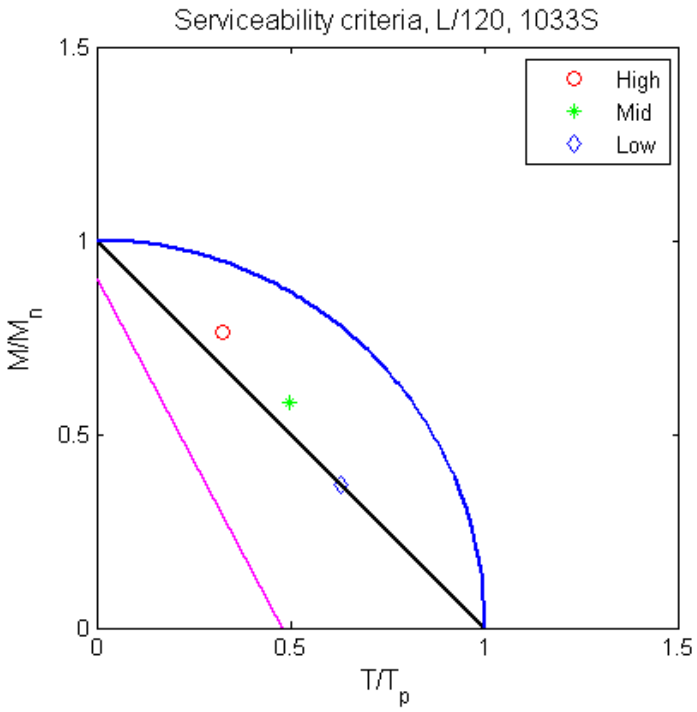

Figure 96 Design criteria comparison, L/120 serviceability, S2 beam

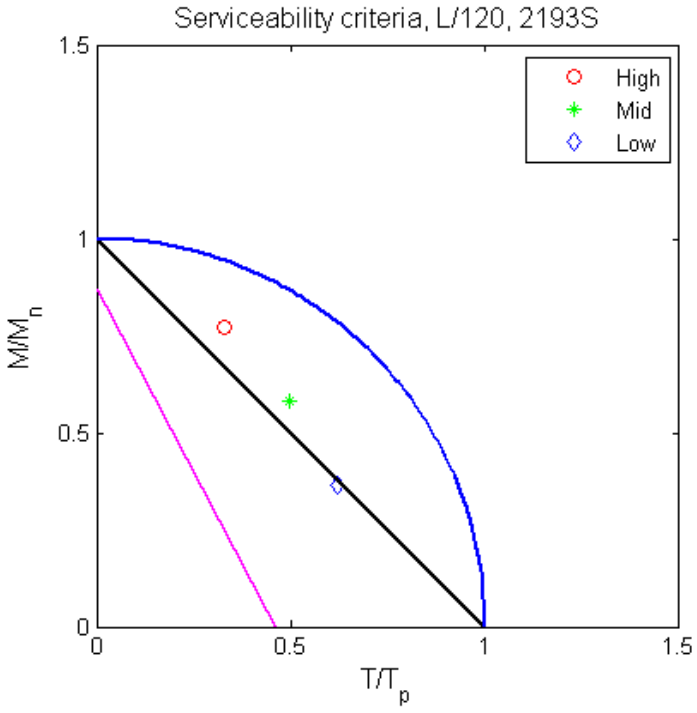

Figure 97 Design criteria comparison, L/120 serviceability, S3 beam

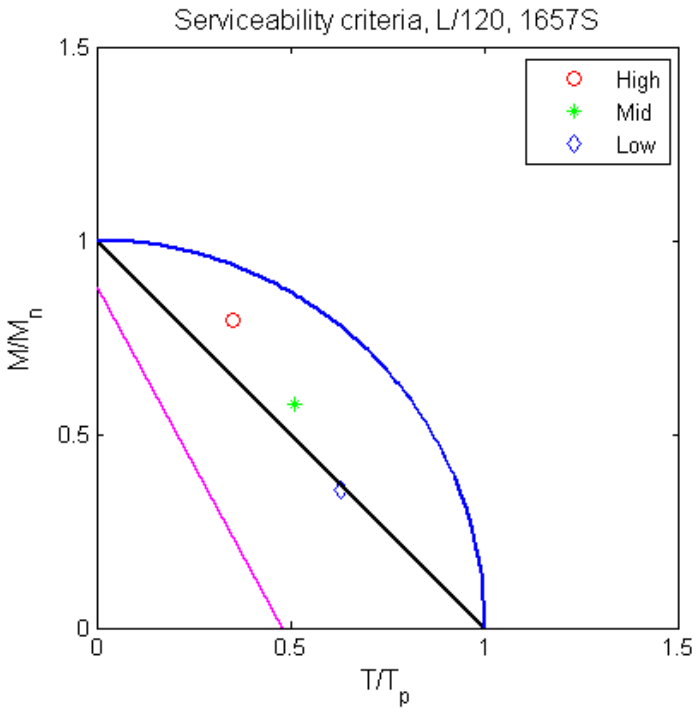

Figure 98 Design criteria comparison, L/120 serviceability, S4 beam

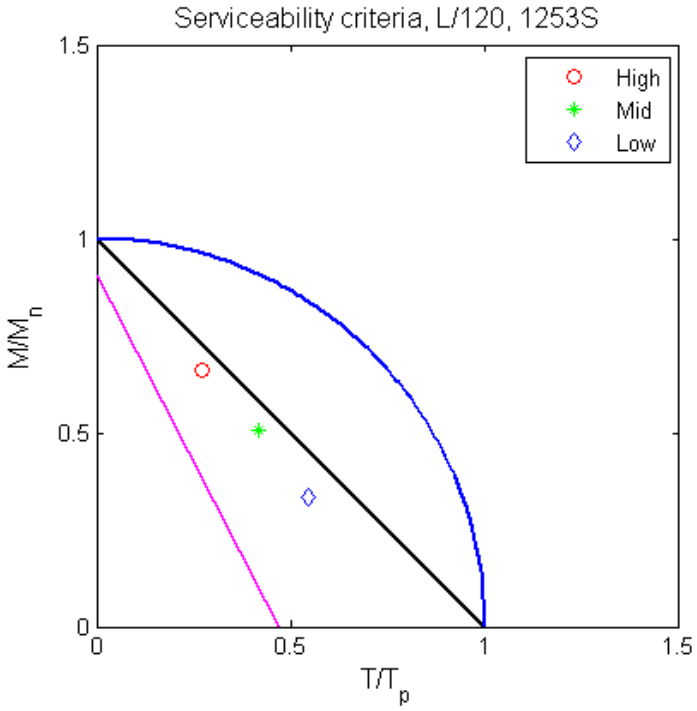

Figure 99 Design criteria comparison, L/120 serviceability, S5 beam

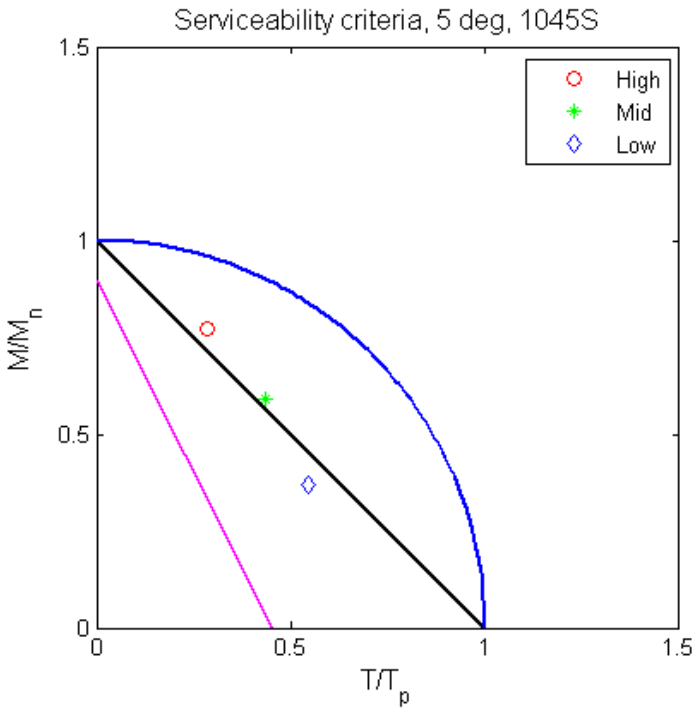

Figure 100 Design criteria comparison, 5deg serviceability, S1 beam

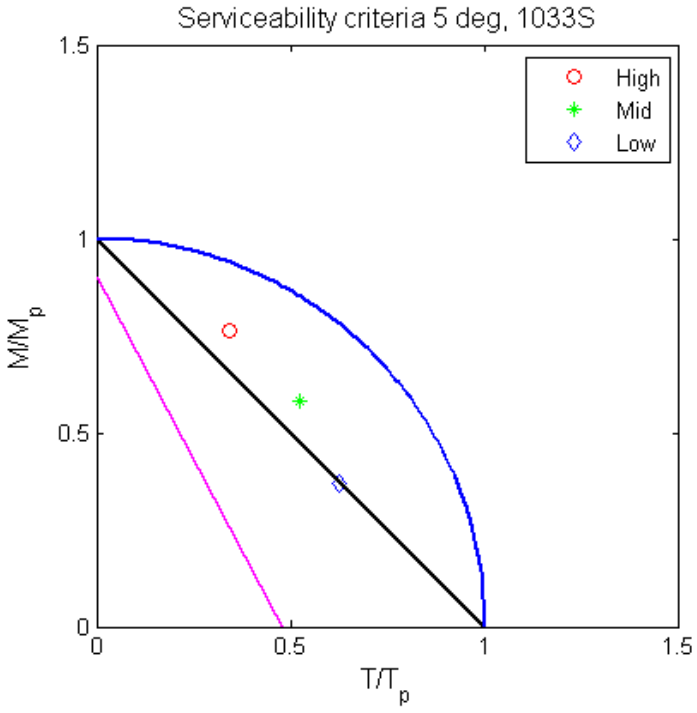

Figure 101 Design criteria comparison, 5deg serviceability, S2 beam

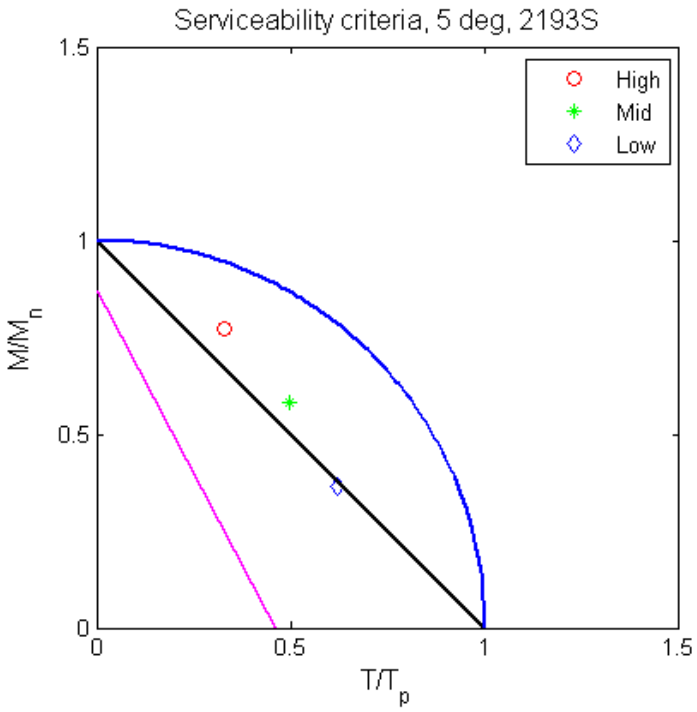

Figure 102 Design criteria comparison, 5deg serviceability, S3 beam

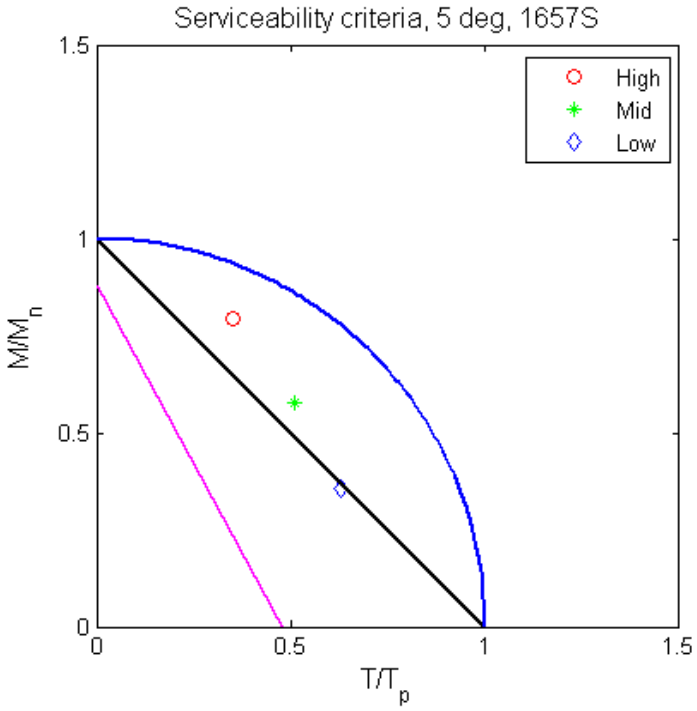

Figure 103 Design criteria comparison, 5deg serviceability, S4 beam

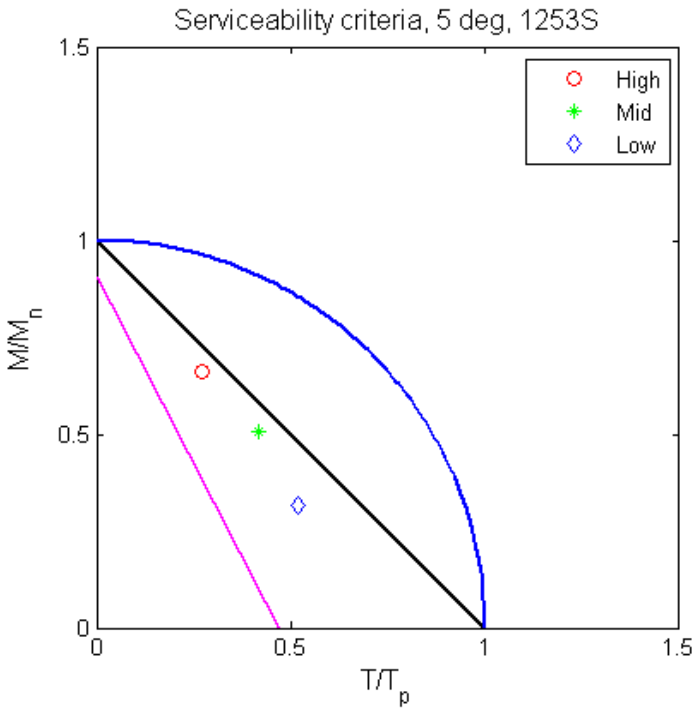

Figure 104 Design criteria comparison, 5deg serviceability, S5 beam

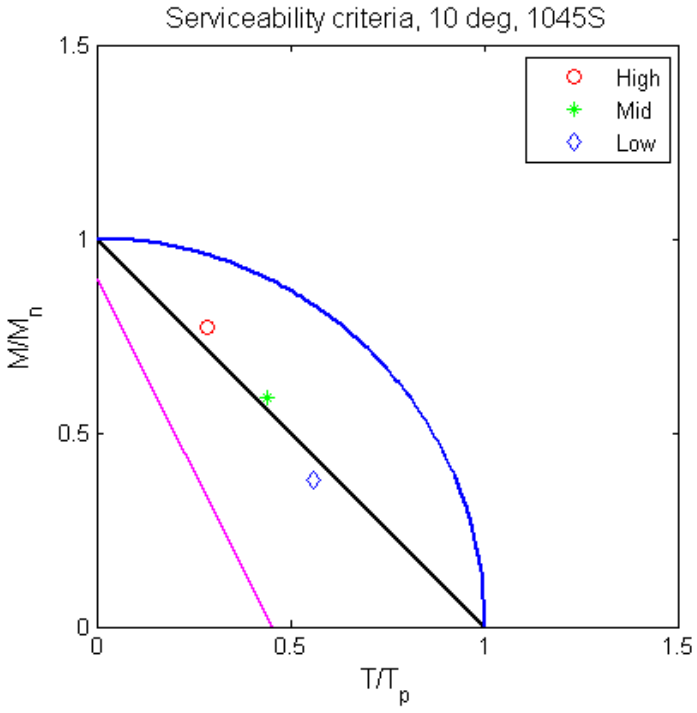

Figure 105 Design criteria comparison, 10deg serviceability, S1 beam

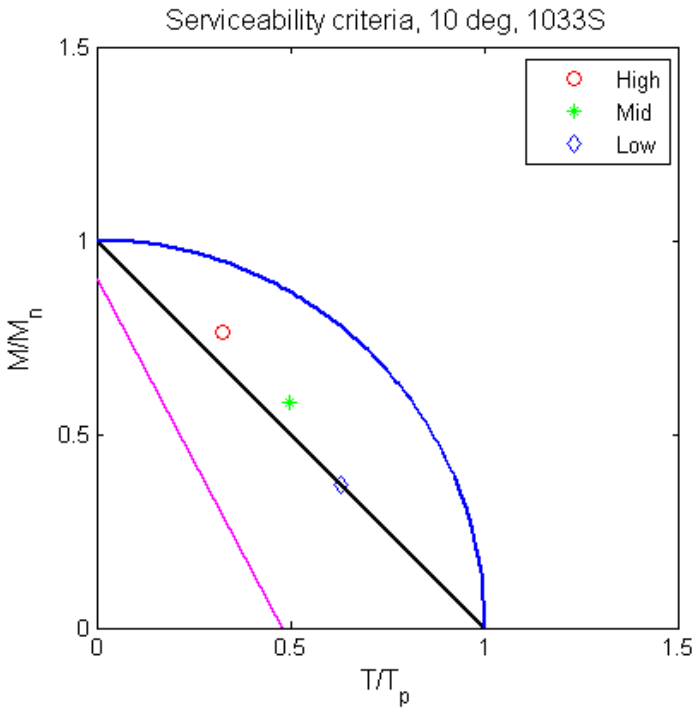

Figure 106 Design criteria comparison, 10deg serviceability, S2 beam

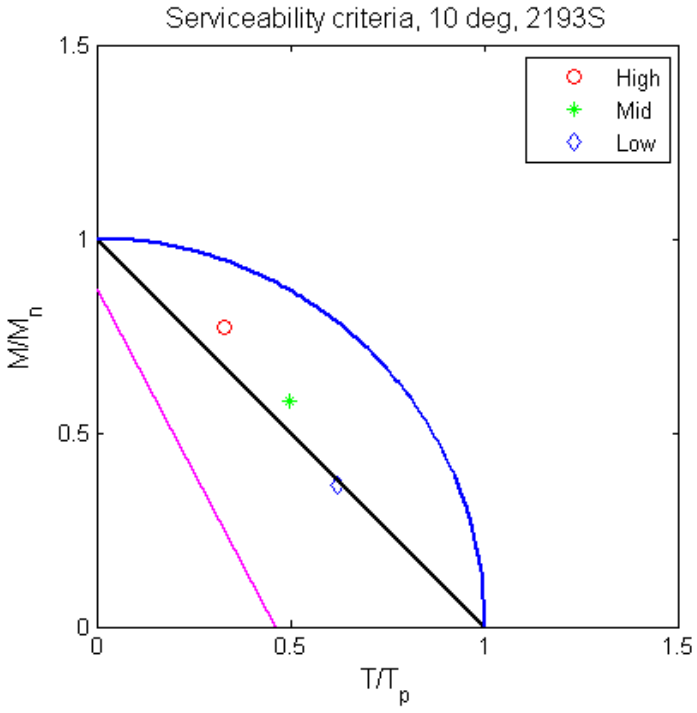

Figure 107 Design criteria comparison, 10deg serviceability, S3 beam

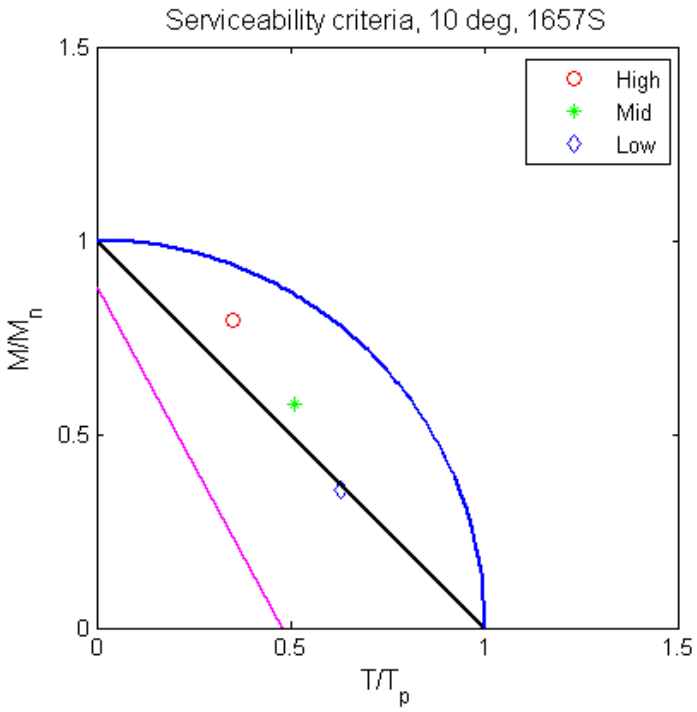

Figure 108 Design criteria comparison, 10deg serviceability, S4 beam

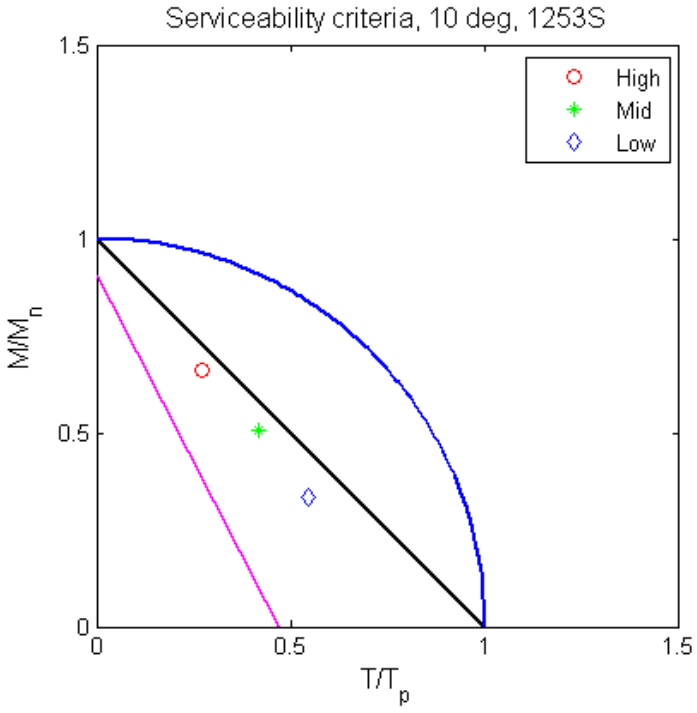

Figure 109 Design criteria comparison, 10deg serviceability, S5 beam

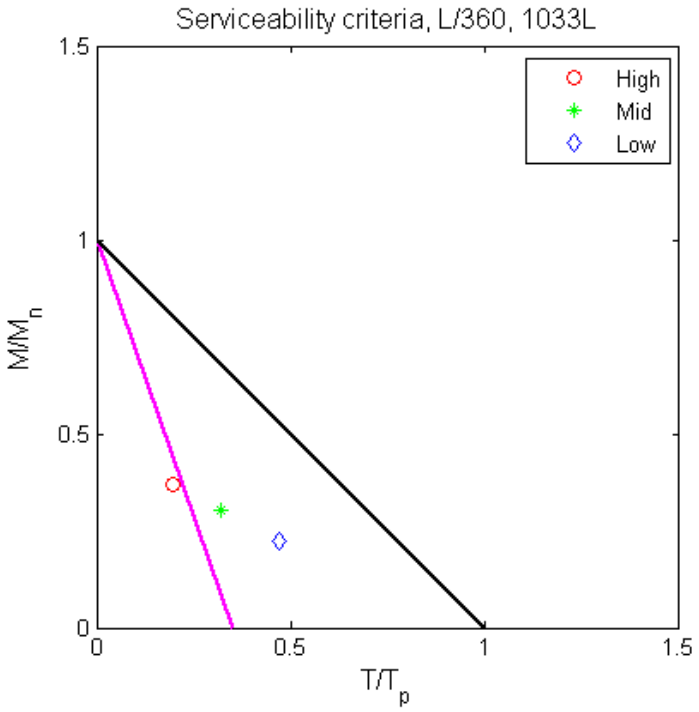

Figure 110 Design criteria comparison, L/360 serviceability, L2 beam

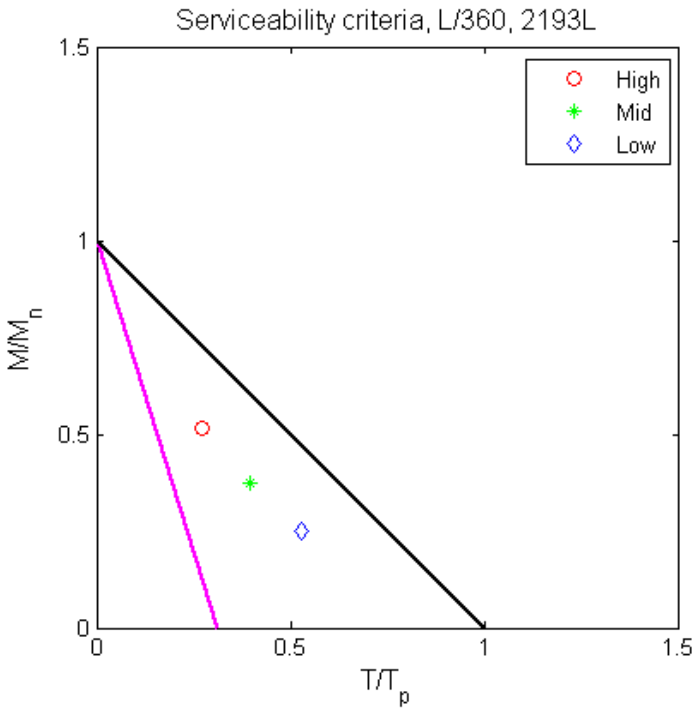

Figure 111 Design criteria comparison, L/360 serviceability, L3 beam

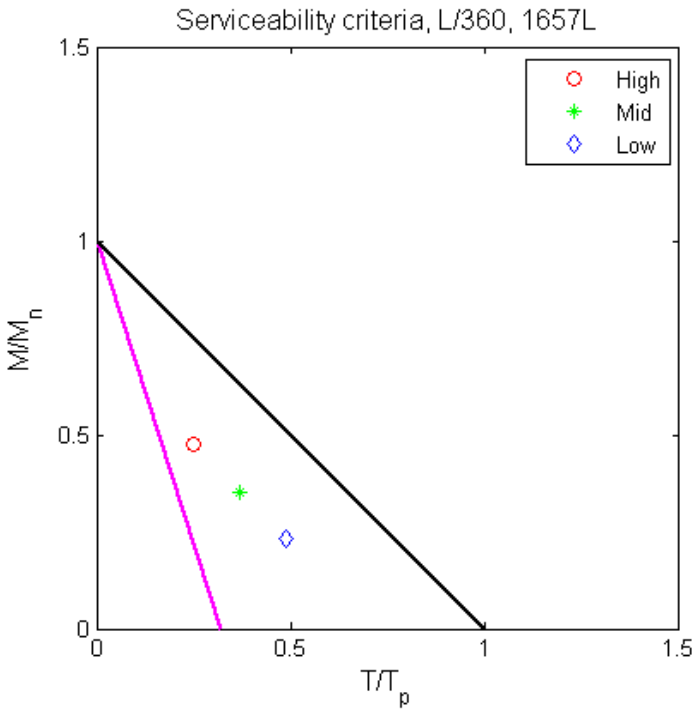

Figure 112 Design criteria comparison, L/360 serviceability, L4 beam

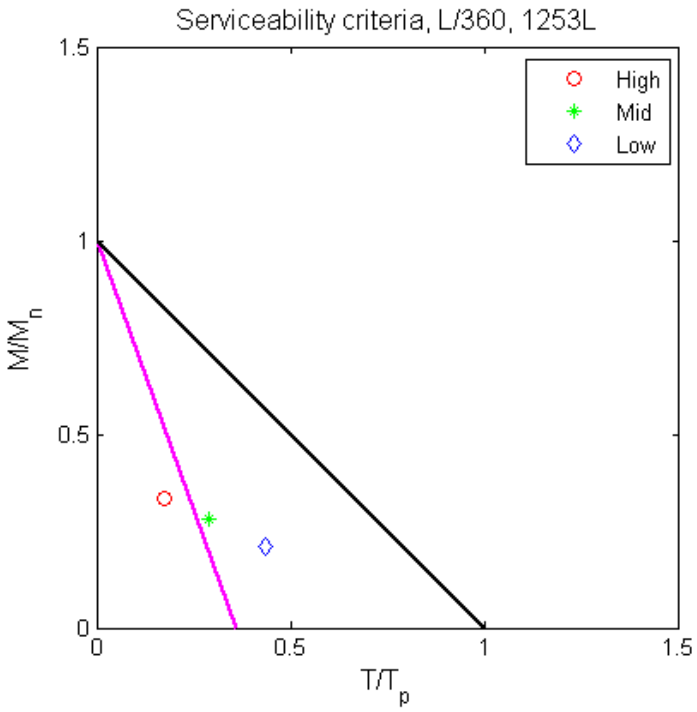

Figure 113 Design criteria comparison, L/360 serviceability, L5 beam

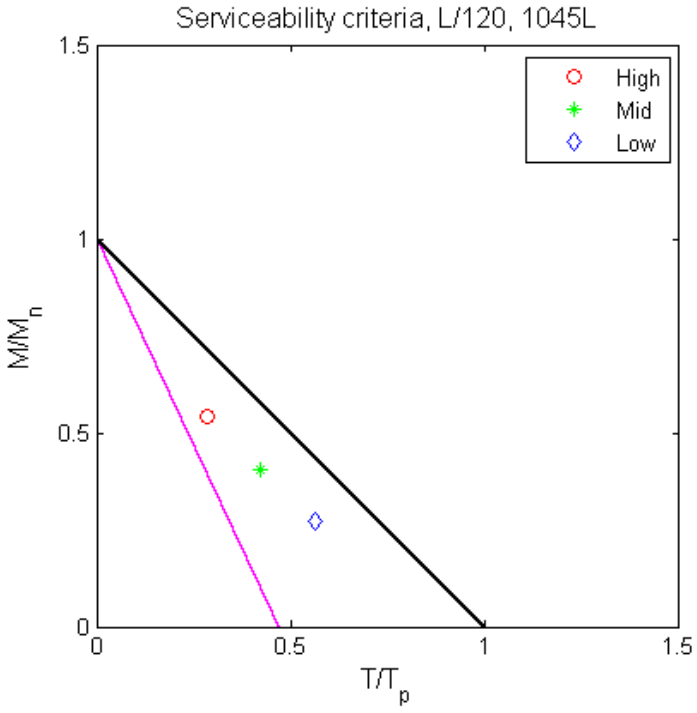

Figure 114 Design criteria comparison, L/120 serviceability, L1 beam

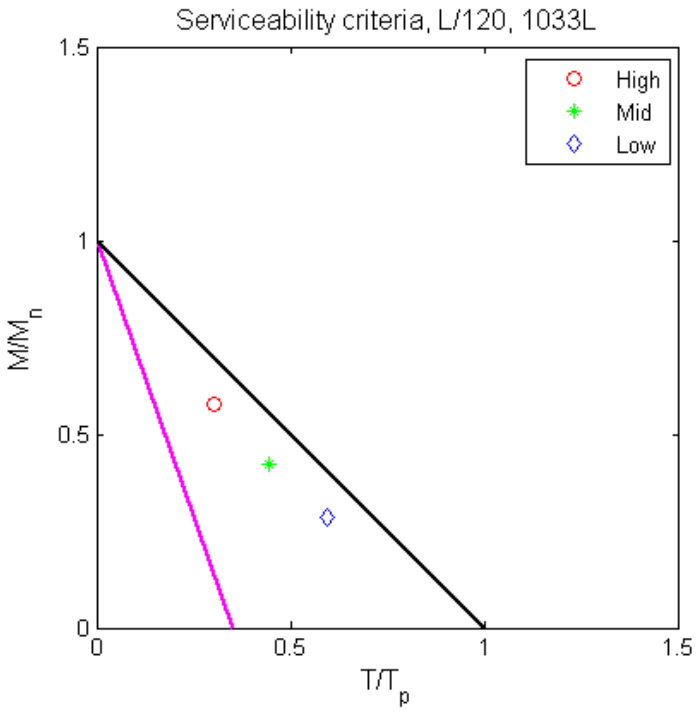

Figure 115 Design criteria comparison, L/120 serviceability, L2 beam

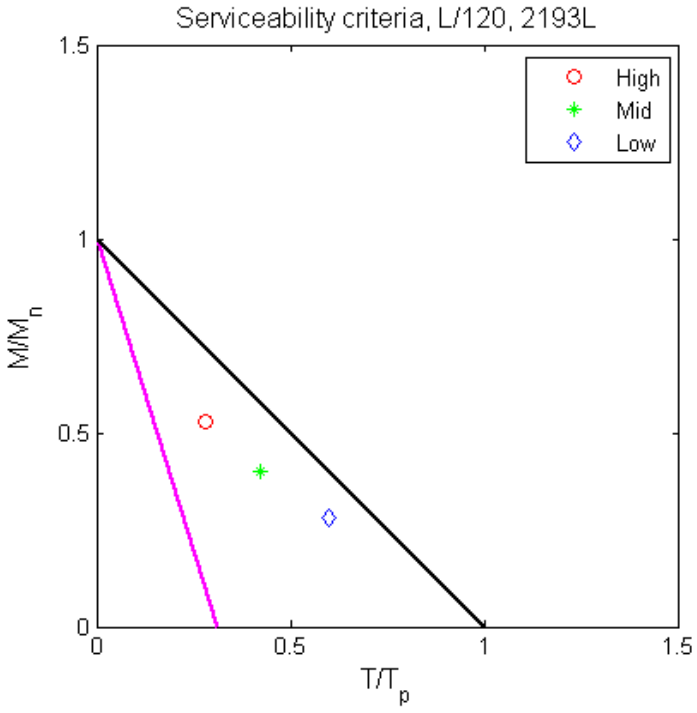

Figure 116 Design criteria comparison, L/120 serviceability, L3 beam

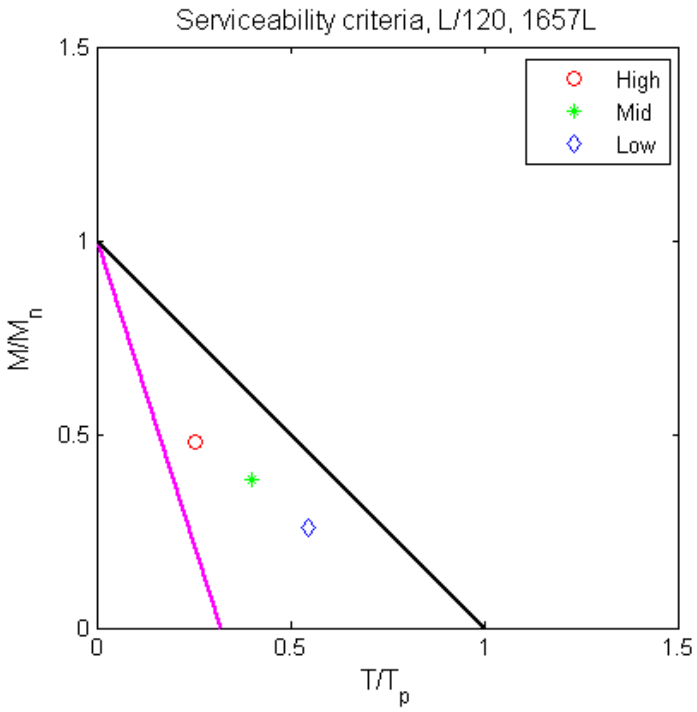

Figure 117 Design criteria comparison, L/120 serviceability, L4 beam

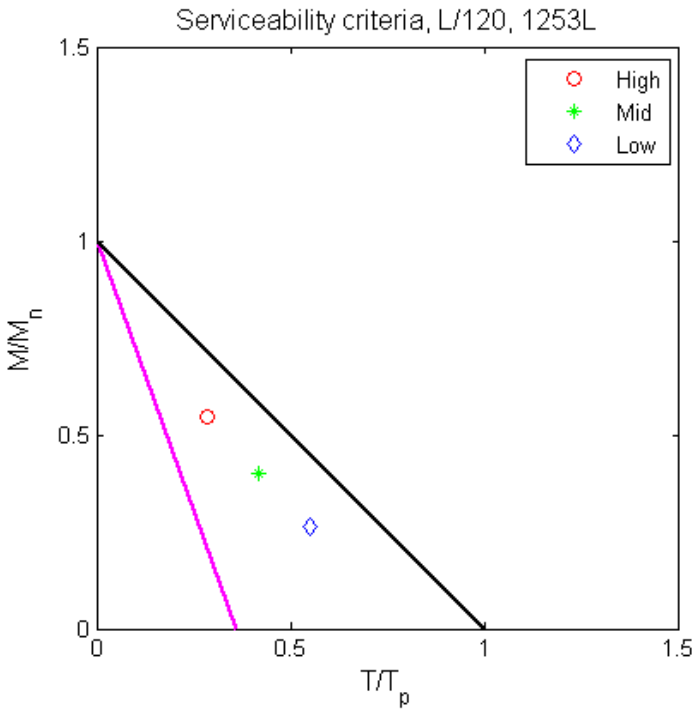

Figure 118 Design criteria comparison, L/120 serviceability, L5 beam

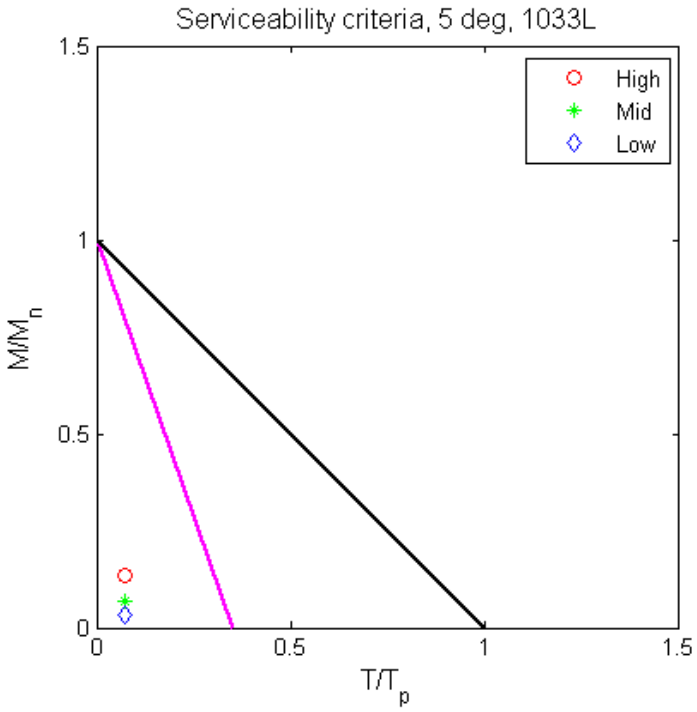

Figure 119 Design criteria comparison, 5 deg serviceability, L2 beam

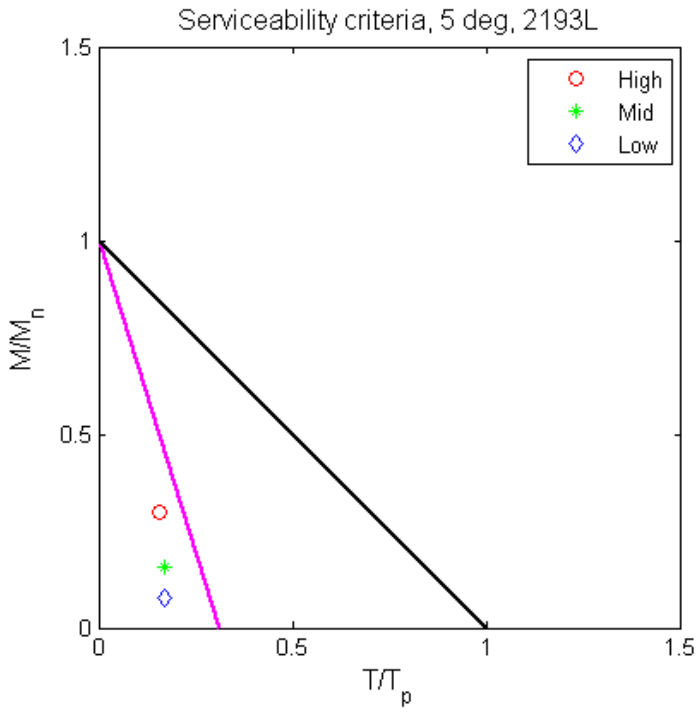

Figure 120 Design criteria comparison, 5 deg serviceability, L3 beam

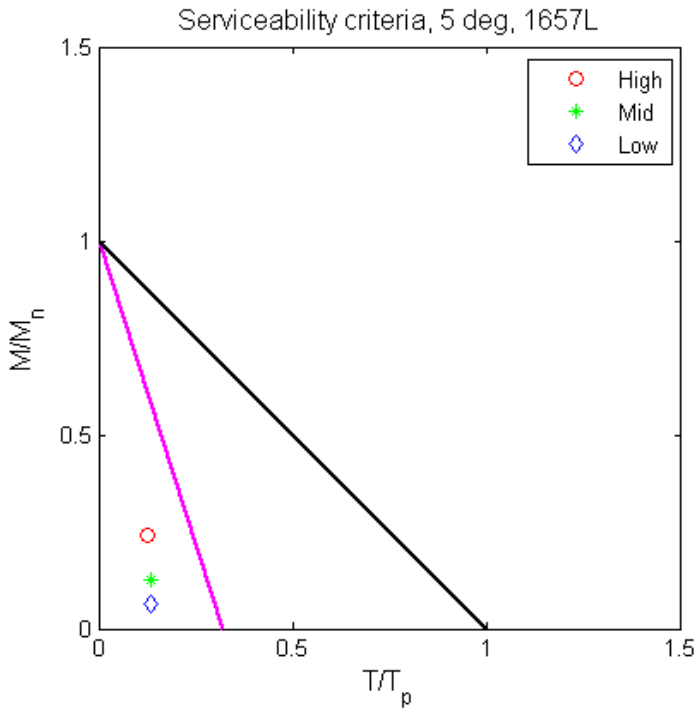

Figure 121 Design criteria comparison, 5 deg serviceability, L4 beam

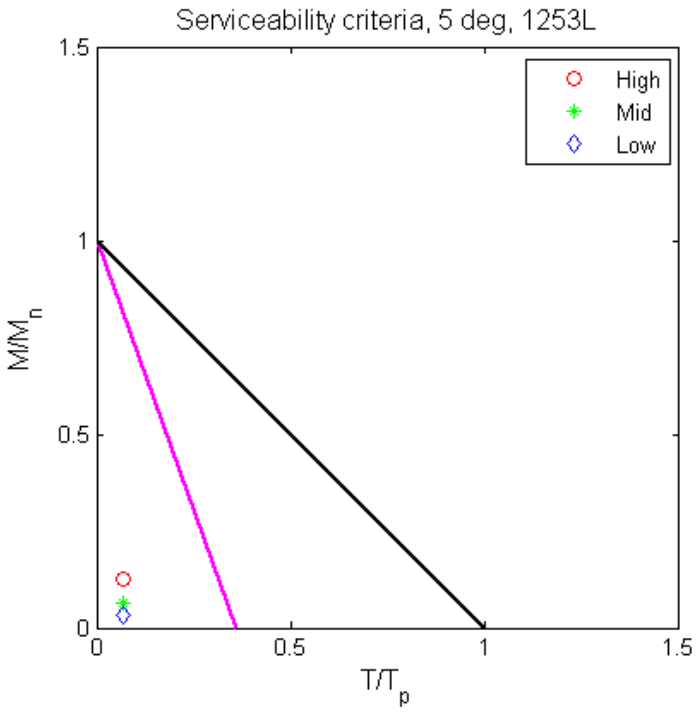

Figure 122 Design criteria comparison, 5 deg serviceability, L5 beam

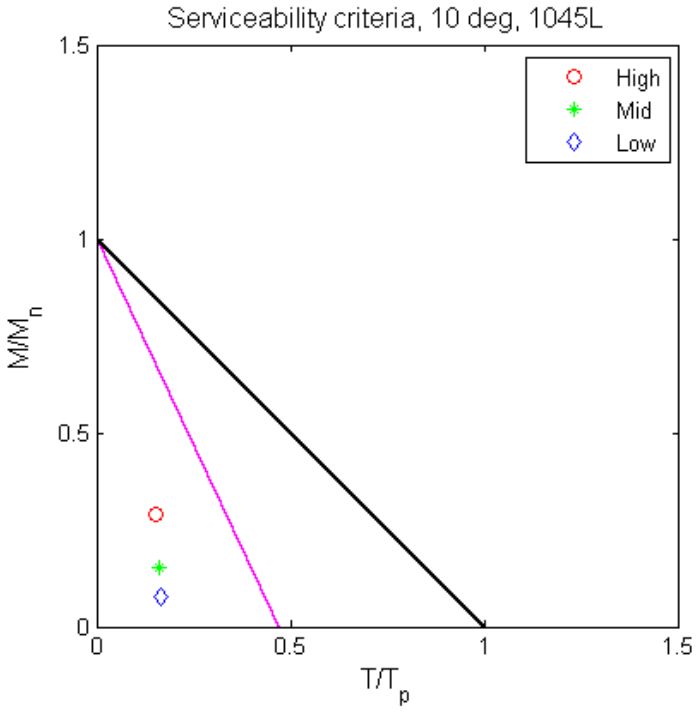

Figure 123 Design criteria comparison, 10 deg serviceability, L1 beam

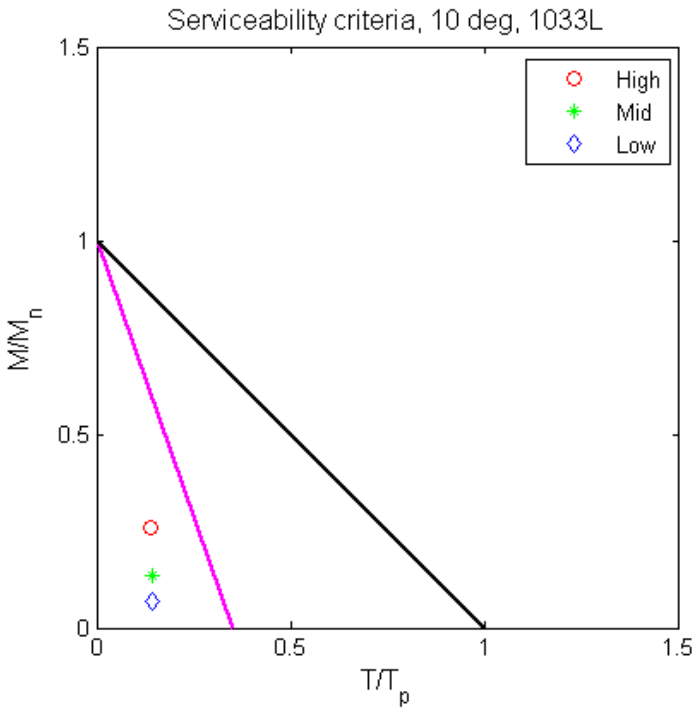

Figure 124 Design criteria comparison, 10 deg serviceability, L2 beam

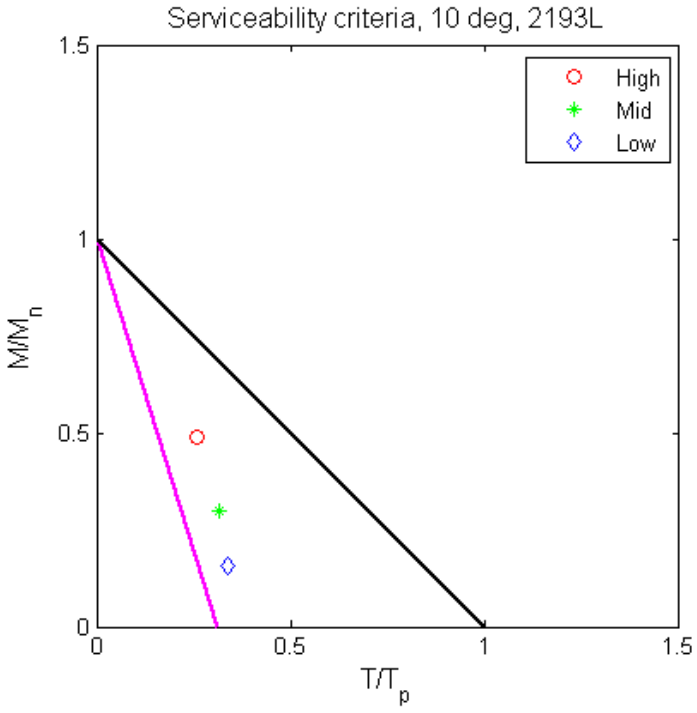

Figure 125 Design criteria comparison, 10 deg serviceability, L3 beam

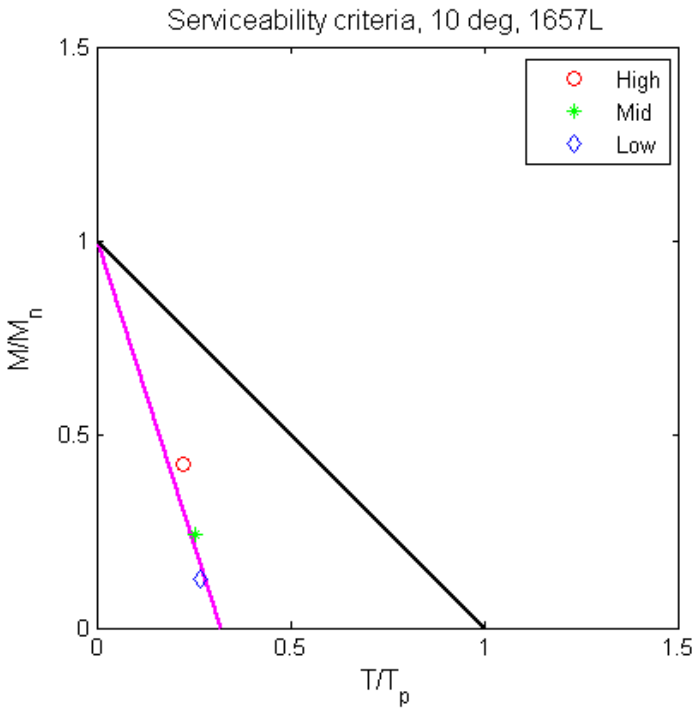

Figure 126 Design criteria comparison, 10 deg serviceability, L4 beam

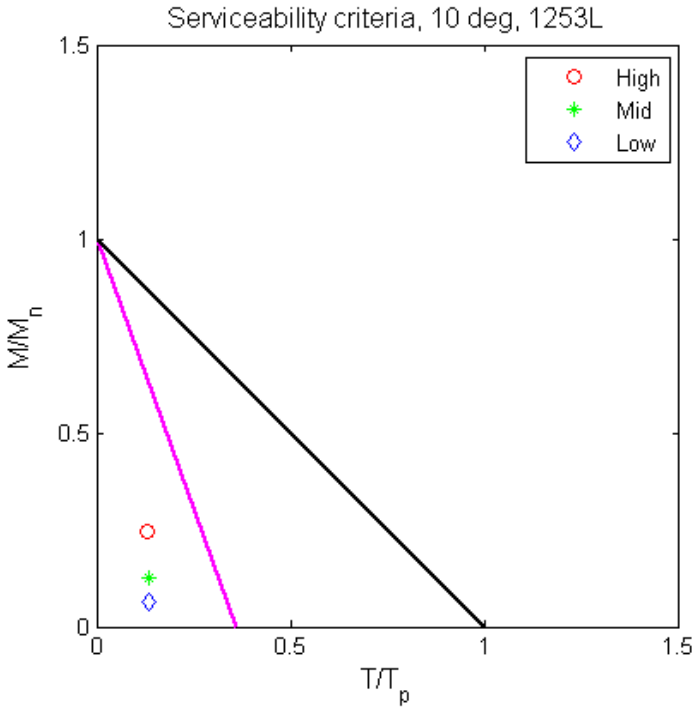

Figure 127 Design criteria comparison, 10 deg serviceability, L5 beam